

LePDF: Standard Model PDFs for High-Energy Lepton Colliders

Francesco Garosi,^{a,b} David Marzocca,^b Sokratis Trifinopoulos^c

^a*SISSA International School for Advanced Studies, Via Bonomea 265, 34136, Trieste, Italy*

^b*INFN, Sezione di Trieste, SISSA, Via Bonomea 265, 34136, Trieste, Italy*

^c*Center for Theoretical Physics, Massachusetts Institute of Technology, Cambridge, MA 02139, USA*

ABSTRACT: The emission of collinear radiation off an elementary lepton can be factorised from the hard scattering process by introducing Parton Distribution Functions of a Lepton (LePDF), which, contrary to protons, can be derived from first principles. In case of multi-TeV lepton colliders, such as the muon colliders currently being proposed, the complete structure of Standard Model interactions must be taken into account. In this work we solve numerically the corresponding DGLAP equations at the double-log order and provide public files with LePDFs for both muons and electrons, including polarisation effects. We discuss several interesting aspects of the resulting PDFs and compare them with the Effective Vector Approximation, showing that the latter fails to describe well the vector bosons PDFs at small momentum fractions, unless it is extended to higher orders.

Contents

1	Introduction	2
2	QED and QCD evolution	4
2.1	Iterative solution for QED	6
3	DGLAP evolution in the SM	7
3.1	Electroweak symmetry breaking effects	7
3.2	Electroweak double logarithms	8
3.3	Top quark as parton	10
3.4	Effective Vector Boson Approximation	11
4	Results	12
4.1	Polarisation	15
4.2	Comparison with the Effective Vector Boson Approximation	16
4.3	Muon neutrino PDF	18
4.4	Mass effects	19
4.5	Top quark PDF	20
4.6	Uncertainties	20
4.7	PDFs for electron beams	22
5	Conclusions	23
A	Inputs and Formalism	25
A.1	Standard Model inputs	25
A.2	Formalism for the DGLAP equations	25
B	Splitting Functions	27
B.1	Massless splitting functions	27
B.2	Ultra-collinear splitting functions	28
C	Radiative corrections	32
D	DGLAP evolution equations in SM	33
D.1	Leptons	34
D.2	Quarks	35
D.3	Transverse gauge bosons	40
D.4	Higgs and longitudinal gauge bosons	43
E	Numerical implementation	45
F	LHAPDF format	47

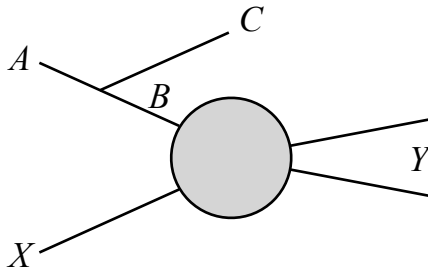


Figure 1. Diagram of a process $AX \rightarrow CY$ with an initial-state splitting $A \rightarrow BC$.

1 Introduction

At present, the Large Hadron Collider at CERN is our only tool for direct exploration of physics at the electroweak scale and above and the high-luminosity phase is planned to last until the early 2040s. It proved to be a formidable machine for both searches of new heavy particles as well as precision studies at the electroweak scale, of which the Higgs discovery and the precision study of its coupling is a prime example. Nevertheless, the next large-scale experiment in high-energy physics is likely to be a lepton collider. The proposed options include circular or linear electron-positron colliders (FCC-ee [1] and CEPC [2] for the former, ILC [3], CLIC [4] and CCC [5] for the latter) as well as $\mu^+\mu^-$ colliders [6–10]. Among these, the linear e^+e^- colliders and the muon colliders could achieve multi-TeV center-of-mass energies.

While leptons are elementary particles in the Standard Model (SM), the process of collinear emission of initial state radiation (ISR), with transverse momentum p_T much smaller than the energy of the hard scattering process, can be factorized and a description in terms of parton distribution functions (PDFs) can be introduced, similarly to what is done in case of proton colliders and the parton content of a proton. The case of collinear photon emission from an electron is known since almost a century and at leading order can be described using the effective photon approximation (EPA) [11–14]

$$f_\gamma^{\text{EPA}}(x) = \frac{\alpha_\gamma}{2\pi} P_{\gamma e}(x) \log \frac{E^2}{m_e^2}, \quad (1.1)$$

where E is the energy of the initial electron and $P_{\gamma e}(x) = \frac{1+(1-x)^2}{x}$ is the splitting function, that describes the probability of an electron to emit a photon with a fraction x of its energy and virtuality $-p_T^2/(1-x)$.

When $E \gg m_e$ the large logarithms can be resummed in order to improve the perturbative expansion, and the factorization scale Q is introduced. Invariance of the physics under the factorization scale leads to the DGLAP equations [15–17]. For a generic splitting of massless partons $A \rightarrow B + C$ (as in Fig. 1), choosing p_T as factorization scale and working at the leading logarithm (LL) order one has

$$Q^2 \frac{df_B(x, Q^2)}{dQ^2} = P_B^v f_B(x, Q^2) + \sum_{A,C} \frac{\alpha_{ABC}(Q)}{2\pi} \int_x^1 \frac{dz}{z} P_{BA}^C(z) f_A\left(\frac{x}{z}, Q^2\right), \quad (1.2)$$

where $P_{BA}^C(z)$ are the leading order (LO) splitting functions (listed in App. B), $\alpha_{ABC}(Q)$ the corresponding running coupling, and the term $P_B^v f_B$ describes virtual corrections (see App. C for details). In case of a proton, due to its non-perturbative nature, the initial conditions for this system must be fitted from collider data. For a lepton, instead, the initial condition can be computed perturbatively and the system can be solved from first principles. The initial condition is

$$f_\ell(x, m_\ell^2) = \delta(1-x) + \mathcal{O}(\alpha) , \quad (1.3)$$

for initially unpolarised beams¹, while all other PDFs vanish for $Q^2 = m_\ell^2$ at this order. Next-to-leading order (NLO) corrections to the initial conditions have also been computed [18] and become relevant when next-to-leading log (NLL) evolution is considered [19, 20]. In this work we limit ourselves to LL evolution and LO initial conditions.

In case of multi-TeV lepton colliders one can be interested in factorization scales much higher than the electroweak scale. In this case all SM interactions and fields should be considered [21]. In this aspect, lepton colliders differ qualitatively from hadron colliders. For the latter, QCD interactions are the dominant contributions to the DGLAP evolution in the whole energy range (see however e.g. Refs. [22–26] about the photon and lepton content of the proton). In the case of lepton collider, instead, QED and electroweak (EW) interactions are the leading ones, with QCD playing an important but not dominant role.

The facts that SM gauge group is non abelian, that it is spontaneously broken at the electroweak scale, and that interactions are chiral have several crucial implications for the evaluation of collinear radiation in this regime. The non abelian nature of EW interactions imply a lack of cancellation of infrared (IR) divergencies between virtual corrections and real emission, which generates Sudakov double logarithms [27–29]. Electroweak symmetry breaking effects have been shown to provide important contributions and to be the dominant ones in case of longitudinal polarisations of electroweak gauge bosons [30]. Since the SM interactions are chiral, PDFs become polarized above the EW scale [31].

The goal of this work is to numerically solve the DGLAP equations from the initial condition at $Q = m_\ell$ up to multi-TeV scales, taking into account all SM interactions (including the effects mentioned above), and to provide public results with the complete LePDFs. For concreteness, in the following we assume the initial lepton to be a muon, since muon colliders could achieve higher energies, for which our discussion is more relevant. However, all results can be equally applied to e^+e^- colliders with suitable substitutions thus we provide numerical results for both.

A preliminary study of PDFs for muon colliders by us, mainly focusing on the fermionic degrees of freedom, was included in Ref. [32]. In this work we extend it by including all SM interactions, Sudakov double logs, polarisation, and EW symmetry breaking effects. One similar study has already been performed in the literature, specifically in Refs. [33, 34], and we compare our results with the plots presented in those works. We also compare against approximate solutions obtained by solving iteratively, at fixed-order, the DGLAP equations,

¹Here we assume unpolarised beams, so that polarisation effects are only due to the DGLAP evolution. If needed, it will be straightforward to implement a given intrinsic beam polarisation in future versions of the code.

which provide the analogous of the Effective Vector Boson Approximation (EVA) [35–37]. A noteworthy result of this comparison is the realisation that the LO EVA for transverse EW gauge bosons PDFs is insufficient for correctly describing the full result, which is instead well approximated by including contributions up to $\mathcal{O}(\alpha^2)$. Crucially, Sudakov double logarithms appear at this order due to the gauge boson splitting $V \rightarrow VV$ and the virtual corrections to the muon PDF.

In Section 2 we present the first part of the evolution below the EW scale, where only QED and QCD interactions are relevant. In Section 3 we discuss the main aspects of the evolution above the EW scale. Our results are collected in Section 4, where several notable features of LePDFs are showed, and a comparison with EVA is presented. We conclude in Section 5, while many details of our computations, the numerical implementation and the formatting of our LePDF files are collected in several Appendices. The numerical results for the LePDFs can be downloaded from GitHub at the link: <https://github.com/DavidMarzocca/LePDF>.

2 QED and QCD evolution

For factorization scales below the EW scale the relevant degrees of freedom are light quarks and charged leptons, with vectorlike QED and QCD gauge interactions. Neutrinos, while having negligible masses, become relevant only above the EW scale where the W boson can go on-shell.² Because the initial condition and the evolution equations are vectorlike, in this regime no polarisation effects are induced, i.e. PDFs will be the same for both fermion chiralities or gauge boson polarisation.

In the DGLAP evolution from the muon mass up to the EW scale one encounters several mass thresholds for each fermion species as well as at the QCD scale Q_{QCD} . At each threshold a matching should be performed. For our purposes, we take all fermions except bottom and top quarks to be massless.³ The Q_{QCD} scale sets the onset of QCD interactions, which become relevant after the $\gamma \rightarrow q\bar{q}$ splitting. This can be interpreted as the QCD structure of a photon, and can be divided into a perturbative and a non-perturbative component, mainly due to the photon mixing with QCD vector mesons [41–45]. The latter one will be power-suppressed at the large scales we are eventually interested in, so we neglect it. The choice of Q_{QCD} depends on how many resonances are included in the non-perturbative component and a value close to m_ρ has been argued to provide a good benchmark [43–45]. In practice, we follow the prescription of Ref. [34, 43] with $Q_{\text{QCD}} = 0.7$ GeV.⁴

Therefore, from m_μ to Q_{QCD} we consider only QED interactions, including all charged leptons as well as the light quarks (u, d, s, c). At Q_{QCD} we match the PDFs and continue the evolution up to the bottom mass scale adding also QCD interactions and setting the

²A possible effect of neutrinos even below the EW scale is due to neutrinos from muon decay $\mu^- \rightarrow e^- \bar{\nu}_e \nu_\mu$ which present IR singularities in the physical region when scattering with the incoming μ^+ (or viceversa) [38]. In case of muon colliders such singularities are cutoff by the finite width of the muon beam [39, 40]. We neglect such effects with our PDF formalism, assuming that it can be described independently of PDFs.

³In future versions we plan to add also the τ and charm quark mass thresholds.

⁴We study the dependence of our results on Q_{QCD} by running the evolution also for values $Q_{\text{QCD}} = 0.52(1.0)$ GeV and interpreting the differences as theory uncertainty on our final results due to non-perturbative QCD dynamics, see dedicated discussion in Sec. 4.6.

initial condition for the gluon PDF as $f_g(x, Q_{\text{QCD}}) = 0$. At $Q = m_b$ we perform another matching and continue the evolution up to the EW scale Q_{EW} including also the bottom quark, setting $f_b(x, m_b) = f_{\bar{b}}(x, m_b) = 0$ as its initial conditions.

Given the C and P symmetries of QED and QCD, and the fact that all fermions except for bottom and top quarks are taken massless, below Q_{EW} several PDFs are related:

$$\begin{aligned}
f_{\ell_{\text{sea}}} &= f_e = f_\tau = f_{\bar{e}} = f_{\bar{\mu}} = f_{\bar{\tau}} , \\
f_{q^u} &= f_u = f_{\bar{u}} = f_c = f_{\bar{c}} , \\
f_{q^d} &= f_d = f_{\bar{d}} = f_s = f_{\bar{s}} , \\
f_b &= f_{\bar{b}} .
\end{aligned} \tag{2.1}$$

The DGLAP equations, according to Eq. (1.2), are then given by

$$\begin{aligned}
\frac{df_\ell}{dt} &= P_\ell^v f_\ell + \frac{\alpha_\gamma(t)}{2\pi} \left[P_{ff}^V \otimes f_\ell + P_{fV}^f \otimes f_\gamma \right] , \\
\frac{df_{q^u}}{dt} &= P_{q^u}^v f_{q^u} + \frac{\alpha_\gamma(t)}{2\pi} Q_u^2 \left[P_{ff}^V \otimes f_{q^u} + N_c P_{fV}^f \otimes f_\gamma \right] \\
&\quad + \frac{\alpha_3(t)}{2\pi} \left[C_F P_{ff}^V \otimes f_{q^u} + T_F P_{fV}^f \otimes f_g \right] , \\
\frac{df_{q^{d,b}}}{dt} &= P_{q^{d,b}}^v f_{q^{d,b}} + \frac{\alpha_\gamma(t)}{2\pi} Q_d^2 \left[P_{ff}^V \otimes f_{q^{d,b}} + N_c P_{fV}^f \otimes f_\gamma \right] \\
&\quad + \frac{\alpha_3(t)}{2\pi} \left[C_F P_{ff}^V \otimes f_{q^{d,b}} + T_F P_{fV}^f \otimes f_g \right] , \\
\frac{df_\gamma}{dt} &= P_\gamma^v f_\gamma + \frac{\alpha_\gamma(t)}{2\pi} \sum_f Q_f^2 P_{Vf}^f \otimes (f_f + f_{\bar{f}}) , \\
\frac{df_g}{dt} &= P_g^v f_g + \frac{\alpha_3(t)}{2\pi} \left[C_A P_{VV} \otimes f_g + C_F P_{Vf}^f \otimes \sum_q (f_q + f_{\bar{q}}) \right] ,
\end{aligned} \tag{2.2}$$

where $\ell = \{\ell_{\text{sea}}, \mu\}$, \otimes indicates a convolution as in Eq. (1.2) and we defined the evolution variable t as

$$t \equiv \log(Q^2/m_\mu^2) , \tag{2.3}$$

such that we start the evolution with the initial condition in Eq. (1.3) at $t = 0$. The splitting functions are listed in App. B (we regulate the $(1-z)^{-1}$ poles using the standard $+$ -distribution, see Eq. (B.1)), while the values of the virtual coefficients P_B^v can be found in App. C. Finally, the details for the RG evolution of QED and QCD couplings are reported in App. A.1. In Fig. 2 we show the result of our numerical solution of DGLAP equations for a muon, evolved from the muon mass up to the EW scale $Q_{\text{EW}} = m_W$ (solid lines). As can be seen, at small x the gluon PDF becomes rather important, while quark PDFs have a size similar to the muon itself or sea leptons, as already showed in Refs. [32–34].

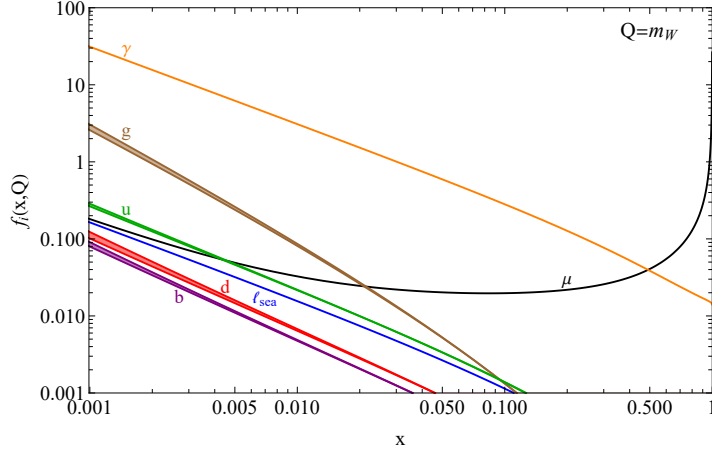


Figure 2. PDFs of a muon evaluated at the EW scale $Q_{EW} = m_W$. The colored regions corresponds to the variation obtained by modifying Q_{QCD} between 0.5 and 1 GeV (see Sec. 4.6 for details). Here ℓ_{sea} is defined as in Eq. (2.1).

2.1 Iterative solution for QED

By solving iteratively the DGLAP equations order by order in $(\alpha_\gamma t) = (\alpha_\gamma \log Q^2/m_Q^2)$, one gets approximate solutions for the PDFs. The LO contribution for the photon PDF is given by Eq. (1.1) with the crucial substitution $E \rightarrow Q$. By including terms up to $\mathcal{O}(\alpha^2 t^2)$ we get

$$\begin{aligned}
 f_\mu^{(\alpha^2)}(x, t) &= \delta(1-x) + \frac{\alpha_\gamma}{2\pi} t \left(\frac{3}{2} \delta(1-x) + P_{ff}^V(x) \right) \\
 &\quad + \frac{1}{2} \left(\frac{\alpha_\gamma}{2\pi} t \right)^2 \left[\frac{9}{4} \delta(1-x) + 3P_{ff}^V(x) + I_{fVVf}(x) + I_{ffff}(x) \right], \\
 f_{\ell_{sea}}^{(\alpha^2)}(x, t) &= \frac{1}{2} \left(\frac{\alpha_\gamma}{2\pi} t \right)^2 I_{fVVf}(x), \\
 f_\gamma^{(\alpha^2)}(x, t) &= \frac{\alpha_\gamma}{2\pi} t P_{Vf}^f(x) + \frac{1}{2} \left(\frac{\alpha_\gamma}{2\pi} t \right)^2 \left[\left(\frac{3}{2} - \frac{2}{3} N_f^{\text{QED}} \right) P_{Vf}^f(x) + I_{Vfff}(x) \right],
 \end{aligned} \tag{2.4}$$

where t is defined in Eq. 2.3 and the $I_{ABBC}(x) \equiv \int_x^1 \frac{dz}{z} P_{AB}^X(z) P_{BC}^Y(x/z)$ integrals are collected in Eq. (B.7). Going up to $\mathcal{O}(\alpha^2 t^2)$ is required in order to describe the low- x behavior of valence and sea lepton PDFs, that is dominated by the $\gamma \rightarrow \ell^+ \ell^-$ splitting (i.e. the $I_{fVVf}(x)$ term above). We find good agreement between these expressions and our numerical results.

The gluon PDF starts formally at $\mathcal{O}(\alpha_\gamma^2 \alpha_s t^3)$. However, due to the large value of α_s at low energies and the importance of a careful treatment of the matching at the Q_{QCD} , a fixed-order solution would not be a good approximation for the correct result. For the same reason we do not report here also the approximated expression for quark PDFs, even if they formally arise already at $\mathcal{O}(\alpha_\gamma^2 t^2)$, since they receive large a QCD contribution from gluon splitting into $q\bar{q}$. A correct description of the quark and gluon PDFs in a lepton therefore motivates a complete numerical solution of the DGLAP equations [34].

Leptons	μ_L	μ_R	e_L	e_R	ν_μ	ν_e	$\bar{\ell}_L$	$\bar{\ell}_R$	$\bar{\nu}_\ell$
Quarks	u_L	d_L	u_R	d_R	t_L	t_R	b_L	b_R	+ h.c.
Gauge Bosons	γ_\pm	Z_\pm	Z/γ_\pm	W_\pm^\pm	g_\pm				
Scalars	h	Z_L	h/Z_L	W_L^\pm					

Table 1. Independent degrees of freedom for our DGLAP evolution above the EW scale.

3 DGLAP evolution in the SM

For energies above the EW scale, the splitting processes in the initial states can involve all SM interactions and fields, which must then be included in the DGLAP equations. The chiral nature of EW interactions induces polarisation effects on PDFs, so in this region all gauge bosons and fermions polarisations are treated separately. Splitting functions for SM interactions in the unbroken phase have been computed in Refs. [21, 30, 31, 46–48], with which we agree. Another well known effect in EW PDFs is the interference between photon and transverse Z_T , which must be described with a Z/γ mixed PDF, as well as between the Higgs boson and the longitudinal Z_L , which induces a h/Z_L mixed PDF [21, 30, 49]. Also, the non-abelian nature of EW interactions induces Sudakov double logarithms, which must be resummed when one is interested at high energies [27–29].

Since we neglect all fermion masses except than the top and bottom quarks, several PDFs are related:

$$\begin{aligned}
f_{e_L} &= f_{\tau_L}, & f_{\bar{\ell}_L} &= f_{\bar{e}_L} = f_{\bar{\mu}_L} = f_{\bar{\tau}_L}, \\
f_{e_R} &= f_{\tau_R}, & f_{\bar{\ell}_R} &= f_{\bar{e}_R} = f_{\bar{\mu}_R} = f_{\bar{\tau}_R}, \\
f_{\nu_e} &= f_{\nu_\tau}, & f_{\bar{\nu}_\ell} &= f_{\bar{\nu}_e} = f_{\bar{\nu}_\mu} = f_{\bar{\nu}_\tau}, \\
f_{u_L} &= f_{c_L}, & f_{\bar{u}_L} &= f_{\bar{c}_L}, & f_{u_R} &= f_{c_R}, & f_{\bar{u}_R} &= f_{\bar{c}_R}, \\
f_{d_L} &= f_{s_L}, & f_{\bar{d}_L} &= f_{\bar{s}_L}, & f_{d_R} &= f_{s_R}, & f_{\bar{d}_R} &= f_{\bar{s}_R}.
\end{aligned} \tag{3.1}$$

The fact that PDFs for right-handed fermions and their conjugate are different is due to the induced polarisation effects in the gluon, photon, and Z boson PDFs. The independent degrees of freedom are given in Table 1 in the case of PDFs of a muon beam, the final count is 42 independent PDFs. Regarding the mass thresholds, we include each degrees of freedom right at the corresponding mass scale.

3.1 Electroweak symmetry breaking effects

EW symmetry breaking effects can be classified as either due to non-vanishing parton masses or as new contributions to the splitting functions that vanish in the limit of unbroken symmetry [30]. The latter are the so-called *ultra-collinear* splittings, which are particularly relevant for the longitudinal polarisations of EW gauge bosons [30, 50], providing the leading contributions for their PDFs even when $Q \gg Q_{\text{EW}}$. In order to easily keep track of all these effects near the EW scale it is convenient to work in the broken phase and with the mass eigenstates. Then, as the DGLAP equations remain the same also for higher energies, we remain in the broken phase for any $Q > Q_{\text{EW}}$. We compute the splitting functions in the Goldstone equivalence gauge, following Ref. [30]. However, we checked that the results are

the same as the ones in [50], in which the theory is formulated in a standard R_ζ -gauge, with a 5-dimensional polarisation vector for the longitudinal component of gauge bosons to take into account the Goldstone contribution.

In case any of the particles involved in the splitting $A \rightarrow B+C$ is massive, the kinematics of the process and the ensuing splitting functions are modified. The relation between the p_T and the virtuality of the parton B entering the hard scattering process becomes

$$\tilde{p}_T^2 \equiv \bar{z}(m_B^2 - p_B^2) = p_T^2 + zm_C^2 + \bar{z}m_B^2 - z\bar{z}m_A^2 + \mathcal{O}\left(\frac{m^2}{E^2}, \frac{p_T^2}{E^2}\right), \quad (3.2)$$

where $\bar{z} = 1-z$ and m^2/E^2 or p_T^2/E^2 terms can be neglected in the regime where factorization can be applied. In the DGLAP equations, this modified propagator of the virtual parton B effectively corresponds to a rescaling of the splitting functions as [30]

$$P_{BA}^C(z) \rightarrow \tilde{P}_{BA}^C(z, p_T^2) = \left(\frac{p_T^2}{\tilde{p}_T^2}\right)^2 P_{BA}^C(z). \quad (3.3)$$

Mass effects in matrix elements that are also present in the unbroken (i.e. massless) theory are instead suppressed by powers of m/E , therefore negligible.

Regarding the ultra-collinear splitting functions, the main feature of these contributions is that they do not scale logarithmically with Q^2 but at large factorization scales are suppressed as v^2/Q^2 . Nevertheless, they provide important contributions that accumulate during the DGLAP evolution in the region $Q \sim Q_{EW}$ and then remain almost constant at higher scales, see for instance the W_L PDF in the right panel of Fig. 3. We report the full set of splitting functions in App. B, while the list of SM DGLAP equations can be found in App. D.

In principle, with massive partons we should care of kinematics bounds: the splittings described by DGLAP equations involve partons A , B and C with energies zE , xE and $(z-x)E$ respectively, all fractions of the energy of the beam E . Since the particle C is emitted on-shell, we need $E_C \geq m_C$, that is $z \geq x + \frac{m_C}{E}$. This means that the lower extreme of integration in Eq. (1.2) should be modified. However, as in Eq. (3.2), m/E terms can be neglected and we can safely start the integration from x .

3.2 Electroweak double logarithms

The fact that the initial and final states are EW non-singlets has important implications, even for inclusive processes. The Bloch-Nordsieck theorem [51], that guarantees cancellation of IR divergencies between real emission and virtual corrections in such processes, is violated for non-abelian symmetries, which implies the presence of Sudakov double logarithms. While in the QCD case this effect vanishes upon averaging over color of the initial states, for $SU(2)_L$ we do not take such average and the initial state breaks explicitly the symmetry, hence double logs do appear also in inclusive processes [27–29, 49, 52]. In our context they can be seen appearing in the terms of the DGLAP equations containing a $1/(1-z)$ pole and can be made explicit by introducing an IR cutoff in the integral, which allows also to resum the Sudakov double logs related to ISR [46–48, 53, 54].⁵ We implement this following

⁵A complete description of all double logarithms in a full process requires, however, the inclusion of further contributions (e.g. virtual corrections, soft radiation, fragmentation, etc.), see for instance [27, 54–59].

Ref. [47], by modifying the boundaries of the integral in Eq. (1.2) as

$$\frac{\alpha_{ABC}(Q)}{2\pi} \int_x^1 \frac{dz}{z} P_{BA}^C(z) f_A\left(\frac{x}{z}, Q^2\right) \rightarrow \frac{\alpha_{ABC}(Q)}{2\pi} \int_x^{z_{\max}^{ABC}(Q)} \frac{dz}{z} P_{BA}^C(z) f_A\left(\frac{x}{z}, Q^2\right), \quad (3.4)$$

where $z_{\max}^{ABC}(Q)$ plays the role of an explicit IR cutoff for the $1/(1-z)$ poles, and is set equal to 1 (in which case we use the $+$ -distribution to regulate the divergence and perform the numerical evaluation) except for the cases where the soft divergence is not cancelled between real emission and virtual corrections, in which case we set $z_{\max}^{ABC}(Q) = 1 - Q_{\text{EW}}/Q$. This modifies the computation of the virtual corrections, that becomes (see App. C)

$$P_A^v(Q) \supset - \sum_{B,C} \frac{\alpha_{ABC}(Q)}{2\pi} \int_0^{z_{\max}^{ABC}(Q)} dz z P_{BA}^C(z) + \text{ultra-collinear}. \quad (3.5)$$

The mismatch of IR divergencies between real and virtual contributions takes place in processes where the emitted radiation (e.g. a W^\pm boson) changes the $SU(2)_L$ component of the initial state, and is always proportional to the amount of explicit breaking of the $SU(2)_L$ symmetry. In fact, the physical effect of these double logs is to restore $SU(2)_L$ invariance at high scales. The case of PDFs of a proton is discussed in Ref. [48]. As an explicit example for leptons, let us consider the DGLAP equations for the μ_L and the corresponding $SU(2)_L$ partner ν_μ

$$\begin{aligned} \frac{df_{\mu_L}}{d \log Q^2} &= \frac{\alpha_2}{2\pi} \frac{1}{2} \int_0^{z_{\max}(Q)} dz P_{ff}^V(z) \left(\frac{1}{z} f_{\nu_\mu}\left(\frac{x}{z}, Q^2\right) - z f_{\mu_L}(x, Q^2) \right) + \dots, \\ \frac{df_{\nu_\mu}}{d \log Q^2} &= \frac{\alpha_2}{2\pi} \frac{1}{2} \int_0^{z_{\max}(Q)} dz P_{ff}^V(z) \left(\frac{1}{z} f_{\mu_L}\left(\frac{x}{z}, Q^2\right) - z f_{\nu_\mu}(x, Q^2) \right) + \dots, \end{aligned} \quad (3.6)$$

where the ellipses include other finite contributions to the integral, as well as other interactions. In the two parentheses, the first term is due to real emission of a W_T^\pm boson, while the second is the corresponding virtual correction. The fact that the muon and neutrino PDFs are different is an explicit breaking of $SU(2)_L$ and implies a non-cancellation of the pole for $z \rightarrow 1$ inside $P_{ff}^V(z)$, which in turn generates the double log. To see this explicitly, let us isolate on the right-hand side only the terms that are singular in $z \rightarrow 1$, fixing $z = 1$ everywhere else:

$$\begin{aligned} \frac{df_{\mu_L}}{d \log Q^2} &\approx -\frac{\alpha_2}{4\pi} \Delta f_{L_2}(x) \int_0^{z_{\max}(Q)} dz \frac{2}{1-z} + \dots \approx -\frac{\alpha_2}{4\pi} \log \frac{Q^2}{Q_{\text{EW}}^2} \Delta f_{L_2}(x) + \dots, \\ \frac{df_{\nu_\mu}}{d \log Q^2} &\approx \frac{\alpha_2}{4\pi} \Delta f_{L_2}(x) \int_0^{z_{\max}(Q)} dz \frac{2}{1-z} + \dots \approx \frac{\alpha_2}{4\pi} \log \frac{Q^2}{Q_{\text{EW}}^2} \Delta f_{L_2}(x) + \dots, \end{aligned} \quad (3.7)$$

where $\Delta f_{L_2} \equiv f_{\mu_L} - f_{\nu_\mu}$. Upon integration in Q^2 , a $\log^2 Q^2/Q_{\text{EW}}^2$ contribution is generated, that tends to deplete the muon PDF and enhance the neutrino one. This example also clearly shows how no such double log is generated for photon or Z_T emission from a fermion or W , since the real and virtual contribution would be proportional to the PDF of the

same parton. A Sudakov double log is instead expected for splittings such that the splitting function is divergent in the soft limit, $z \rightarrow 1$, and the A and B partons are different:

$$z_{\max}^{ABC}(Q) = 1 - \frac{Q_{\text{EW}}}{Q} \quad \text{if } P_{BA}^C, U_{BA}^C \propto \frac{1}{1-z} \text{ and } A \neq B, \quad (3.8)$$

otherwise we put $z_{\max} = 1$ and employ the standard +-distribution (see Eq. (B.1)) to regulate the $z \rightarrow 1$ divergence, for a more stable numerical evaluation of the DGLAP equations.

In practice, this happens for W_T^\pm emission off any parton (in correspondence to the poles in the P_{ff}^V , P_{VV}^V , and P_{hh}^V splittings) and for Z_T boson emission from an initial longitudinal Z_L or Higgs (due to the P_{hh}^V splitting), since Z emission changes $Z_L \longleftrightarrow h$. Analogously, for ultra-collinear splittings this takes place for any W_L emission and for Z_L emission off and initial Higgs or Z_L .

This procedure amounts to a double-logarithmic (DL) approximation to the Sudakov factor for initial-state radiation. This could be further improved to LL or NLL resummation by suitably modifying the scale at which the coupling constant $\alpha_2(Q)$ is evaluated, as discussed in Refs. [31, 60]. Since we are interested in energies where $\alpha_2 \log^2 Q^2/Q_{\text{EW}}^2 \sim \mathcal{O}(1)$ but $\alpha_2 \log Q^2/Q_{\text{EW}}^2 \ll 1$, we limit ourselves to the DL approximation for electroweak corrections in the present work.

3.3 Top quark as parton

When the energy of the hard process Q is much larger than the top mass, processes with a collinearly emitted top quark can develop a logarithmic enhancement proportional to $\log Q^2/m_t^2$. It can therefore become useful to resum these logarithms by including the top quark among the other partons [61, 62]. The question of whether or not one should include it as a parton depends on the process considered and on the optimal way to rearrange the perturbative series [63, 64]. With this in mind, we provide two versions of our PDFs of leptons, one in the 5-flavour-scheme (5FS) and one in a 6FS, where the top quark is added in the DGLAP evolution for scales above m_t . While codes that include the top quark in proton PDFs assume it is massless, in our approach we keep a finite top mass in the same spirit in which we keep finite W and Z masses for the weak bosons PDFs. This is justified by the fact that in our case, contrary to proton PDFs, EW interactions and EW symmetry breaking effects are crucial, and the top mass is one of such effects. For a detailed discussion of different schemes for the top mass in the computation of hadron collider observables with a top quark PDF see [64].

The DGLAP equations for the $t_L, \bar{t}_L, t_R, \bar{t}_R$ are reported explicitly in Eqs. (D.11, D.12, D.19, D.20). We checked numerically that the dominant contributions are those from initial transverse gauge bosons, with electroweak bosons, photon and gluon terms being approximately of similar size. Instead, ultra-collinear contributions are practically negligible. Nevertheless, in our numerical evaluation we keep all terms.

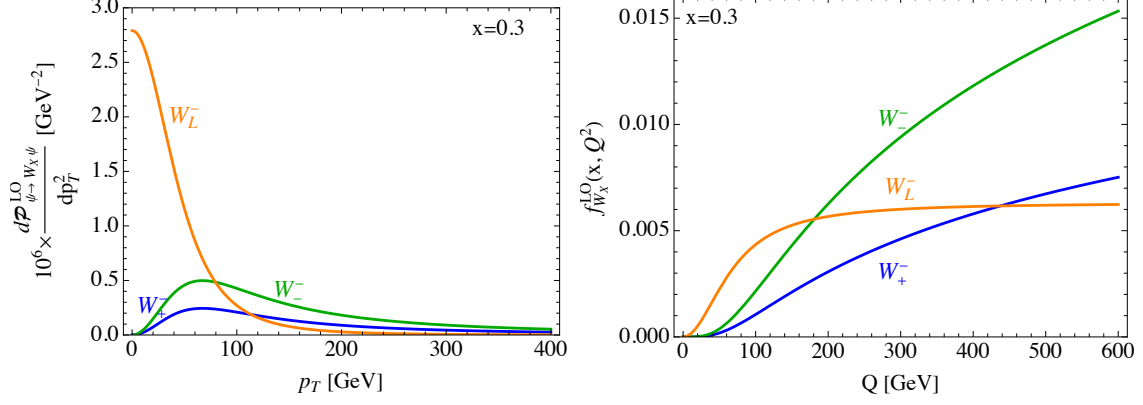


Figure 3. Integrand functions (left) and resulting PDFs (right) for the computation of the EW PDFs for transverse and longitudinal W boson of Eqs. (3.9,3.10).

3.4 Effective Vector Boson Approximation

The EPA has been generalized to describe EW gauge bosons in high-energy collisions since the '80s [65–68], in what is now known as the Effective Vector Boson Approximation (EVA) [36, 37]. When the hard scattering energy is much larger than the EW gauge boson mass and the p_T of the collinearly emitted gauge boson, then the cross section of the process can be factorized into an almost on-shell collinear emission and the subsequent hard scattering [35, 69–71].

One can compute the EW gauge bosons PDFs by evaluating the DGLAP equations at fixed order, similarly to what we did in Section 2 for QED, using $f_{\mu_L}^{(0)}(x) = f_{\mu_R}^{(0)}(x) = \frac{1}{2}\delta(1-x)$ for the muon PDF. Taking the DGLAP equations for the transverse and longitudinal W^- boson, Eqs. (D.33,D.34,D.38) one gets the leading order results

$$\begin{aligned}
 f_{W_{\pm}}^{(\alpha)}(x, Q^2) &= \int_{m_{\mu}^2}^{Q^2} dp_T^2 \frac{1}{2} \frac{d\mathcal{P}_{\psi \rightarrow W_T \psi}}{dp_T^2}(x, p_T^2) = \int_{m_{\mu}^2}^{Q^2} dp_T^2 \frac{\alpha_2}{8\pi} \frac{p_T^2}{(p_T^2 + (1-x)m_W^2)^2} P_{V_{\pm}f_L}^f(x) = \\
 &= \frac{\alpha_2}{8\pi} P_{V_{\pm}f_L}^f(x) \left(\log \frac{Q^2 + (1-x)m_W^2}{m_{\mu}^2 + (1-x)m_W^2} - \frac{Q^2}{Q^2 + (1-x)m_W^2} \right) = \\
 &\approx \frac{\alpha_2}{8\pi} P_{V_{\pm}f_L}^f(x) \left(\log \frac{Q^2}{m_W^2} - \log(1-x) - 1 \right) + \mathcal{O}\left(\frac{m_W^2}{Q^2}\right), \quad (3.9)
 \end{aligned}$$

$$\begin{aligned}
 f_{W_L}^{(\alpha)}(x, Q^2) &= \int_0^{Q^2} dp_T^2 \frac{1}{2} \frac{d\mathcal{P}_{\psi \rightarrow W_L \psi}}{dp_T^2}(x, p_T^2) = \int_0^{Q^2} dp_T^2 \frac{\alpha_2}{4\pi} \frac{m_W^2}{(p_T^2 + (1-x)m_W^2)^2} \frac{(1-x)^2}{x} = \\
 &= \frac{\alpha_2}{4\pi} \frac{1-x}{x} \frac{Q^2}{Q^2 + (1-x)m_W^2} \approx \frac{\alpha_2}{4\pi} \frac{1-x}{x} + \mathcal{O}\left(\frac{m_W^2}{Q^2}\right), \quad (3.10)
 \end{aligned}$$

and analogously for the Z and Z/γ PDFs

$$\begin{aligned}
 f_{Z_{\pm}}^{(\alpha)}(x, Q^2) &= \frac{\alpha_2}{4\pi c_W^2} \left(P_{V_{\pm}f_L}^f(x)(Q_{\mu_L}^Z)^2 + P_{V_{\pm}f_R}^f(x)(Q_{\mu_R}^Z)^2 \right) \\
 &\quad \left(\log \frac{Q^2 + (1-x)m_Z^2}{m_{\mu}^2 + (1-x)m_Z^2} - \frac{Q^2}{Q^2 + (1-x)m_Z^2} \right), \quad (3.11)
 \end{aligned}$$

$$f_{Z/\gamma\pm}^{(\alpha)}(x, Q^2) = -\frac{\sqrt{\alpha_\gamma\alpha_2}}{2\pi c_W} \left(P_{V_\pm f_L}^f(x) Q_{\mu_L}^Z + P_{V_\pm f_R}^f(x) Q_{\mu_R}^Z \right) \log \frac{Q^2 + (1-x)m_Z^2}{m_\mu^2 + (1-x)m_Z^2}, \quad (3.12)$$

$$f_{Z_L}^{(\alpha)}(x, Q^2) = \frac{\alpha_2}{2\pi c_W^2} \frac{1-x}{x} \left((Q_{\mu_L}^Z)^2 + (Q_{\mu_R}^Z)^2 \right) \frac{Q^2}{Q^2 + (1-x)m_Z^2}, \quad (3.13)$$

where $P_{V_+ f_L}^f(x) = P_{V_- f_R}^f(x) = (1-x)^2/x$ and $P_{V_- f_L}^f(x) = P_{V_+ f_R}^f(x) = 1/x$. The muon mass here serves as an IR cutoff for the logarithm in the transverse case to cure the $x \rightarrow 1$ limit, while we neglect it in the other terms. Notably, the W^+ has no contribution at this order.

In Fig. 3 we show the dependence in $\sqrt{p_T^2}$ of the integrands (left), and the resulting PDFs (right), fixing a value $x = 0.3$ and showing separately the two polarisation of the transverse W_\pm^- . One can see that the integrands are peaked before the EW scale and, while in the case of W_T it decreases as $\sim 1/p_T^2$ inducing the logarithmic grow of the PDF, for the longitudinal W polarisation the contribution to the integral is localised in p_T^2 before the EW scale and the PDF tends to a constant at large scales.

In our numerical integration of DGLAP equations, the effects due to EW interactions are introduced only above the Q_{EW} matching scale. Since we employ p_T as factorization scale, this effectively corresponds to performing the integration in Eqs. (3.9,3.10) only for $p_T^2 > Q_{EW}^2$, missing the region $0 < p_T^2 < Q_{EW}^2$. To address this issue we match the gauge bosons PDFs at Q_{EW} to the analytically computed one for the same scale and use it as boundary conditions,

$$f_A(x, Q_{EW}^2) \equiv f_A^{(\alpha)}(x, Q_{EW}^2) \quad \text{for } A = W_{L,\pm}^-, Z_{L,\pm}, Z/\gamma_\pm, \quad (3.14)$$

and then continue the integration numerically to higher scales. The boundary conditions for the PDFs of other heavy states (h , h/Z_L , top quark) are instead set to zero at the corresponding mass scales.

4 Results

Here we discuss several aspects of our LePDFs. The details of our numerical implementation of the DGLAP equations are collected in App. E.

Fig. 4 (top panel) collects, as an example, a set of PDFs evaluated at the scale $Q = 3$ TeV. One first thing to notice is that, as expected, for $x \gtrsim 0.5$ the muon PDF dominates, while for smaller x the largest PDF is the photon one. However, the transverse negative W_T^- PDF is only a factor ~ 2 smaller and the transverse Z_T boson is another factor of 2 smaller than that: they both receive contributions from the emission off an initial muon. Analogously, the muon neutrino ν_μ has a large PDF at large x values due to the emission off a μ_L^- , which has also a Sudakov double-log enhancement. The positive transverse W_T^+ PDF is instead more suppressed because its leading contribution arises from the emission off the muon neutrino and off another gauge boson. The importance of EW gauge bosons PDFs reflects the common lore that *a high-energy lepton collider is also a weak boson collider*.

In the bottom panel of Fig. 4 we show the PDFs for the longitudinal polarisations of EW gauge bosons and the Higgs, evaluated at scales of 3 TeV (solid lines) and 30 TeV (dashed lines). The PDFs for W_L^- and Z_L are mostly scale independent, since they receive

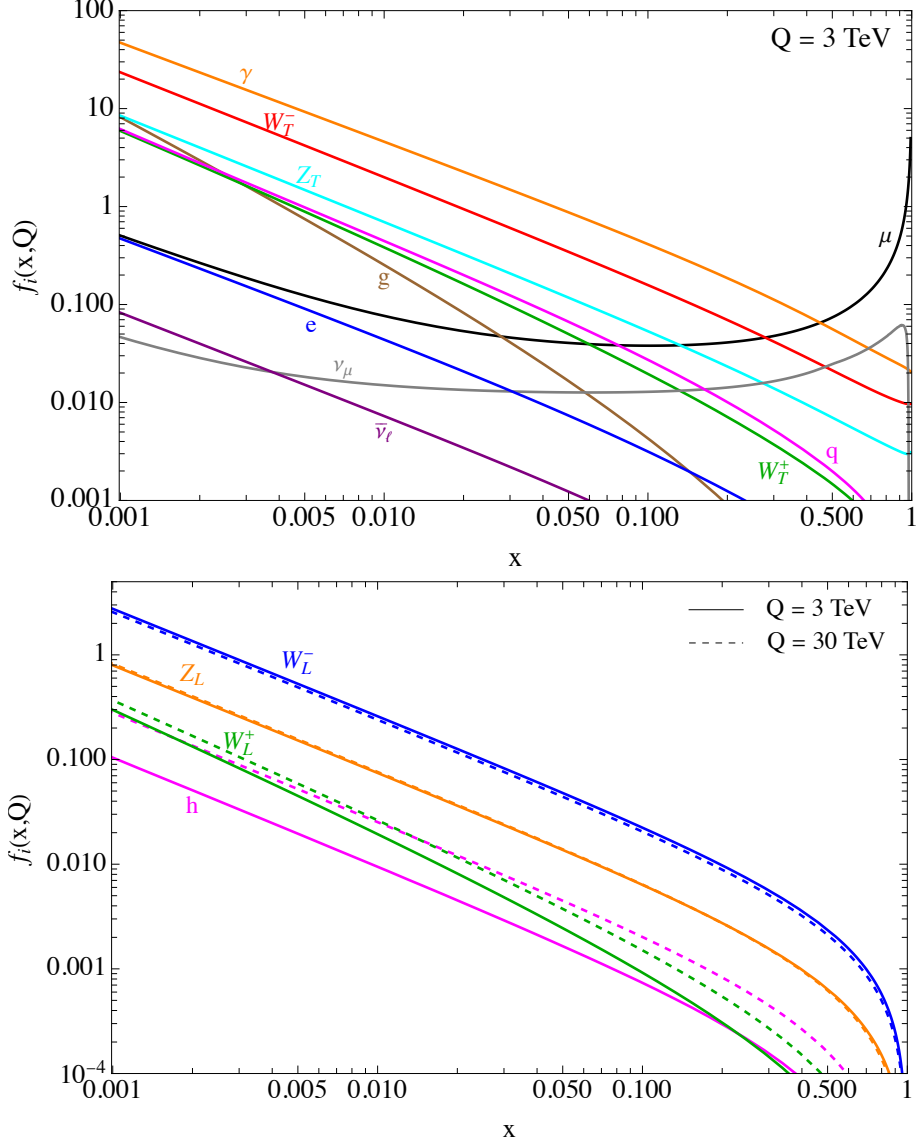


Figure 4. (Top panel): Sample of PDFs evaluated at a scale $Q = 3$ TeV for a muon. For this plot we sum over polarisations and q represents the sum of all quark PDFs except for the top. (Bottom panel): PDFs for the scalar degrees of freedom in the SM. Solid (dashed) lines are evaluated at a scale of $Q = 3$ (30) TeV.

the dominant contribution from the ultra-collinear splitting off a muon. On the other hand, the ultra-collinear contribution to the W_L^+ PDF comes mostly from the muon neutrino, which has a PDF suppressed with respect to the muon one. Therefore, other contributions from standard splitting functions (e.g. from P_{hV}^h and P_{hh}^V) are sizeable and induce a scale dependence. In case of the Higgs boson there is no ultra-collinear contribution from massless fermions, so one does not expect ultra-collinear terms to dominate and indeed its PDF shows a large scale dependence.

The fraction of the momentum carried by each of the partonic components is given by

field	$Q = 3$ TeV	$Q = 10$ TeV	$Q = 30$ TeV
μ_L	49.48%	48.72%	47.76%
μ_R	46.98%	44.12%	41.12%
ν_μ	1.28%	2.83%	4.85%
ν_ℓ	0.0004%	0.0009%	0.001%
ℓ	0.005%	0.007%	0.01%
q	0.038%	0.05%	0.07%
γ	1.3%	1.4%	1.46%
W_T^-	0.52%	0.64%	0.74%
W_T^+	0.03%	0.06%	0.11%
Z_T	0.17%	0.22%	0.28%
g	0.001%	0.002%	0.003%

Table 2. Fraction of the momentum carried by each parton at $Q = 3, 10, 30$ TeV.

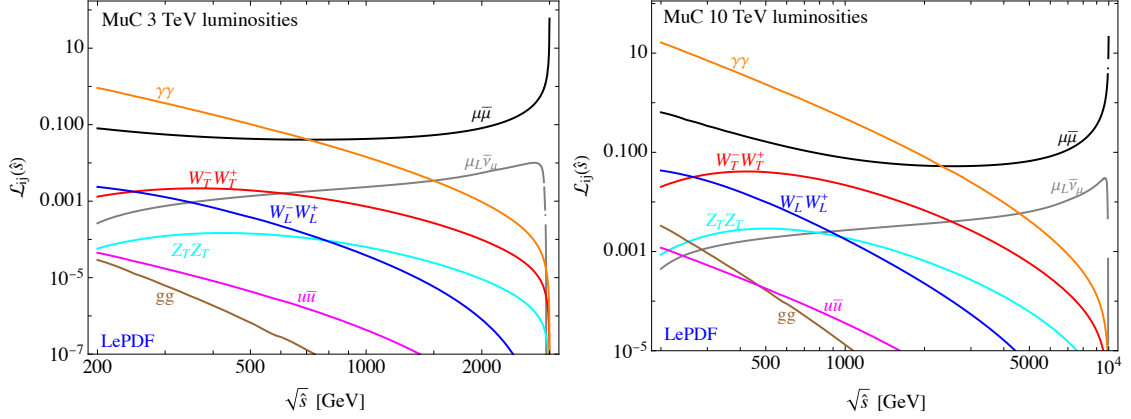


Figure 5. Examples of parton luminosities at a 3 TeV (left) and 10 TeV (right) MuC. Unless specified, for this plot we sum over polarizations.

the $n = 2$ Mellin transform of the PDF (see App. C for more details) and it can be used to evaluate the relevant role of the various individual components at different scales. To this end, in Table 2 we give three examples for the set of PDFs shown in Fig. 4 at scales 3 TeV, 10 TeV, and 30 TeV. We observe that as the energy of the hard process is increased the percentages of both the left- and right-handed muon components are decreased and those of all other partons increased, which illustrates the importance of electroweak interactions at higher energies.

In Fig. 5 we show some examples of parton luminosities for a 3 and 10 TeV muon colliders where, unless specified, we sum over polarizations. Parton luminosities can be useful for computing cross sections integrated over angular variables. In case of a muon collider they are defined from the convolution of the PDFs of parton i from the muon and parton j from the anti-muon, as follows:

$$\mathcal{L}_{ij}(\hat{s}) \equiv \int_{\hat{s}/s_0}^1 \frac{dx}{x} f_i^{(\mu)} \left(x, \frac{\sqrt{\hat{s}}}{2} \right) f_j^{(\bar{\mu})} \left(\frac{\hat{s}}{xs_0}, \frac{\sqrt{\hat{s}}}{2} \right), \quad (4.1)$$

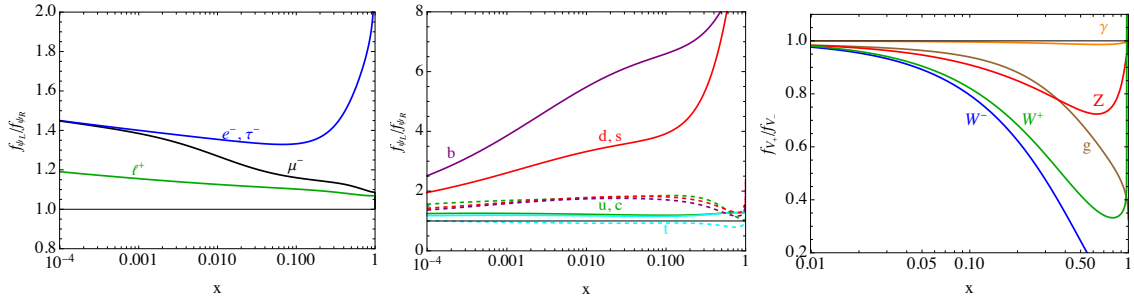


Figure 6. Polarisation ratios for the PDFs of leptons (left), quarks (center), and gauge bosons (right) at a scale $Q = 3$ TeV. Dashed lines in the central panel are for the corresponding anti-quarks.

where $\sqrt{s_0}$ is the collider center of mass energy and $\sqrt{\hat{s}}$ is the invariant mass of the two-parton system. From Fig. 5 we can notice that, even at small invariant masses, the $\mu\bar{\mu}$ luminosity is much larger than the W^+W^- luminosity (also the charged-current $\mu_L\bar{\nu}_\mu$ luminosity is sizeable). The impact of this channel in VBF studies at muon colliders should therefore be studied in more details. It is also interesting to point out that the QCD-related luminosities (gluons and quarks) are very small, which is going to strongly suppress QCD-induced backgrounds in electroweak processes.

4.1 Polarisation

The chiral structure of SM interactions above the EW scale induces polarisation effects for the PDFs [31]. In Fig. 6 we show polarisation ratios for several PDFs at a scale $Q = 3$ TeV. The observed behavior can be easily understood as follows. The W_T^-, W_T^+ , and Z_T PDFs receive the dominant contribution from the emission off an initial $\mu_{L,R}^-$ or ν_μ . Since the $P_{V_+ f_L}^f$ splitting function goes to zero for $z \rightarrow 1$, while $P_{V_- f_L}^f$ tends to a constant, the positive helicity of the EW gauge bosons will be suppressed for $x \rightarrow 1$. In case of the photon, the leading contribution comes from the muon splitting and it is vector-like at leading order, so the polarisation effect will be suppressed.

In case of fermions, left-handed chiralities (and their conjugate) receive contributions from W bosons splitting to $\psi_L\bar{\psi}'_L$, therefore their PDF is expected to be larger than the right-handed counterparts. The tendency increases with x in the case of the leptons (except for the muon) and down-type quarks as opposed to antileptons and up-type quarks, since the left-handed parts of the former receive contributions from W_T^- , while the latter from W_T^+ , and the W_T^+ PDF falls faster than the W_T^- PDF at high x (see Fig. 4) This effect can be of $\mathcal{O}(1)$, since the W^- PDF is comparable in size to the photon one. The b_L PDF is further enhanced compared to b_R due to the $W_L^- \rightarrow b_L\bar{t}_R$ splitting proportional to y_t .

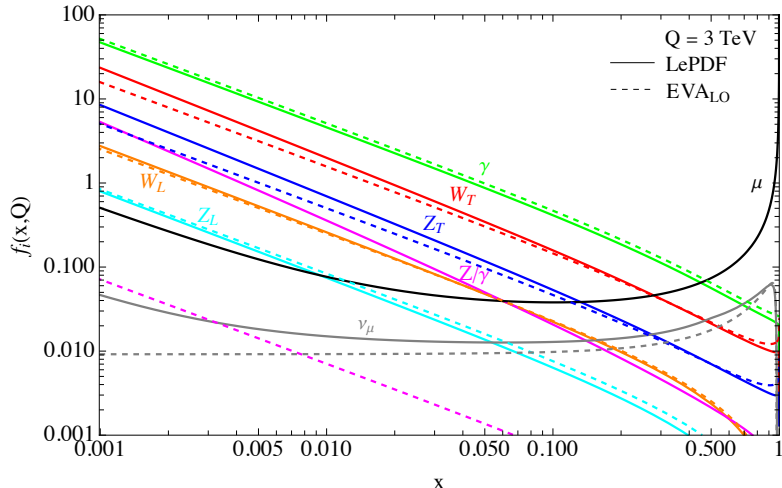


Figure 7. PDFs for EW gauge bosons (plus muon and muon neutrino) at a scale $Q = 3$ TeV. Solid lines are from the numerical solution of DGLAP equations while dashed ones are from the LO EVA expressions in Eqs. (3.9)-(3.13).

4.2 Comparison with the Effective Vector Boson Approximation

In Fig. 7 we show our results for EW gauge bosons PDFs, compared with the LO EVA result discussed in Section 3.4 (to reduce the number of lines plotted we show the sum of transverse polarisations). Several things can be noticed.

For Z/γ , the EVA result is two orders of magnitude smaller than what we find with the numerical evolution. This is due to the fact that $Q_{\mu_L}^Z + Q_{\mu_R}^Z = -\frac{1}{2} + 2s_W^2 \ll 1$ is accidentally suppressed (indeed, it becomes zero when evolving the Weinberg angle at a scale of about 3.6 TeV). This cancellation takes place because in EVA it is assumed that the initial-state muon is not polarised. However, in the evolution from the EW scale upward, electroweak interactions induce a polarisation of the muon PDF, which becomes up to $\sim 40\%$ at a scale of 3 TeV, as can be seen in Fig. 6 (left panel). Therefore, in the full numerical evolution there is no such tuned cancellation in the Z/γ PDF. This clearly shows that the EVA result is not reliable for this PDF.

For the longitudinal polarisations, the EVA provides a good description of the PDFs, to within $\sim 10\%$ accuracy. In case of the transverse W and Z polarisations, instead, there is a noticeable discrepancy which grows even up to $\mathcal{O}(50\%)$ at multi-TeV scales for small x values. This is dominantly due to the missing contributions from $V \rightarrow VV$ splittings, that start at NLO. Such contributions become important due to two effects: the PDF of the initial-state gauge boson at small x is much larger than the muon PDF and they include IR Sudakov corrections that induce a parametric dependence as $\alpha^2 \log^3(Q^2/m_W^2)$. We perform two checks to verify this. First, we do a run of our numerical code setting to zero the P_{VV} splitting functions (both in real emission and radiative corrections): the resulting EW gauge bosons PDFs agree well with LO EVA. Second, focussing only on the W_+^- PDF for simplicity, we compute iteratively the $\mathcal{O}(\alpha^2)$ contributions to the weak bosons PDFs, adding the real emissions from P_{VV}^V and P_{Vf}^f splittings, and the corresponding virtual

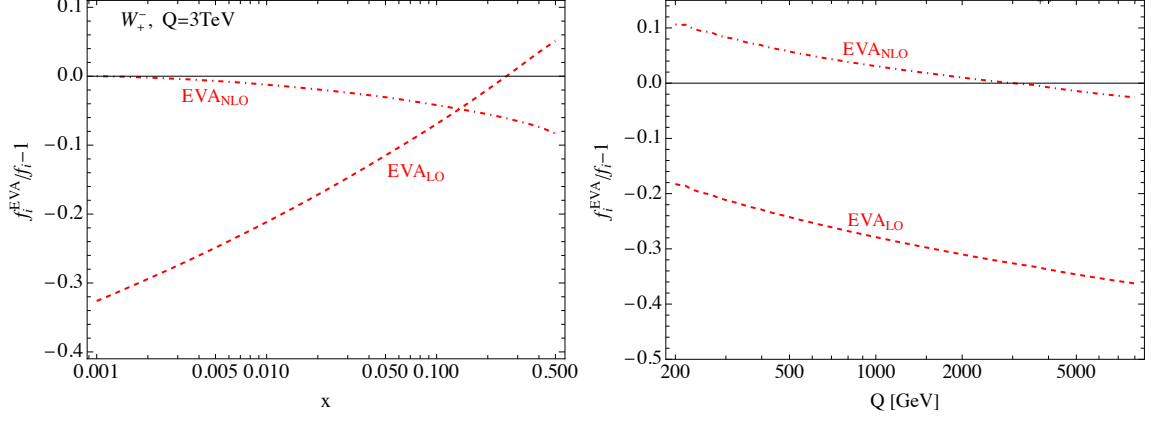


Figure 8. Relative difference between the numerical result for the W_+ PDF and the LO (dashed) or NLO (dot-dashed) EVA expression for a fixed scale $Q = 3$ TeV (left) and for fixed $x = 0.001$ (right).

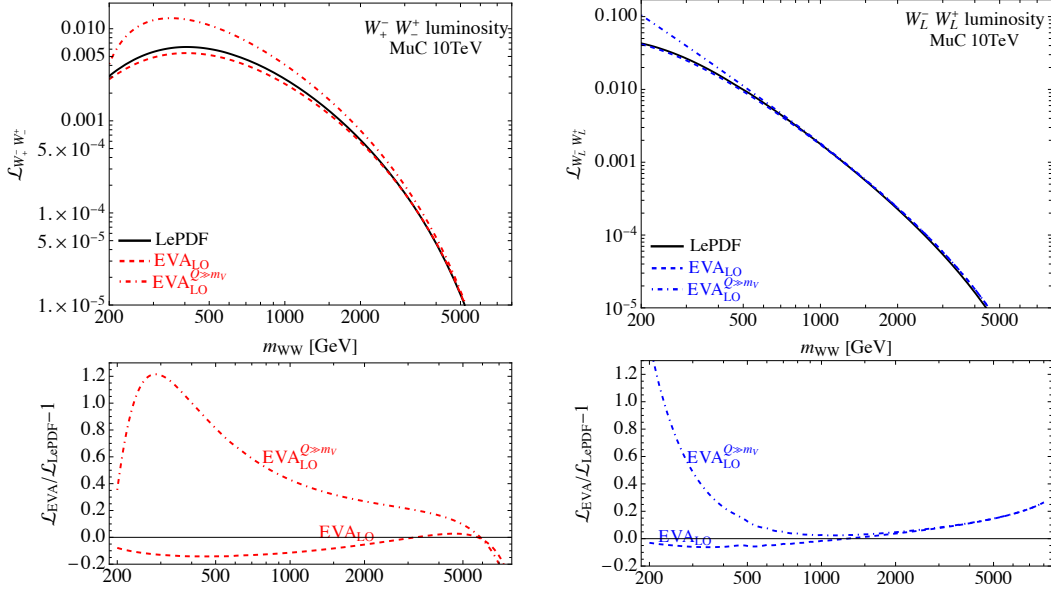


Figure 9. Parton luminosities for $W_+ W_-$ (left) and $W_L W_L^+$ (right) at a 10 TeV muon collider. We show a comparison with luminosities obtained with the LO EVA result in Eq. (3.9) (dashed) and with the $Q \gg m_W$ approximation, implemented in [37] (dot-dashed).

corrections. In practice, we take the DGLAP equations for transverse EW gauge bosons in Section D.3 and use the $\mathcal{O}(\alpha)$ results for the gauge bosons PDFs (i.e. the LO EVA of Eqs. (3.9-3.13)) and the muon. For simplicity, at this step we use approximate expressions for the LO EVA by keeping only the $\log \frac{Q^2}{m_{W,Z}^2}$ term, which makes our NLO EVA result reliable only for $Q \gg m_W$ and $x \ll 1$. We also neglect contributions from longitudinal modes and ultra-collinear ones. We then perform analytically the convolution with the

splitting functions and finally the integral from m_W up to the factorization scale Q :

$$\begin{aligned}
f_{\mu_L}^{(\alpha)}(x, t) &\simeq \int_{t_{m_W}}^t dt' \left(\frac{1}{2} P_{\mu_L}^v(t') \delta(1-x) + \frac{\alpha_\gamma}{4\pi} P_{ff}^V(x) + \frac{\alpha_2}{4\pi c_W^2} (Q_{\mu_L}^Z)^2 P_{ff}^V(x) \right), \\
f_{W_+}^{(\alpha^2)}(x, t) &\simeq \int_{t_{m_W}}^t dt' \left(P_{W_+}^v f_{W_+}^{(\alpha)} + \frac{\alpha_2}{4\pi} P_{V_+ f_L}^f \otimes f_{\mu_L}^{(\alpha)} + \frac{\alpha_2}{2\pi} c_W^2 P_{V_+ V_s} \otimes (f_{W_s^-}^{(\alpha)} + f_{Z_s}^{(\alpha)}) + \right. \\
&\quad \left. + \frac{\alpha_\gamma}{2\pi} P_{V_+ V_s} \otimes (f_{W_s^-}^{(\alpha)} + f_{\gamma_s}^{(\alpha)}) + \frac{\sqrt{\alpha_\gamma \alpha_2}}{2\pi} c_W P_{V_+ V_s} \otimes f_{Z/\gamma_s}^{(\alpha)} \right).
\end{aligned} \tag{4.2}$$

It can be noted that Sudakov double logs appear here in the virtual contributions to $f_{\mu_L}^{(\alpha)}$ and to $f_{W_+}^{(\alpha^2)}$, as well as in the $P_{V_+ V_s}$ terms from the neutral gauge bosons.

In Fig. 8 we show the relative deviation of the LO (dashed) and NLO (dot-dashed) EVA results from the complete numerical PDF as function of x (left panel) and as function of the scale (right panel). We observe that the NLO EVA result improves substantially the agreement with the full numerical result, while the LO EVA has large deviations at small x . The missing terms in the LO EVA become more and more important with larger scales, confirming the argument made above.

In Fig. 9, instead, we plot the $W_+^- W_-^+$ (left panel) and $W_L^- W_L^+$ (right panel) parton luminosities for a 10 TeV MuC. We show a comparison between the LePDF result (solid lines) and the LO EVA expression in the $Q \gg m_W$ approximation (dot-dashed), that is the one implemented in Ref. [37], or with the complete W mass dependence as in Eq. (3.9) (dashed). We see that, at the level of luminosity, the LO EVA with the complete mass dependence provides a good approximation of the resummed LePDF result up to $\sim 15\%$ deviations for the transverse modes. This means that the much larger deviations we observe at the PDF level for small x are diluted when the luminosities are calculated. On the other hand, the massless approximation deviates up to $\mathcal{O}(1)$ even at the luminosity level and in particular at partonic center of mass energies of few hundreds of GeV, where the weak-boson fusion process cross sections are the largest.

4.3 Muon neutrino PDF

The leading contribution to the muon neutrino PDF arises already at $\mathcal{O}(\alpha_2)$ from the $\mu_L \rightarrow W^- \nu_\mu$ splitting, which presents an IR soft divergence that is cutoff by the W mass. As already discussed in Sec. 3.2, the missing counterpart of this divergence in the virtual correction is at the origin of the Sudakov double log. In the same spirit as done for the EVA, we can compute the neutrino PDF by iteratively solving the DGLAP equations up to $\mathcal{O}(\alpha)$, using the zeroth-order expression for the μ_L PDF:

$$\begin{aligned}
\frac{df_{\nu_\mu}}{d \log Q^2} &= \frac{\alpha_2}{4\pi} \int_x^{1-m_W/Q} \frac{dz}{z} \frac{Q^4}{(Q^2 + z m_W^2)^2} P_{ff}^V(z) \frac{1}{2} \delta\left(1 - \frac{x}{z}\right) + \mathcal{O}(\alpha^2) = \\
&= \frac{\alpha_2}{8\pi} \frac{Q^4}{(Q^2 + x m_W^2)^2} P_{ff}^V(x) \theta\left(1 - \frac{m_W}{Q} - x\right) + \mathcal{O}(\alpha^2).
\end{aligned} \tag{4.3}$$

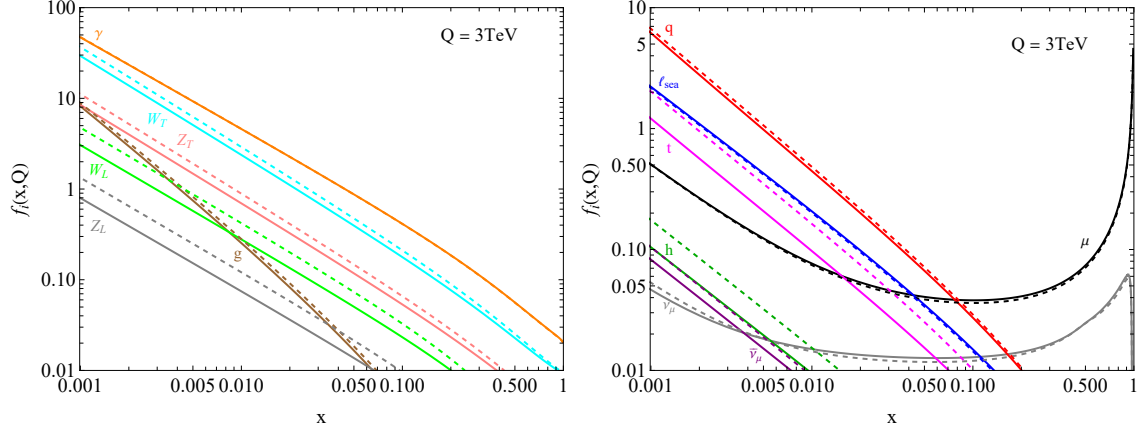


Figure 10. PDFs for gauge bosons (left), fermions and Higgs (right) at a scale $Q = 3$ TeV. Solid lines are the full result while dashed ones are obtained neglecting the masses in the propagators. For simplicity in this plot we sum over polarisations.

The Heaviside theta is the result of the IR cutoff $z_{\max} = 1 - \frac{m_W}{Q}$ in the integral. Integrating this differential equation from m_W^2 up to Q^2 we get:

$$f_{\nu_\mu}^{(\alpha)}(x, Q^2) = \frac{\alpha_2}{8\pi} \theta\left(Q^2 - \frac{m_W^2}{(1-x)^2}\right) P_{ff}^V(x) \left(\log \frac{Q^2 + xm_W^2}{m_W^2} + \log \frac{(1-x)^2}{1+x(1-x)^2} + \frac{xm_W^2}{Q^2 + xm_W^2} + \frac{1}{1+x(1-x)^2} - 1 \right). \quad (4.4)$$

We observe here the single logarithm due to the standard collinear divergence, while the Sudakov log is absent because the initial muon PDF at zeroth order is just a delta function. It will appear, however, in the computation of an inclusive cross section upon integration of the PDF, due to the $x \rightarrow 1$ divergence inside $P_{ff}^V(x)$, that is not cancelled by a virtual correction at the same order but is instead cut off at the W mass by the theta function.

In Fig. 7 we show a comparison between this $\mathcal{O}(\alpha)$ approximation of the muon neutrino PDF (dashed gray line) with the one from LePDF (solid gray), at a scale $Q = 3$ TeV. We observe a very good agreement at large x values, i.e. where the $\mu_L \rightarrow W^- \nu_\mu$ splitting dominates. At smaller x values the $\mathcal{O}(\alpha^2)$ contribution from $Z \rightarrow \nu_\mu \bar{\nu}_\mu$ will instead dominate. Comparing to the results of Refs. [33, 34], we observe a different behavior of the ν_μ PDF for $x \rightarrow 1$: while both our analytic result described above and LePDF show a cutoff (due to the IR m_W cutoff) at $x \lesssim 1$, in their result the ν_μ PDF increases similarly to the muon PDF up to $x = 1$.

4.4 Mass effects

We showed in Section 3.1 that massive particles modify the virtuality of the particle B as in Eq. (3.2). As already discussed in [30, 36], the impact of the latter effect is important since, due to the presence of the masses in the denominators of the DGLAP equations, the PDFs are lowered or enhanced when $m_{B,C} \neq 0$ and $m_A \neq 0$ respectively. In Fig. 10 we show the

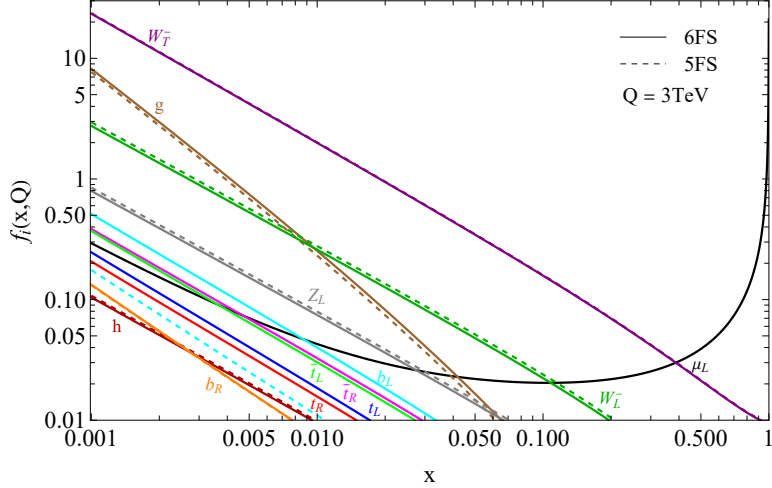


Figure 11. Comparison between 5-flavour-scheme (dashed) and 6-flavour-schemes (solid) at a scale $Q = 3$ TeV.

PDFs computed keeping and neglecting the masses in \tilde{p}_T , still starting the evolution of a given massive parton at the scale corresponding to its mass.

For instance, in case of EW gauge bosons (both transverse and longitudinal) one can expect that mass effects lower their PDFs, with the biggest effects at small x due to the $(1-x)$ factor appearing in front of the mass corrections. This can also be verified from the LO EVA in Eqs. (3.9-3.13). In case of the Higgs, its interactions have the form $A \rightarrow h + A$, with $A = W, Z, t$, which implies $\delta_{p_T}^2 = x^2 m_A^2 + (1-x)m_h^2 > 0$, which explains why the Higgs PDF is bigger when masses are neglected.

4.5 Top quark PDF

In Fig. 11 we compare the results between the 5FS and the 6FS showing the top PDFs together with the PDFs mostly affected by the inclusion of the top. As already mentioned in Section 3.3 the top PDFs are mainly driven by the collinear emission off the transverse gauge bosons and the differences are more noticeable in high energies (we use the benchmark $Q = 3$ TeV). Since the PDFs of W_T^- and W_L^- are large compared to the Z and W_T^+ , we expect a larger PDF for \bar{t}_L and \bar{t}_R than t_L or t_R . Also, the same splittings $W_T^- \rightarrow b_L \bar{t}_L$ and $W_L^- \rightarrow b_L \bar{t}_R$ will induce a large enhancement of the b_L PDF compared to b_R in the 6FS.

Additionally, we observe that the PDFs of the EW transverse gauge bosons themselves are almost unaffected, since they are dominated by splitting off a muon. The gluon PDF, instead, receives a noticeable further contribution. Shifts of comparable size are also induced in the PDFs of the longitudinal gauge bosons (and even smaller for the Higgs), but in this case the PDFs are decreased due to a mass effect similar to the ones discussed in the previous Section 4.4.

4.6 Uncertainties

Here we discuss several sources of uncertainties in our computation. Some are physical, such as the choice of Q_{QCD} or missing higher orders, while others are intrinsic in the numerical

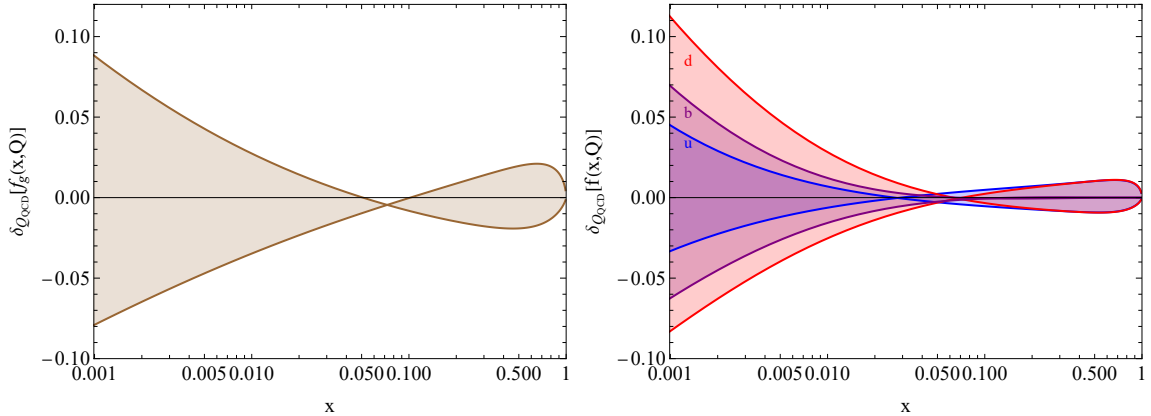


Figure 12. Effects of the choice of Q_{QCD} on the PDFs of gluon (left) and quarks (right) at the EW scale $Q = m_W$.

implementation of the DGLAP equations and can be improved simply by dedicating more computational time to the task.

QCD matching scale

As already discussed in Section 2 the QCD scale Q_{QCD} is not clearly determined and different choices of this parameter can have a non negligible impact on the PDF, in particular for the colored particles. To study the dependence of our results on Q_{QCD} we repeat the evolution for $Q_{\text{QCD}} = 0.52$ GeV and $Q_{\text{QCD}} = 1$ GeV and we compute the relative differences with respect to the chosen value of 0.7 GeV

$$\delta_{Q_{\text{QCD}}}[f_A(x, Q)] = \frac{f_A(x, Q)|_{Q_{\text{QCD}}} - f_A(x, Q)|_{0.7 \text{ GeV}}}{f_A(x, Q)|_{0.7 \text{ GeV}}}, \quad Q_{\text{QCD}} = \{0.52 \text{ GeV}, 1 \text{ GeV}\}. \quad (4.5)$$

In Fig. 12 we show the results for the colored particles, which are the most affected by the choice of the QCD scale, while for the photon and the leptons the relative differences are smaller than 10^{-5} . We report the results at $Q = m_W$ after the QED+QCD evolution, since this is the phase in which these effects are stronger.

Discretization

The second source of uncertainty we take into account is the discretization, that is the number of grid points N_x . Again we focus for simplicity on the first phase of the evolution, since these effects do not change much with the energy scale⁶. As for Q_{QCD} we repeat the evolution for different values of N_x and compute the relative differences of the PDFs obtained. The results at the EW scale m_W , obtained varying N_x from 300 to 600 and then to 1000, are reported in Fig. 13: it is clear that as we increase N_x the relative differences are reduced, as expected since in this way we are approaching the continuum limit. Being

⁶We checked that this is actually the case computing the PDFs in the full SM both with $N_x = 600$ and $N_x = 1000$: for instance at a scale $Q = 3\text{TeV}$ the relative differences are smaller than 2%.

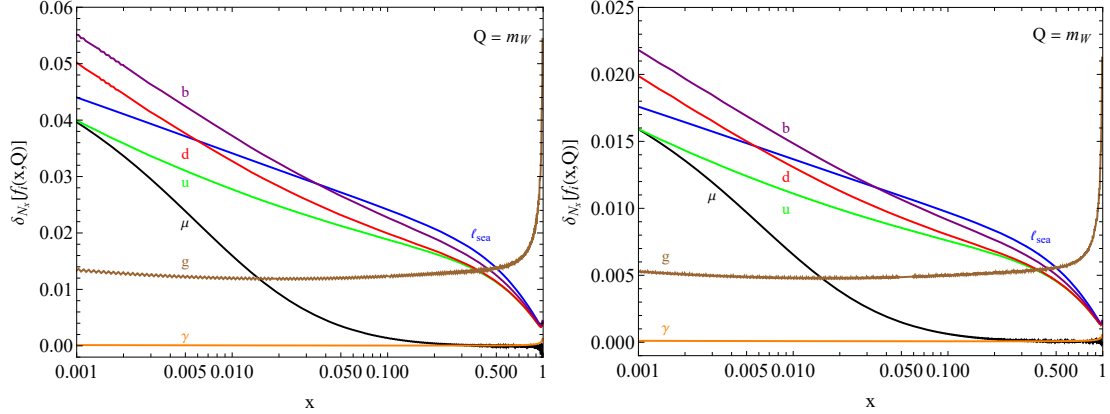


Figure 13. Effects of N_x on the PDFs at the EW scale $Q = m_W$. The relative differences correspond to $N_x = \{300; 600\}$ (left) and to $N_x = \{600; 1000\}$ (right).

the relative difference between $N_x = 600$ and $N_x = 1000$ already of $\mathcal{O}(10^{-2})$, we take the latter as reference value, since a further increase will introduce even smaller corrections.

Integration step

Numerical uncertainties also arise due to the discretization in t , depending on the choice of the integration step dt , as shown in Eq. (E.7). As for the previous cases, we compute the relative differences of the PDFs obtained for two different values of dt , in particular we choose $dt = t(m_W)/N_t$, with $N_t = \{100; 200\}$: this means that we consider N_t steps in the first phase of the evolution. We do not report any plot, since we checked that the relative differences are at most of $\mathcal{O}(10^{-3})$, both at $Q = m_W$ and at higher scales.

Higher orders

The largest theoretical uncertainties in our results originate from neglecting higher order corrections. In particular, in the DL approximation terms of $\mathcal{O}(\alpha_2 \log(Q/Q_{EW}))$ are not consistently resummed [60]. For example, at $Q = 3$ TeV, these terms already amount to 10%, while at $Q = 10$ TeV to 14%. We notice that promoting our approximation to the full LL result does not improve the situation [60], since single-log terms of the same size from the NLL expansion are still present. However, performing the NLO matching as prescribed in Refs. [48] can reduce the uncertainties to 4% for $Q = 3$ TeV. Extending our formalism to NLL order would eventually correspond to $< 3\%$ accuracy regardless of the energy scale.

4.7 PDFs for electron beams

Our numerical code, with obvious substitutions, can also be used to derive LePDFs for electron beams. While most future projects for e^+e^- colliders are focussed on EW-scale energies to perform high-precision studies of EW gauge bosons, the Higgs, and top quark, linear collider projects also envisage later stages with TeV-scale center of mass energies. In this case our SM PDFs can provide a useful tool. We therefore provide public PDFs for electron/positron beams alongside those for muons and anti-muons. In Fig. 14 we show

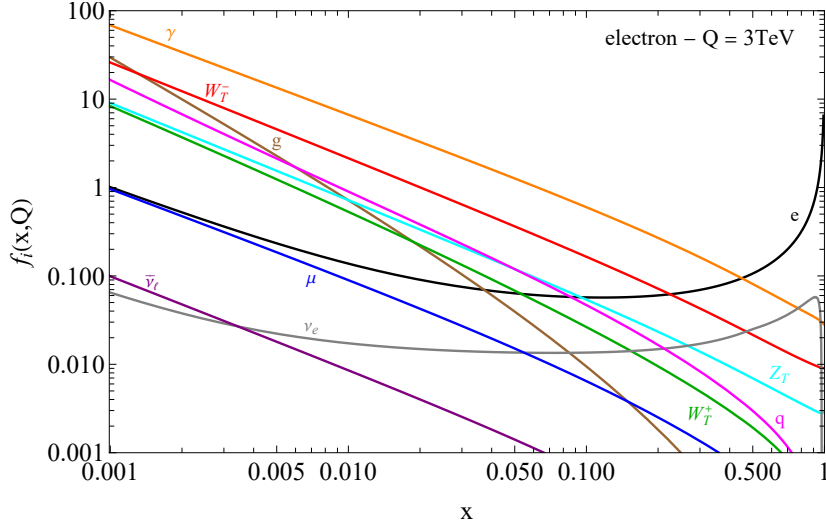


Figure 14. In this plot we show some PDFs evaluated at a scale $Q = 3$ TeV for an electron beam. For this plot we sum over polarisations and q represents the sum of all quark PDFs except for the top.

only an example plot for some PDFs of an electron. As for the muon case, in case of EW gauge bosons PDFs we did a comparison with the EVA approximation at LO and NLO, obtaining similar results as shown above for the muon. The main difference in the PDFs of an electron compared to those of a muon is that photon, charged leptons and quarks PDFs are larger. This is due to the longer QED evolution from m_e to m_μ . A consequence of larger quarks PDF is also a larger gluon one, even if $Q_{\text{QCD}} > m_\mu$. On the other hand, EW gauge boson PDFs are very similar since, at first order, their PDF is insensitive on physics at scales below the EW one.

5 Conclusions

Obtaining precise predictions for multi-TeV lepton colliders is a topic of active studies. In fact, while QCD radiation plays a minor role, in comparison to hadron colliders, electroweak corrections in this energy regime can become very large due to single and double logarithmic enhancements. Furthermore, the electroweak sector presents several features that are absent when dealing with QED or QCD radiation. Within this context, the resummation of a subset of large logarithms related to the factorisable emission of initial-state radiation can be viewed as an ingredient for a complete description of collider phenomenology at such machines.

In this paper we solved the set of DGLAP equations for an initial-state lepton, evolving the complete set of PDFs from the infrared up to multi-TeV scales. Our computation is performed with LO splitting functions, keeping into account all relevant mass thresholds, EW symmetry breaking terms, masses of all EW states, and resumming EW Sudakov logs at the double-logarithmic level. The residual uncertainty is dominated by the incomplete single-log EW resummation and can be estimated to be of $\mathcal{O}(10\%)$, while we show that

other systematic uncertainties are fully under control. Improving our results to include single-log resummation is left for future work.

Using this result we discuss several notable features of LePDFs. Polarisation effects, due to the chiral nature of SM interactions, are shown to be of $\mathcal{O}(1)$ in Fig. 6, or even larger than that in case of the b quark. This last effect is due to the interaction with the top quark via the large top Yukawa coupling, and becomes much smaller in the 5FS, where the top is not included in the evolution. As already observed in previous studies, we confirm that including EW states masses in the propagators gives sizeable correction to the PDFs, even for large factorisation scales.

Furthermore, we perform a detailed comparison of our results for the EW gauge bosons PDFs with the widely used Effective Vector Approximation. This comparison, presented in Fig. 7, illustrates how the EVA fails to describe correctly the transverse EW gauge bosons PDFs at small x values, with deviations reaching even $\mathcal{O}(50\%)$ for W_T^\pm and Z_T at large scales, or even missing the target by more than one order of magnitude in case of the off-diagonal Z/γ PDF. The cause of the latter large deviation is the well-known accidental cancellation in the vector-like coupling of a lepton to the Z boson, which does not take place in the full result since the muon gains a strong polarisation. The smaller, but still substantial deviations in the PDFs of transverse EW gauge bosons are due to the fact that the EVA, treated at LO, does not include contributions from gauge boson splitting off an initial gauge boson. Such terms, while being formally of higher order, become enhanced due to the large γ, W, Z PDFs and the fact that these splittings come with associated Sudakov double logs. In fact, by extending iteratively the EVA up to $\mathcal{O}(\alpha^2)$ we obtain a much better agreement with the complete numerical result, as shown in Fig. 8. In light of this, we recommend the use of LePDF to derive precision predictions for SM and BSM processes at high-energy electron or muon colliders (they could also be used for lepton-hadron collisions), when one is interested in being inclusive on radiation emitted at small p_T compared to the typical energy of the hard scattering, $E \gg p_T^{\text{coll.rad.}}$, and when $E \gg m_W$, which are the conditions for factorisation to be valid.

Our numerical results for the LePDFs are made public⁷ in the LHAPDF6 format (with some modifications due to the necessity of describing independently all helicity states). We provide results for initial-state muons, anti-muons, electrons, and positrons, all in both the 5 and 6 flavour schemes.

Acknowledgments

We would like to thank Thomas Gehrmann, Johannes Michel, Luca Vecchi, and Andrea Wulzer for fruitful discussions. DM acknowledges partial support by MIUR grant PRIN 2017L5W2PT and the European Research Council (ERC) under the European Union’s Horizon 2020 research and innovation programme, grant agreement 833280 (FLAY). ST is supported by the Swiss National Science Foundation - project n. P500PT_203156, and by the Center of Theoretical Physics at MIT.

⁷They are available from GitHub at <https://github.com/DavidMarzocca/LePDF>.

Parameter	α_3	α_2	α_1	α_{y_t}
Value	0.1057	0.03329	0.01025	0.0679

Table 3. Numerical inputs for the SM parameters at a scale $Q = 200$ GeV from [72].

A Inputs and Formalism

A.1 Standard Model inputs

In order to set our notation, we define the covariant derivatives as

$$D_\mu = \partial_\mu - ig_3 G_\mu^A t_A - ig_2 W_\mu^a T^a - ig_1 Y B_\mu, \quad (\text{A.1})$$

where t^A and T^a are $SU(3)$ and $SU(2)$ generators, respectively, while Y is the hypercharge. The electric charge is given by $Q = Y + T^3$. In our analysis we neglect the CKM matrix and work with diagonal Yukawas

$$\mathcal{L}_Y = -y_u^i \bar{Q}_L^i u_R^i H^c - y_d^i \bar{Q}_L^i d_R^i H - y_e^i \bar{L}_L^i e_R^i H + h.c., \quad (\text{A.2})$$

where $H^c = i\sigma_2 H^*$. In particular, in our implementation we keep only $y_u^3 \equiv y_t \neq 0$. Finally, we define the Higgs potential as

$$V(H) = \lambda_h \left(H^\dagger H - \frac{v^2}{2} \right)^2. \quad (\text{A.3})$$

To shorten the notation, we define the following quantities

$$\begin{aligned} c_W^2 &= \frac{g_2^2}{g_1^2 + g_2^2}, \quad e = g_1 c_W, \quad \alpha_{g_x} \equiv \frac{g_x^2}{4\pi}, \quad \alpha_\gamma = \frac{e^2}{4\pi}, \quad Q_f^Z = T_3 - Q_f s_W^2, \\ \alpha_{\gamma 2}(t) &= \sqrt{\alpha_\gamma(t) \alpha_2(t)}, \quad C_F = \frac{N_c^2 - 1}{2N_c}, \quad T_F = 1/2, \end{aligned} \quad (\text{A.4})$$

where $N_c = 3$.

We evaluate the RG evolution for the QCD coupling using the 3-loop result [73] with mass thresholds for the charm, bottom, and top quarks. For the QED and EW couplings, as well as for the top Yukawa, we employ the corresponding 1-loop RGE. The numerical boundary conditions are taken at $Q = 200$ GeV from [72], we report the relevant ones in Table 3 for convenience.

A.2 Formalism for the DGLAP equations

We consider a process $A + X \rightarrow C + Y$ mediated by the particle B at tree level, with B carrying a fraction $z \in [0, 1]$ of the energy of A , as in Fig. 1. The kinematics, up to quadratic order in the transverse momentum p_T , is the following

$$p_A^\mu = \left(E_A, 0, 0, \sqrt{E_A^2 - m_A^2} \right), \quad (\text{A.5})$$

$$p_B^\mu = \left(zE_A, p_T, 0, \sqrt{E_A^2 - m_A^2} - \sqrt{\bar{z}^2 E_A^2 - m_C^2} + \frac{p_T^2}{2\sqrt{\bar{z}^2 E_A^2 - m_C^2}} \right), \quad (\text{A.6})$$

$$p_C^\mu = \left(\bar{z}E_A, -p_T, 0, \sqrt{\bar{z}^2 E_A^2 - m_C^2} - \frac{p_T^2}{2\sqrt{\bar{z}^2 E_A^2 - m_C^2}} \right), \quad (\text{A.7})$$

where we remind that $\bar{z} = 1 - z$. In this way the emitted particle C is on-shell ($p_C^2 = m_C^2$), while for the particle B , neglecting $\mathcal{O}(p_T^4)$ terms, we have

$$p_B^2 = m_A^2 + m_C^2 - 2\bar{z}E_A^2 + 2\sqrt{(E_A^2 - m_A^2)(\bar{z}^2 E_A^2 - m_C^2)} - \sqrt{\frac{(E_A^2 - m_A^2)}{(\bar{z}^2 E_A^2 - m_C^2)}} p_T^2. \quad (\text{A.8})$$

Since we are working with high-energy initial beams, we can expand p_B^2 neglecting terms of order m/E and p_T/E or higher, so that the virtuality of the particle B is given by

$$m_B^2 - p_B^2 = \frac{1}{\bar{z}}(p_T^2 + zm_C^2 + \bar{z}m_B^2 - z\bar{z}m_A^2) + \mathcal{O}\left(\frac{m^2}{E^2}, \frac{p_T^2}{E^2}\right) \equiv \frac{\tilde{p}_T^2}{\bar{z}}. \quad (\text{A.9})$$

Invariance of the cross section on the factorization scale Q , that we choose to be the p_T of the emitted parton, gives the DGLAP equations [43, 74]

$$Q^2 \frac{df_B(x, Q^2)}{dQ^2} = P_B^v(x, Q^2) f_B(x, Q^2) + \sum_{A,C} \int_x^{z_{\max}^{ABC}} \frac{dz}{z} Q^2 \frac{d\mathcal{P}_{A \rightarrow B+C}}{dz dp_T^2}(z, Q^2) f_A\left(\frac{x}{z}, Q^2\right), \quad (\text{A.10})$$

where P_B^v represents the virtual corrections (see App. C) and

$$\frac{d\mathcal{P}_{A \rightarrow B+C}}{dz dp_T^2}(z, p_T^2) = \frac{1}{16\pi^2 \tilde{p}_T^4} z \bar{z} |\mathcal{M}_{A \rightarrow B+C}|^2, \quad (\text{A.11})$$

describes the splitting process. The standard matrix elements, which are also present in the unbroken phase (i.e. in a massless theory), are typically parametrized as

$$|\mathcal{M}_{A \rightarrow B+C}|^2 \equiv 8\pi\alpha_{ABC} \frac{p_T^2}{z\bar{z}} P_{BA}^C(z), \quad (\text{A.12})$$

where $P_{BA}^C(z)$ is the splitting function and α_{ABC} the corresponding coupling. Ultra-collinear matrix elements are instead proportional to v^2 and they can be parametrized with new splitting functions U_{BA}^C as

$$|\mathcal{M}_{A \rightarrow B+C}|^2 \supset \frac{v^2}{z\bar{z}} U_{BA}^C(z). \quad (\text{A.13})$$

The general DGLAP equation for a parton B is then given by

$$Q^2 \frac{df_B(x, Q^2)}{dQ^2} = P_B^v f_B(x, Q^2) + \sum_{A,C} \frac{\alpha_{ABC}}{2\pi} \tilde{P}_{BA}^C \otimes f_A + \frac{v^2}{16\pi^2 Q^2} \sum_{A,C} \tilde{U}_{BA}^C \otimes f_A, \quad (\text{A.14})$$

where \tilde{P} and \tilde{U} are the splitting functions for massive partons and are obtained from those for massless ones with the redefinition in Eq. (3.3)

$$\tilde{P}_{BA}^C(z, p_T^2) = \left(\frac{p_T^2}{\tilde{p}_T^2} \right)^2 P_{BA}^C(z), \quad (\text{A.15})$$

with

$$\tilde{p}_T^2 \equiv \bar{z}(m_B^2 - p_B^2) = p_T^2 + zm_C^2 + \bar{z}m_B^2 - z\bar{z}m_A^2 + \mathcal{O}\left(\frac{m^2}{E^2}, \frac{p_T^2}{E^2}\right). \quad (\text{A.16})$$

B Splitting Functions

Here we list all the splitting functions, including ultra-collinear ones. Some of them have a \bar{z} pole and therefore they introduce divergences in the DGLAP equations when $z_{\max} = 1$. To deal with such divergences, we use the $+$ distribution, defined as

$$\int_x^1 dz \frac{f(z)}{(1-z)_+} = \int_x^1 dz \frac{f(z) - f(1)}{1-z} - f(1) \int_0^x \frac{dz}{1-z} = \int_x^1 dz \frac{f(z) - f(1)}{1-z} + f(1) \log(1-x). \quad (\text{B.1})$$

As already discussed, since the SM is a chiral theory we separate vector polarizations and fermion helicities in the splitting functions.

B.1 Massless splitting functions

We start with the splitting functions of the form in Eq. (A.12). Here f labels a fermion, V a gauge boson and h a scalar. We do not specify the polarization of the particle C , since in the computation we sum over it.

$$\begin{aligned} P_{ff}^V(z) &\equiv P_{f_L f_L}^V(z) = P_{f_R f_R}^V(z) = \frac{1+z^2}{\bar{z}_+}, \\ P_{V_+ f_L}^f(z) &= P_{V_- f_R}^f(z) = \frac{\bar{z}^2}{z}, \\ P_{V_- f_L}^f(z) &= P_{V_+ f_R}^f(z) = \frac{1}{z}, \\ P_{f_L V_+}^f(z) &= P_{f_R V_-}^f(z) = \bar{z}^2, \\ P_{f_L V_-}^f(z) &= P_{f_R V_+}^f(z) = z^2, \end{aligned} \quad (\text{B.2})$$

$$\begin{aligned} P_{ff}^h(z) &\equiv P_{f_L f_R}^h(z) = P_{f_R f_L}^h(z) = \frac{\bar{z}}{2}, \\ P_{hf}^f(z) &\equiv P_{h f_L}^f(z) = P_{h f_R}^f(z) = \frac{z}{2}, \\ P_{fh}^f(z) &\equiv P_{f_L h}^f(z) = P_{f_R h}^f(z) = \frac{1}{2}, \end{aligned} \quad (\text{B.3})$$

$$\begin{aligned} P_{V_\pm h}^h(z) &= \frac{\bar{z}}{z}, \\ P_{V_h}^h(z) &\equiv P_{V_+ h}^h(z) + P_{V_- h}^h(z) = \frac{2\bar{z}}{z}, \end{aligned} \quad (\text{B.4})$$

$$\begin{aligned} P_{hh}^V(z) &= \frac{2z}{\bar{z}_+}, \\ P_{hV}^h(z) &\equiv P_{hV_+}^h(z) = P_{hV_-}^h(z) = z\bar{z}, \\ P_{V_+ V_+}^V(z) &= P_{V_- V_-}^V(z) = \frac{1+z^4}{z\bar{z}_+}, \\ P_{V_+ V_-}^V(z) &= P_{V_- V_+}^V(z) = \frac{\bar{z}^3}{z}. \end{aligned} \quad (\text{B.5})$$

Since QED and QCD are vectorlike theories, we also define the splitting functions properly summed over the vector polarizations and fermion helicities:

$$\begin{aligned}
P_{Vf}^f(z) &\equiv \frac{P_{V_+f_L}^f(z) + P_{V_+f_R}^f(z) + P_{V_-f_L}^f(z) + P_{V_-f_R}^f(z)}{2} = \frac{1 + \bar{z}^2}{z}, \\
P_{fV}^f(z) &\equiv \frac{P_{fLV_+}^f(z) + P_{fRV_+}^f(z) + P_{fLV_-}^f(z) + P_{fRV_-}^f(z)}{2} = z^2 + \bar{z}^2, \\
P_{VV}^V(z) &\equiv \frac{P_{V_+V_+}^V(z) + P_{V_+V_-}^V(z) + P_{V_-V_+}^V(z) + P_{V_-V_-}^V(z)}{2} = 2 \frac{(1 - z\bar{z})^2}{z\bar{z}_+}.
\end{aligned} \tag{B.6}$$

Finally, we report here the integrals appearing in Eq. (2.4):

$$\begin{aligned}
I_{fVVf}(x) &= \int_x^1 \frac{dz}{z} P_{fV}^f(z) P_{Vf}^f\left(\frac{x}{z}\right) = \frac{4 + 3x - 3x^2 - 4x^3}{3x} + 2(1+x) \log x, \\
I_{Vfff}(x) &= \int_x^1 \frac{dz}{z} P_{Vf}^f\left(\frac{x}{z}\right) P_{ff}^V(z) = \\
&= 2 \log(1-x) P_{Vf}^f(x) + \frac{(1-x)(2x-3)}{x} + (2-x) \log x, \\
I_{ffff}(x) &= \int_x^1 \frac{dz}{z} P_{ff}^V\left(\frac{x}{z}\right) P_{ff}^V(z) = \\
&= \frac{-2(1-x)^2 + 4(1+x^2) \log(1-x) - (1+3x^2) \log x}{1-x}.
\end{aligned} \tag{B.7}$$

B.2 Ultra-collinear splitting functions

The top quark is explicitly written, while for other fermions we write f . $s = L, R$ is the helicity of the fermion, $T = \pm$ is a transverse polarization of the gauge bosons. If inside a splitting we write $f_s f_{-s}$ it means that the two fermions have opposite helicity (same for the gauge bosons). N_c^f is 1 for leptons and N_c for quarks.

Splitting $f \rightarrow f + V_T$ ($f = t, b$):

$$\begin{aligned}
U_{t_R b_L}^{W^-}(z) &= U_{\bar{t}_R \bar{b}_L}^{W^+}(z) = \frac{1}{2} g_2^2 y_t^2 \bar{z}, \\
U_{W_- b_L}^{t_R}(z) &= U_{W_+ \bar{b}_L}^{\bar{t}_R}(z) = \frac{1}{2} g_2^2 y_t^2 z, \\
U_{b_L t_R}^{W^+}(z) &= U_{\bar{b}_L \bar{t}_R}^{W^-}(z) = \frac{1}{2} g_2^2 y_t^2 \bar{z} z^2, \\
U_{W_+ t_R}^{b_L}(z) &= U_{W_- \bar{t}_R}^{\bar{b}_L}(z) = \frac{1}{2} g_2^2 y_t^2 z \bar{z}^2,
\end{aligned} \tag{B.8}$$

$$\begin{aligned}
U_{tt}^g(z) &\equiv U_{t_R t_L}^{g-}(z) = U_{\bar{t}_R \bar{t}_L}^{g+}(z) = U_{t_L t_R}^{g+}(z) = U_{\bar{t}_L \bar{t}_R}^{g-}(z) = C_F g_3^2 y_t^2 \bar{z}^3, \\
U_{gt}^t(z) &\equiv U_{g_- t_L}^{t_R}(z) = U_{g_+ \bar{t}_L}^{\bar{t}_R}(z) = U_{g_+ t_R}^{t_L}(z) = U_{g_- \bar{t}_R}^{\bar{t}_L}(z) = C_F g_3^2 y_t^2 z^3, \\
U_{tt}^\gamma(z) &\equiv U_{t_R t_L}^{\gamma-}(z) = U_{\bar{t}_R \bar{t}_L}^{\gamma+}(z) = U_{t_L t_R}^{\gamma+}(z) = U_{\bar{t}_L \bar{t}_R}^{\gamma-}(z) = Q_u^2 e^2 y_t^2 \bar{z}^3, \\
U_{\gamma t}^t(z) &\equiv U_{\gamma_- t_L}^{t_R}(z) = U_{\gamma_+ \bar{t}_L}^{\bar{t}_R}(z) = U_{\gamma_+ t_R}^{t_L}(z) = U_{\gamma_- \bar{t}_R}^{\bar{t}_L}(z) = Q_u^2 e^2 y_t^2 z^3,
\end{aligned} \tag{B.9}$$

$$\begin{aligned}
U_{t_R t_L}^{Z-}(z) &= U_{\bar{t}_R \bar{t}_L}^{Z+}(z) = \frac{g_2^2 y_t^2}{c_W^2} \bar{z} \left(\frac{1}{2} - Q_u s_W^2 \bar{z} \right)^2, \\
U_{Z- t_L}^{t_R}(z) &= U_{Z+ \bar{t}_L}^{\bar{t}_R}(z) = \frac{g_2^2 y_t^2}{c_W^2} z \left(\frac{1}{2} - Q_u s_W^2 z \right)^2, \\
U_{t_L t_R}^{Z+}(z) &= U_{\bar{t}_L \bar{t}_R}^{Z-}(z) = \frac{g_2^2 y_t^2}{c_W^2} \bar{z} \left(\frac{z}{2} + Q_u s_W^2 \bar{z} \right)^2, \\
U_{Z+ t_R}^{t_L}(z) &= U_{Z- \bar{t}_R}^{\bar{t}_L}(z) = \frac{g_2^2 y_t^2}{c_W^2} z \left(\frac{\bar{z}}{2} + Q_u s_W^2 z \right)^2, \\
U_{Z/\gamma- t_L}^{t_R}(z) &= U_{Z/\gamma+ \bar{t}_L}^{\bar{t}_R}(z) = 2Q_u \frac{e g_2}{c_W} y_t^2 z^2 \left(\frac{1}{2} - Q_u s_W^2 z \right), \\
U_{Z/\gamma+ t_R}^{t_L}(z) &= U_{Z/\gamma- \bar{t}_R}^{\bar{t}_L}(z) = -2Q_u \frac{e g_2}{c_W} y_t^2 z^2 \left(\frac{\bar{z}}{2} + Q_u s_W^2 z \right).
\end{aligned} \tag{B.10}$$

Splitting $V_T \rightarrow f + \bar{f}$ ($f = t, b$):

$$\begin{aligned}
U_{b_L W_-}^{\bar{t}_R}(z) &= U_{b_L W_+}^{t_R}(z) = \frac{N_c}{2} g_2^2 y_t^2 z^2, \\
U_{\bar{t}_R W_-}^{b_L}(z) &= U_{\bar{t}_R W_+}^{b_L}(z) = \frac{N_c}{2} g_2^2 y_t^2 \bar{z}^2,
\end{aligned} \tag{B.11}$$

$$\begin{aligned}
U_{t g}^t(z) &\equiv U_{t_L g_-}^{\bar{t}_R}(z) = U_{\bar{t}_R g_-}^{t_L}(z) = U_{t_R g_+}^{\bar{t}_L}(z) = U_{\bar{t}_L g_+}^{t_R}(z) = T_F g_3^2 y_t^2, \\
U_{t \gamma}^t(z) &\equiv U_{t_L \gamma_-}^{\bar{t}_R}(z) = U_{\bar{t}_R \gamma_-}^{t_L}(z) = U_{t_R \gamma_+}^{\bar{t}_L}(z) = U_{\bar{t}_L \gamma_+}^{t_R}(z) = N_c Q_u^2 e^2 y_t^2,
\end{aligned} \tag{B.12}$$

$$\begin{aligned}
U_{t_L Z_-}^{\bar{t}_R}(z) &= U_{t_L Z_+}^{t_R}(z) = N_c \frac{g_2^2 y_t^2}{c_W^2} \left(\frac{z}{2} - Q_u s_W^2 \right)^2, \\
U_{\bar{t}_R Z_-}^{t_L}(z) &= U_{\bar{t}_R Z_+}^{\bar{t}_L}(z) = N_c \frac{g_2^2 y_t^2}{c_W^2} \left(\frac{\bar{z}}{2} - Q_u s_W^2 \right)^2, \\
U_{t_L Z/\gamma_-}^{\bar{t}_R}(z) &= U_{t_L Z/\gamma_+}^{t_R}(z) = N_c Q_u e \frac{g_2}{c_W} y_t^2 \left(\frac{z}{2} - Q_u s_W^2 \right), \\
U_{\bar{t}_R Z/\gamma_-}^{t_L}(z) &= U_{\bar{t}_R Z/\gamma_+}^{\bar{t}_L}(z) = N_c Q_u e \frac{g_2}{c_W} y_t^2 \left(\frac{\bar{z}}{2} - Q_u s_W^2 \right).
\end{aligned} \tag{B.13}$$

Splitting $f \rightarrow f + V_L$:

$$\begin{aligned}
U_{f_L f_L}^{Z_L}(z) &= U_{\bar{f}_L \bar{f}_L}^{Z_L}(z) = \left(T_3 y_f^2 \bar{z}^2 + \frac{g_2^2}{c_W^2} Q_{f_L}^Z z \right)^2 \frac{1}{z_+}, \\
U_{Z_L f_L}^{f_L}(z) &= U_{Z_L \bar{f}_L}^{\bar{f}_L}(z) = \left(T_3 y_f^2 z^2 + \frac{g_2^2}{c_W^2} Q_{f_L}^Z \bar{z} \right)^2 \frac{1}{z}, \\
U_{f_R f_R}^{Z_L}(z) &= U_{\bar{f}_R \bar{f}_R}^{Z_L}(z) = \left(T_3 y_f^2 \bar{z}^2 - \frac{g_2^2}{c_W^2} Q_{f_R}^Z z \right)^2 \frac{1}{\bar{z}_+}, \\
U_{Z_L f_R}^{f_R}(z) &= U_{Z_L \bar{f}_R}^{\bar{f}_R}(z) = \left(T_3 y_f^2 z^2 - \frac{g_2^2}{c_W^2} Q_{f_R}^Z \bar{z} \right)^2 \frac{1}{z}, \\
U_{f_L^{(2)} f_L^{(1)}}^{W_L}(z) &= U_{\bar{f}_L^{(2)} \bar{f}_L^{(1)}}^{W_L}(z) = (y_{f_1}^2 z \bar{z} - y_{f_2}^2 \bar{z} - g_2^2 z)^2 \frac{1}{2 \bar{z}_+}, \\
U_{W_L f_L^{(1)}}^{f_L^{(2)}}(z) &= U_{W_L \bar{f}_L^{(1)}}^{\bar{f}_L^{(2)}}(z) = (y_{f_1}^2 z \bar{z} - y_{f_2}^2 z - g_2^2 \bar{z})^2 \frac{1}{2 z}.
\end{aligned} \tag{B.14}$$

Splitting $V_L \rightarrow f + \bar{f}$:

$$\begin{aligned}
U_{f_L Z_L}^{\bar{f}_L}(z) &= U_{f_L Z_L}^{f_L}(z) = N_c^f \left(T_3 y_f^2 - \frac{g_2^2}{c_W^2} Q_{f_L}^Z z \bar{z} \right)^2, \\
U_{f_R Z_L}^{\bar{f}_R}(z) &= U_{f_R Z_L}^{f_R}(z) = N_c^f \left(T_3 y_f^2 - \frac{g_2^2}{c_W^2} Q_{f_R}^Z z \bar{z} \right)^2, \\
U_{f_L^{(1)} W_L}^{\bar{f}_L^{(2)}}(z) &= U_{f_L^{(1)} W_L}^{f_L^{(2)}}(z) = \frac{N_c^f}{2} (y_{f_1}^2 \bar{z} + y_{f_2}^2 z - g_2^2 z \bar{z})^2.
\end{aligned} \tag{B.15}$$

Splitting $t \rightarrow t + h$:

$$\begin{aligned}
U_{tt}^h(z) &\equiv U_{t_L t_L}^h(z) = U_{t_R t_R}^h(z) = U_{\bar{t}_R \bar{t}_R}^h(z) = U_{\bar{t}_L \bar{t}_L}^h(z) = \frac{y_t^4}{4} \bar{z} (1+z)^2, \\
U_{ht}^t(z) &\equiv U_{ht_L}^{t_L}(z) = U_{ht_R}^{t_R}(z) = U_{h\bar{t}_R}^{\bar{t}_R}(z) = U_{h\bar{t}_L}^{\bar{t}_L}(z) = \frac{y_t^4}{4} z (1+\bar{z})^2.
\end{aligned} \tag{B.16}$$

Splitting $h \rightarrow t + \bar{t}$:

$$U_{th}^t(z) \equiv U_{t_L h}^{\bar{t}_L}(z) = U_{\bar{t}_R h}^{\bar{t}_R}(z) = U_{\bar{t}_R h}^{t_R}(z) = U_{\bar{t}_L h}^{t_L}(z) = N_c \frac{y_t^4}{4} (\bar{z} - z)^2. \tag{B.17}$$

Splitting $V_T \rightarrow V_L + V_T$:

$$\begin{aligned}
U_{W_L W_T}^{\gamma_T}(z) &= e^2 g_2^2 \frac{\bar{z}^3}{z}, \\
U_{\gamma_T W_T}^{W_L}(z) &= e^2 g_2^2 \frac{z^3}{\bar{z}_+}, \\
U_{W_L W_T}^{Z_T}(z) &= \frac{1}{4} c_W^2 g_2^4 (1 + \bar{z} + t_W^2 z)^2 \frac{\bar{z}}{z}, \\
U_{Z_T W_T}^{W_L}(z) &= \frac{1}{4} c_W^2 g_2^4 (1 + z + t_W^2 \bar{z})^2 \frac{z}{\bar{z}_+}, \\
U_{Z/\gamma_T W_T}^{W_L}(z) &= c_W e g_2^3 (1 + z + t_W^2 \bar{z}) \frac{z^2}{\bar{z}_+}, \\
U_{Z_L W_T}^{W_T}(z) &= \frac{1}{4} g_2^4 (1 + \bar{z})^2 \frac{\bar{z}}{z}, \\
U_{W_T W_T}^{Z_L}(z) &= \frac{1}{4} g_2^4 (1 + z)^2 \frac{z}{\bar{z}_+}, \\
U_{W_L \gamma_T}^{W_T}(z) &= e^2 g_2^2 \frac{\bar{z}}{z}, \\
U_{W_T \gamma_T}^{W_L}(z) &= e^2 g_2^2 \frac{z}{\bar{z}_+}, \\
U_{W_L Z_T}^{W_T}(z) &= \frac{1}{4} c_W^2 g_2^4 (1 + \bar{z} - t_W^2 z)^2 \frac{\bar{z}}{z}, \\
U_{W_T Z_T}^{W_L}(z) &= \frac{1}{4} c_W^2 g_2^4 (1 + z - t_W^2 \bar{z})^2 \frac{z}{\bar{z}_+}, \\
U_{W_L Z/\gamma_T}^{W_T}(z) &= \frac{1}{2} c_W e g_2^3 (1 + \bar{z} - t_W^2 z) \frac{\bar{z}}{z}, \\
U_{W_T Z/\gamma_T}^{W_L}(z) &= \frac{1}{2} c_W e g_2^3 (1 + z - t_W^2 \bar{z}) \frac{z}{\bar{z}_+}.
\end{aligned} \tag{B.18}$$

Splitting $V_L \rightarrow V_T + V_{-T}$:

$$\begin{aligned}
U_{\gamma_T W_L}^{W_{-T}}(z) &= e^2 g_2^2 z^3 \bar{z} , \\
U_{W_T W_L}^{\gamma_{-T}}(z) &= e^2 g_2^2 z \bar{z}^3 , \\
U_{Z_T W_L}^{W_{-T}}(z) &= \frac{1}{4} c_W^2 g_2^4 z \bar{z} (\bar{z} - z + t_W^2)^2 , \\
U_{W_T W_L}^{Z_{-T}}(z) &= \frac{1}{4} c_W^2 g_2^4 z \bar{z} (z - \bar{z} + t_W^2)^2 , \\
U_{Z/\gamma_T W_L}^{W_{-T}}(z) &= -c_W e g_2^3 z^2 \bar{z} (\bar{z} - z + t_W^2) , \\
U_{W_T Z_L}^{W_{-T}}(z) &= \frac{1}{4} g_2^4 z \bar{z} (\bar{z} - z)^2 .
\end{aligned} \tag{B.19}$$

Splitting $V_T \rightarrow h + V_T$:

$$\begin{aligned}
U_{h W_T}^{W_T}(z) &= U_{W_T W_T}^h(z) = \frac{1}{4} g_2^4 z \bar{z} , \\
U_{h Z_T}^{Z_T}(z) &= U_{Z_T Z_T}^h(z) = \frac{1}{4} \frac{g_2^4}{c_W^4} z \bar{z} .
\end{aligned} \tag{B.20}$$

Splitting $h \rightarrow V_T + V_{-T}$:

$$\begin{aligned}
U_{W_T h}^{W_{-T}}(z) &= \frac{1}{4} g_2^4 z \bar{z} , \\
U_{Z_T h}^{Z_{-T}}(z) &= \frac{1}{8} \frac{g_2^4}{c_W^4} z \bar{z} .
\end{aligned} \tag{B.21}$$

Splitting $V_L \rightarrow V_L + V_L$:

$$\begin{aligned}
U_{Z_L W_L}^{W_L}(z) &= \frac{1}{16} g_2^4 [(\bar{z} - z)(2 + z\bar{z}) - t_W^2 \bar{z}(1 + \bar{z})]^2 \frac{1}{z\bar{z}_+} , \\
U_{W_L W_L}^{Z_L}(z) &= \frac{1}{16} g_2^4 [(z - \bar{z})(2 + z\bar{z}) - t_W^2 z(1 + z)]^2 \frac{1}{z\bar{z}_+} , \\
U_{W_L Z_L}^{W_L}(z) &= \frac{1}{16} g_2^4 (z - \bar{z})^2 (2 + z\bar{z} - t_W^2 z\bar{z})^2 \frac{1}{z\bar{z}_+} .
\end{aligned} \tag{B.22}$$

Splitting $h \rightarrow V_L + V_L$:

$$\begin{aligned}
U_{Z_L h}^{Z_L}(z) &= \frac{1}{8} \left[\frac{g_2^2}{c_W^2} (1 - z\bar{z}) - 4\lambda_h z\bar{z} \right]^2 \frac{1}{z\bar{z}_+} , \\
U_{W_L h}^{W_L}(z) &= \frac{1}{4} [g_2^2 (1 - z\bar{z}) - 4\lambda_h z\bar{z}]^2 \frac{1}{z\bar{z}_+} .
\end{aligned} \tag{B.23}$$

Splitting $V_L \rightarrow h + V_L$:

$$\begin{aligned}
U_{h Z_L}^{Z_L}(z) &= \frac{1}{4} \left[\frac{g_2^2}{c_W^2} (1 - z\bar{z}) + 4\lambda_h \bar{z} \right]^2 \frac{z}{\bar{z}_+} , \\
U_{Z_L Z_L}^h(z) &= \frac{1}{4} \left[\frac{g_2^2}{c_W^2} (1 - z\bar{z}) + 4\lambda_h z \right]^2 \frac{\bar{z}}{z} , \\
U_{h W_L}^{W_L}(z) &= \frac{1}{4} [g_2^2 (1 - z\bar{z}) + 4\lambda_h \bar{z}]^2 \frac{z}{\bar{z}_+} , \\
U_{W_L W_L}^h(z) &= \frac{1}{4} [g_2^2 (1 - z\bar{z}) + 4\lambda_h z]^2 \frac{\bar{z}}{z} .
\end{aligned} \tag{B.24}$$

Splitting $h \rightarrow h + h$:

$$U_{hh}^h(z) = 18\lambda_h^2 z \bar{z} . \quad (\text{B.25})$$

Splitting involving the mixed state hZ_L :

$$\begin{aligned} U_{hZ_L t_L}^{t_L} (z) &= -U_{hZ_L \bar{t}_L}^{\bar{t}_L} (z) = y_t^2 (1 + \bar{z}) \left(\frac{y_t^2}{2} z^2 + g_Z^2 Q_{t_L}^Z \bar{z} \right) , \\ U_{hZ_L t_R}^{t_R} (z) &= -U_{hZ_L \bar{t}_R}^{\bar{t}_R} (z) = -y_t^2 (1 + \bar{z}) \left(\frac{y_t^2}{2} z^2 - g_Z^2 Q_{t_R}^Z \bar{z} \right) , \\ U_{t_L hZ_L}^{\bar{t}_L} (z) &= U_{\bar{t}_L hZ_L}^{t_L} (z) = -\frac{y_t^2}{2} (\bar{z} - z) \left(\frac{y_t^2}{2} - g_Z^2 Q_{t_L}^Z z \bar{z} \right) , \\ U_{t_R hZ_L}^{\bar{t}_R} (z) &= U_{\bar{t}_R hZ_L}^{t_R} (z) = \frac{y_t^2}{2} (\bar{z} - z) \left(\frac{y_t^2}{2} - g_Z^2 Q_{t_R}^Z z \bar{z} \right) , \end{aligned} \quad (\text{B.26})$$

$$\begin{aligned} U_{hZ_L W_L}^{W_L} (z) &\equiv U_{hZ_L W_L^+}^{W_L^+} (z) = -U_{hZ_L W_L^-}^{W_L^-} (z) \\ &= \frac{g_2^2}{4} [g_2^2 (1 - z\bar{z}) + 4\lambda_h \bar{z}] [(\bar{z} - z)(2 + z\bar{z}) - t_W^2 \bar{z}(1 - \bar{z})] \frac{1}{\bar{z}_+} , \end{aligned} \quad (\text{B.27})$$

$$\begin{aligned} U_{W_L hZ_L}^{W_L} (z) &\equiv U_{W_L^+ hZ_L}^{W_L^-} (z) = -U_{W_L^- hZ_L}^{W_L^+} (z) \\ &= \frac{g_2^2}{8} [g_2^2 (1 - z\bar{z}) - 4\lambda_h z \bar{z}] (\bar{z} - z) [(2 + (1 - t_W^2) z \bar{z})] \frac{1}{z \bar{z}_+} , \end{aligned}$$

$$\begin{aligned} U_{hZ_L W_T}^{W_T} (z) &\equiv U_{hZ_L W_T^+}^{W_T^+} (z) = U_{hZ_L W_T^-}^{W_T^-} (z) = \frac{g_2^4}{2} \bar{z}(1 + \bar{z}) , \\ U_{W_T hZ_L}^{W_T} (z) &\equiv U_{W_T^+ hZ_L}^{W_T^-} (z) = -U_{W_T^- hZ_L}^{W_T^+} (z) = -\frac{g_2^4}{4} z \bar{z} (\bar{z} - z) . \end{aligned} \quad (\text{B.28})$$

C Radiative corrections

To cancel the IR divergences appearing in the splitting functions in the soft limit $z \rightarrow 1$ we need to add virtual corrections. Instead of explicitly computing the corresponding Feynman diagrams, we use that virtual corrections correspond to a process in which the particles B and A are the same and C is absent, so in the splitting formalism they can be treated introducing a new splitting function for each particle of the form $P_{BB}^v(x, t) = P_B^v(t) \delta(1 - x)$. Inserting the new term in the DGLAP equations we get

$$\frac{df_B(x, t)}{dt} \supset P_{BB}^v \otimes f_B = P_B^v(t) f_B(x, t) . \quad (\text{C.1})$$

The coefficients $P_B^v(t)$ can be computed using momentum conservation

$$\sum_i \int_0^1 dx x f_i(x, t) = \sum_i f_i^{(2)}(t) = 1 \quad \forall t , \quad (\text{C.2})$$

where $f_i^{(2)}$ represents the $n = 2$ Mellin transform of the PDF

$$f^{(n)} = \int_0^1 \frac{dx}{x} x^n f(x) . \quad (\text{C.3})$$

Deriving in t and using Eqs. (A.10, C.1) we obtain for each particle A

$$P_A^v(t) + \sum_{B,C} \left(\frac{d\mathcal{P}_{A \rightarrow B+C}}{dz dp_T^2} \right)^{(2)} = 0 . \quad (\text{C.4})$$

From the definitions in Eqs. (A.11, A.12, 3.3, A.13), we get

$$P_A^v(t) = - \sum_{B,C} \left(\frac{\alpha_{ABC}}{2\pi} \tilde{P}_{BA}^{C(2)} + \frac{v^2}{16\pi^2 Q^2(t)} \tilde{U}_{BA}^{C(2)} \right) . \quad (\text{C.5})$$

In order to reproduce the non cancellation of IR divergences in $SU(2)_L$ interactions, the computation of virtual corrections is modified by changing the boundary of the integral as discussed in Section 3.2

$$P_A^v(t) = - \sum_{B,C} \int_0^{z_{\max}^{ABC}(t)} dz z \left(\frac{\alpha_{ABC}}{2\pi} \tilde{P}_{BA}^C(z) + \frac{v^2}{16\pi^2 Q^2(t)} \tilde{U}_{BA}^C(z) \right) . \quad (\text{C.6})$$

We show explicitly the virtual corrections for the QED+QCD phase, with N_ℓ charged leptons, N_u up and N_d down quarks. All the particles are treated as massless, so momentum conservation equations become just relations between the $n = 2$ Mellin transform of the splitting functions and the virtual coefficients. Applying Eq. (C.6) respectively to the fermions, the photon and the gluon we get, using Eq. (2.2)

$$\begin{aligned} P_f^v &= \frac{3}{2} \left(\frac{\alpha_\gamma}{2\pi} Q_f^2 + \frac{\alpha_3}{2\pi} C_F \delta_{f,q} \right) , \\ P_\gamma^v &= - \frac{\alpha_\gamma}{2\pi} \frac{2}{3} N_f^{\text{QED}} , \\ P_g^v &= \frac{\alpha_3}{2\pi} \left(\frac{11}{6} C_A - \frac{2}{3} T_F N_q \right) , \end{aligned} \quad (\text{C.7})$$

where $N_f^{\text{QED}} = N_\ell + N_c(N_u Q_u^2 + N_d Q_d^2)$ is the effective number of fermions, $N_q = N_u + N_d$ is the number of quarks and $\delta_{f,q} = 1$ for quarks and 0 for leptons. In our specific setup, $N_\ell = N_d = 3$ and $N_u = 2$, so $N_q = 5$ and $N_f^{\text{QED}} = \frac{20}{3}$. We omit writing the explicit expressions for virtual corrections in the full SM phase, as they are many and too lengthy.

D DGLAP evolution equations in SM

Here we list the full set of DGLAP equations we used above the EW scale. We use the following notation for transverse vector polarization:

$$P_{BV_s}^C \otimes f_{V_s} = P_{BV_+}^C \otimes f_{V_+} + P_{BV_-}^C \otimes f_{V_-} , \quad (\text{D.1})$$

$$P_{BV_s}^C \otimes f_{V_{-s}} = P_{BV_+}^C \otimes f_{V_-} + P_{BV_-}^C \otimes f_{V_+} . \quad (\text{D.2})$$

In the ultra-collinear terms the factor $v^2/(16\pi^2 Q(t)^2)$ appearing in front of each splitting function is omitted to shorten the notation.

D.1 Leptons

$$\begin{aligned}
\frac{df_{\nu_i}}{dt} &= P_{\nu_i}^v f_{\nu_i} + \frac{\alpha_2(t)}{2\pi c_W^2(t)} \frac{1}{4} \left[\tilde{P}_{ff}^V \otimes f_{\nu_i} + \tilde{P}_{fLV_s}^f \otimes f_{Z_s} \right] \\
&+ \frac{\alpha_2(t)}{2\pi} \frac{1}{2} \left[\tilde{P}_{ff}^V \otimes f_{\ell_{L,i}} + \tilde{P}_{fLV_s}^f \otimes f_{W_s^+} \right] \\
&+ \tilde{U}_{\nu\ell_L}^{W_L^-} \otimes f_{\ell_{L,i}} + \tilde{U}_{\nu W_L^+}^{\ell_L} \otimes f_{W_L^+} + \tilde{U}_{\nu\nu}^{Z_L} \otimes f_{\nu_i} + \tilde{U}_{\nu Z_L}^{\nu} \otimes f_{Z_L} ,
\end{aligned} \tag{D.3}$$

$$\begin{aligned}
\frac{df_{\bar{\nu}_i}}{dt} &= P_{\bar{\nu}_i}^v f_{\bar{\nu}_i} + \frac{\alpha_2(t)}{2\pi c_W^2(t)} \frac{1}{4} \left[\tilde{P}_{ff}^V \otimes f_{\bar{\nu}_i} + \tilde{P}_{fLV_s}^f \otimes f_{Z_{-s}} \right] \\
&+ \frac{\alpha_2(t)}{2\pi} \frac{1}{2} \left[\tilde{P}_{ff}^V \otimes f_{\bar{\ell}_{L,i}} + \tilde{P}_{fLV_s}^f \otimes f_{W_{-s}^-} \right] \\
&+ \tilde{U}_{\bar{\nu}\bar{\ell}_L}^{W_L^+} \otimes f_{\bar{\ell}_{L,i}} + \tilde{U}_{\bar{\nu}W_L^-}^{\ell_L} \otimes f_{W_L^-} + \tilde{U}_{\bar{\nu}\bar{\nu}}^{Z_L} \otimes f_{\bar{\nu}_i} + \tilde{U}_{\bar{\nu}Z_L}^{\nu} \otimes f_{Z_L} ,
\end{aligned} \tag{D.4}$$

$$\begin{aligned}
\frac{df_{\ell_{L,i}}}{dt} &= P_{\ell_{L,i}}^v f_{\ell_{L,i}} + \frac{\alpha_\gamma(t)}{2\pi} Q_\ell^2 \left[\tilde{P}_{ff}^V \otimes f_{\ell_{L,i}} + \tilde{P}_{fLV_s}^f \otimes f_{\gamma_s} \right] \\
&+ \frac{\alpha_2(t)}{2\pi c_W^2(t)} \left(\frac{1}{2} + Q_\ell s_W^2(t) \right)^2 \left[\tilde{P}_{ff}^V \otimes f_{\ell_{L,i}} + \tilde{P}_{fLV_s}^f \otimes f_{Z_s} \right] \\
&+ \frac{\alpha_2(t)}{2\pi} \frac{1}{2} \left[\tilde{P}_{ff}^V \otimes f_{\nu_i} + \tilde{P}_{fLV_s}^f \otimes f_{W_s^-} \right] \\
&- \frac{\alpha_\gamma 2(t)}{2\pi c_W(t)} Q_\ell \left(\frac{1}{2} + Q_\ell s_W^2(t) \right) \tilde{P}_{fLV_s}^f \otimes f_{Z_{\gamma_s}} \\
&+ \tilde{U}_{\ell_L\nu}^{W_L^+} \otimes f_{\nu_i} + \tilde{U}_{\ell_L W_L^-}^{\nu} \otimes f_{W_L^-} + \tilde{U}_{\ell_L \ell_L}^{Z_L} \otimes f_{\ell_{L,i}} + \tilde{U}_{\ell_L Z_L}^{\ell_L} \otimes f_{Z_L} ,
\end{aligned} \tag{D.5}$$

$$\begin{aligned}
\frac{df_{\bar{\ell}_{L,i}}}{dt} &= P_{\bar{\ell}_{L,i}}^v f_{\bar{\ell}_{L,i}} + \frac{\alpha_\gamma(t)}{2\pi} Q_\ell^2 \left[\tilde{P}_{ff}^V \otimes f_{\bar{\ell}_{L,i}} + \tilde{P}_{fLV_s}^f \otimes f_{\gamma_{-s}} \right] \\
&+ \frac{\alpha_2(t)}{2\pi c_W^2(t)} \left(\frac{1}{2} + Q_\ell s_W^2(t) \right)^2 \left[\tilde{P}_{ff}^V \otimes f_{\bar{\ell}_{L,i}} + \tilde{P}_{fLV_s}^f \otimes f_{Z_{-s}} \right] \\
&+ \frac{\alpha_2(t)}{2\pi} \frac{1}{2} \left[\tilde{P}_{ff}^V \otimes f_{\bar{\nu}_i} + \tilde{P}_{fLV_s}^f \otimes f_{W_{-s}^+} \right] \\
&- \frac{\alpha_\gamma 2(t)}{2\pi c_W(t)} Q_\ell \left(\frac{1}{2} + Q_\ell s_W^2(t) \right) \tilde{P}_{fLV_s}^f \otimes f_{Z_{\gamma_{-s}}} \\
&+ \tilde{U}_{\bar{\ell}_L \bar{\nu}}^{W_L^-} \otimes f_{\bar{\nu}_i} + \tilde{U}_{\bar{\ell}_L W_L^+}^{\nu} \otimes f_{W_L^+} + \tilde{U}_{\bar{\ell}_L \bar{\ell}_L}^{Z_L} \otimes f_{\bar{\ell}_{L,i}} + \tilde{U}_{\bar{\ell}_L Z_L}^{\ell_L} \otimes f_{Z_L} ,
\end{aligned} \tag{D.6}$$

$$\begin{aligned}
\frac{df_{\ell_{R,i}}}{dt} &= P_{\ell_{R,i}}^v f_{\ell_{R,i}} + \frac{\alpha_\gamma(t)}{2\pi} Q_\ell^2 \left[\tilde{P}_{ff}^V \otimes f_{\ell_{R,i}} + \tilde{P}_{fLV_s}^f \otimes f_{\gamma_{-s}} \right] \\
&+ \frac{\alpha_2(t)}{2\pi c_W^2(t)} Q_\ell^2 s_W^4(t) \left[\tilde{P}_{ff}^V \otimes f_{\ell_{R,i}} + \tilde{P}_{fLV_s}^f \otimes f_{Z_{-s}} \right] \\
&- \frac{\alpha_\gamma 2(t)}{2\pi c_W(t)} Q_\ell^2 s_W^2(t) \tilde{P}_{fLV_s}^f \otimes f_{Z_{\gamma_{-s}}} \\
&+ \tilde{U}_{\ell_R \ell_R}^{Z_L} \otimes f_{\ell_{R,i}} + \tilde{U}_{\ell_R Z_L}^{\ell_R} \otimes f_{Z_L} ,
\end{aligned} \tag{D.7}$$

$$\begin{aligned}
\frac{df_{\bar{\ell}_{R,i}}}{dt} &= P_{\bar{\ell}_{R,i}}^v f_{\bar{\ell}_{R,i}} + \frac{\alpha_\gamma(t)}{2\pi} Q_\ell^2 \left[\tilde{P}_{ff}^V \otimes f_{\bar{\ell}_{R,i}} + \tilde{P}_{f_L V_s}^f \otimes f_{\gamma_s} \right] \\
&+ \frac{\alpha_2(t)}{2\pi c_W^2(t)} Q_\ell^2 s_W^4(t) \left[\tilde{P}_{ff}^V \otimes f_{\bar{\ell}_{R,i}} + \tilde{P}_{f_L V_s}^f \otimes f_{Z_s} \right] \\
&- \frac{\alpha_{\gamma 2}(t)}{2\pi c_W(t)} Q_\ell^2 s_W^2(t) \tilde{P}_{f_L V_s}^f \otimes f_{Z_{\gamma_s}} \\
&+ \tilde{U}_{\bar{\ell}_R \bar{\ell}_R}^{Z_L} \otimes f_{\bar{\ell}_{R,i}} + \tilde{U}_{\bar{\ell}_R Z_L}^{\ell_R} \otimes f_{Z_L} .
\end{aligned} \tag{D.8}$$

D.2 Quarks

$$\begin{aligned}
\frac{df_{u_{L,i}}}{dt} &= P_{u_{L,i}}^v f_{u_{L,i}} + \frac{\alpha_\gamma(t)}{2\pi} Q_u^2 \left[\tilde{P}_{ff}^V \otimes f_{u_{L,i}} + N_c \tilde{P}_{f_L V_s}^f \otimes f_{\gamma_s} \right] \\
&+ \frac{\alpha_2(t)}{2\pi c_W^2(t)} \left(\frac{1}{2} - Q_u s_W^2(t) \right)^2 \left[\tilde{P}_{ff}^V \otimes f_{u_{L,i}} + N_c \tilde{P}_{f_L V_s}^f \otimes f_{Z_s} \right] \\
&+ \frac{\alpha_2(t)}{2\pi} \frac{1}{2} \left[\tilde{P}_{ff}^V \otimes f_{d_{L,i}} + N_c \tilde{P}_{f_L V_s}^f \otimes f_{W_s^+} \right] \\
&+ \frac{\alpha_{\gamma 2}(t)}{2\pi} Q_u N_c \left(\frac{1}{2} - Q_u s_W^2(t) \right) \tilde{P}_{f_L V_s}^f \otimes f_{Z_{\gamma_s}} \\
&+ \frac{\alpha_3(t)}{2\pi} \left[C_F \tilde{P}_{ff}^V \otimes f_{u_{L,i}} + T_F \tilde{P}_{f_L V_s}^f \otimes f_{g_s} \right] \\
&+ \tilde{U}_{u_L d_L}^{W_L^-} \otimes f_{d_{L,i}} + \tilde{U}_{u_L W_L^+}^{d_L} \otimes f_{W_L^+} + \tilde{U}_{u_L u_L}^{Z_L} \otimes f_{u_{L,i}} + \tilde{U}_{u_L Z_L}^{\bar{u}_L} \otimes f_{Z_L} ,
\end{aligned} \tag{D.9}$$

$$\begin{aligned}
\frac{df_{\bar{u}_{L,i}}}{dt} &= P_{\bar{u}_{L,i}}^v f_{\bar{u}_{L,i}} + \frac{\alpha_\gamma(t)}{2\pi} Q_u^2 \left[\tilde{P}_{ff}^V \otimes f_{\bar{u}_{L,i}} + N_c \tilde{P}_{f_L V_s}^f \otimes f_{\gamma_{-s}} \right] \\
&+ \frac{\alpha_2(t)}{2\pi c_W^2(t)} \left(\frac{1}{2} - Q_u s_W^2(t) \right)^2 \left[\tilde{P}_{ff}^V \otimes f_{\bar{u}_{L,i}} + N_c \tilde{P}_{f_L V_s}^f \otimes f_{Z_{-s}} \right] \\
&+ \frac{\alpha_2(t)}{2\pi} \frac{1}{2} \left[\tilde{P}_{ff}^V \otimes f_{\bar{d}_{L,i}} + N_c \tilde{P}_{f_L V_s}^f \otimes f_{W_{-s}^-} \right] \\
&+ \frac{\alpha_{\gamma 2}(t)}{2\pi} Q_u N_c \left(\frac{1}{2} - Q_u s_W^2(t) \right) \tilde{P}_{f_L V_s}^f \otimes f_{Z_{\gamma_{-s}}} \\
&+ \frac{\alpha_3(t)}{2\pi} \left[C_F \tilde{P}_{ff}^V \otimes f_{\bar{u}_{L,i}} + T_F \tilde{P}_{f_L V_s}^f \otimes f_{g_{-s}} \right] \\
&+ \tilde{U}_{\bar{u}_L \bar{d}_L}^{W_L^+} \otimes f_{\bar{d}_{L,i}} + \tilde{U}_{\bar{u}_L W_L^-}^{d_L} \otimes f_{W_L^-} + \tilde{U}_{\bar{u}_L \bar{u}_L}^{Z_L} \otimes f_{\bar{u}_{L,i}} + \tilde{U}_{\bar{u}_L Z_L}^{u_L} \otimes f_{Z_L} ,
\end{aligned} \tag{D.10}$$

$$\begin{aligned}
\frac{df_{t_L}}{dt} = & P_{t_L}^v f_{t_L} + \frac{\alpha_\gamma(t)}{2\pi} Q_u^2 \left[\tilde{P}_{ff}^V \otimes f_{t_L} + N_c \tilde{P}_{f_L V_s}^f \otimes f_{\gamma_s} \right] \\
& + \frac{\alpha_2(t)}{2\pi c_W^2(t)} \left(\frac{1}{2} - Q_u s_W^2(t) \right)^2 \left[\tilde{P}_{ff}^V \otimes f_{t_L} + N_c \tilde{P}_{f_L V_s}^f \otimes f_{Z_s} \right] \\
& + \frac{\alpha_2(t)}{2\pi} \frac{1}{2} \left[\tilde{P}_{ff}^V \otimes f_{b_L} + N_c \tilde{P}_{f_L V_s}^f \otimes f_{W_s^+} \right] \\
& + \frac{\alpha_{\gamma 2}(t)}{2\pi} Q_u N_c \left(\frac{1}{2} - Q_u s_W^2(t) \right) \tilde{P}_{f_L V_s}^f \otimes f_{Z\gamma_s} \\
& + \frac{\alpha_3(t)}{2\pi} \left[C_F \tilde{P}_{ff}^V \otimes f_{t_L} + T_F \tilde{P}_{f_L V_s}^f \otimes f_{g_s} \right] \\
& + \frac{\alpha_y(t)}{2\pi} \frac{1}{2} \left[\tilde{P}_{ff}^h \otimes \left(f_{t_R}^{(h)} + f_{t_R}^{(Z_L)} \right) + N_c \tilde{P}_{fh}^f \otimes (f_h + f_{Z_L} + f_{hZ_L}) \right] \\
& + \tilde{U}_{tt}^g \otimes f_{t_R} + \tilde{U}_{tg}^t \otimes f_{g-} \\
& + \tilde{U}_{tt}^\gamma \otimes f_{t_R} + \tilde{U}_{t\gamma}^t \otimes f_{\gamma-} + \tilde{U}_{t_L t_R}^{Z+} \otimes f_{t_R} + \tilde{U}_{t_L Z-}^{t_R} \otimes f_{Z-} + \tilde{U}_{t_L Z/\gamma-}^{t_R} \otimes f_{Z/\gamma-} \\
& + \tilde{U}_{t_L b_L}^{W_L^-} \otimes f_{b_L} + \tilde{U}_{t_L W_L^+}^{b_L} \otimes f_{W_L^+} \\
& + \tilde{U}_{t_L t_L}^{Z_L} \otimes f_{t_L} + \tilde{U}_{t_L Z_L}^{t_L} \otimes f_{Z_L} + \tilde{U}_{tt}^h \otimes f_{t_L} + \tilde{U}_{th}^t \otimes f_h + \tilde{U}_{t_L h Z_L}^{t_L} \otimes f_{hZ_L} ,
\end{aligned} \tag{D.11}$$

$$\begin{aligned}
\frac{df_{\bar{t}_L}}{dt} = & P_{\bar{t}_L}^v f_{\bar{t}_L} + \frac{\alpha_\gamma(t)}{2\pi} Q_u^2 \left[\tilde{P}_{ff}^V \otimes f_{\bar{t}_L} + N_c \tilde{P}_{f_L V_s}^f \otimes f_{\gamma_{-s}} \right] \\
& + \frac{\alpha_2(t)}{2\pi c_W^2(t)} \left(\frac{1}{2} - Q_u s_W^2(t) \right)^2 \left[\tilde{P}_{ff}^V \otimes f_{\bar{t}_L} + N_c \tilde{P}_{f_L V_s}^f \otimes f_{Z_{-s}} \right] \\
& + \frac{\alpha_2(t)}{2\pi} \frac{1}{2} \left[\tilde{P}_{ff}^V \otimes f_{\bar{b}_L} + N_c \tilde{P}_{f_L V_s}^f \otimes f_{W_{-s}^-} \right] \\
& + \frac{\alpha_{\gamma 2}(t)}{2\pi} Q_u N_c \left(\frac{1}{2} - Q_u s_W^2(t) \right) \tilde{P}_{f_L V_s}^f \otimes f_{Z\gamma_{-s}} \\
& + \frac{\alpha_3(t)}{2\pi} \left[C_F \tilde{P}_{ff}^V \otimes f_{\bar{t}_L} + T_F \tilde{P}_{f_L V_s}^f \otimes f_{g_{-s}} \right] \\
& + \frac{\alpha_y(t)}{2\pi} \frac{1}{2} \left[\tilde{P}_{ff}^h \otimes \left(f_{\bar{t}_R}^{(h)} + f_{\bar{t}_R}^{(Z_L)} \right) + N_c \tilde{P}_{fh}^f \otimes (f_h + f_{Z_L} - f_{hZ_L}) \right] \\
& + \tilde{U}_{tt}^g \otimes f_{\bar{t}_R} + \tilde{U}_{tg}^t \otimes f_{g+} \\
& + \tilde{U}_{tt}^\gamma \otimes f_{\bar{t}_R} + \tilde{U}_{t\gamma}^t \otimes f_{\gamma+} + \tilde{U}_{t_L \bar{t}_R}^{Z-} \otimes f_{\bar{t}_R} + \tilde{U}_{t_L Z+}^{t_R} \otimes f_{Z+} + \tilde{U}_{t_L Z/\gamma+}^{t_R} \otimes f_{Z/\gamma+} \\
& + \tilde{U}_{\bar{t}_L \bar{b}_L}^{W_L^+} \otimes f_{\bar{b}_L} + \tilde{U}_{\bar{t}_L W_L^-}^{b_L} \otimes f_{W_L^-} \\
& + \tilde{U}_{\bar{t}_L \bar{t}_L}^{Z_L} \otimes f_{\bar{t}_L} + \tilde{U}_{\bar{t}_L Z_L}^{t_L} \otimes f_{Z_L} + \tilde{U}_{tt}^h \otimes f_{\bar{t}_L} + \tilde{U}_{th}^t \otimes f_h + \tilde{U}_{\bar{t}_L h Z_L}^{t_L} \otimes f_{hZ_L} ,
\end{aligned} \tag{D.12}$$

$$\begin{aligned}
\frac{df_{d_{L,i}}}{dt} &= P_{d_{L,i}}^v f_{d_{L,i}} + \frac{\alpha_\gamma(t)}{2\pi} Q_d^2 \left[\tilde{P}_{ff}^V \otimes f_{d_{L,i}} + N_c \tilde{P}_{f_{LV_s}}^f \otimes f_{\gamma_s} \right] \\
&+ \frac{\alpha_2(t)}{2\pi c_W^2(t)} \left(\frac{1}{2} + Q_d s_W^2(t) \right)^2 \left[\tilde{P}_{ff}^V \otimes f_{d_{L,i}} + N_c \tilde{P}_{f_{LV_s}}^f \otimes f_{Z_s} \right] \\
&+ \frac{\alpha_2(t)}{2\pi} \frac{1}{2} \left[\tilde{P}_{ff}^V \otimes f_{u_{L,i}} + N_c \tilde{P}_{f_{LV_s}}^f \otimes f_{W_s^-} \right] \\
&- \frac{\alpha_{\gamma 2}(t)}{2\pi} Q_d N_c \left(\frac{1}{2} + Q_d s_W^2(t) \right) \tilde{P}_{f_{LV_s}}^f \otimes f_{Z_{\gamma_s}} \\
&+ \frac{\alpha_3(t)}{2\pi} \left[C_F \tilde{P}_{ff}^V \otimes f_{d_{L,i}} + T_F \tilde{P}_{f_{LV_s}}^f \otimes f_{g_s} \right] \\
&+ \tilde{U}_{d_{L,u_L}^+} \otimes f_{u_{L,i}} + \tilde{U}_{d_{L,W_L}^-} \otimes f_{W_L^-} + \tilde{U}_{d_{L,d_L}^{Z_L}} \otimes f_{d_{L,i}} + \tilde{U}_{d_{L,Z_L}^{\bar{d}_L}} \otimes f_{Z_L} ,
\end{aligned} \tag{D.13}$$

$$\begin{aligned}
\frac{df_{\bar{d}_{L,i}}}{dt} &= P_{\bar{d}_{L,i}}^v f_{\bar{d}_{L,i}} + \frac{\alpha_\gamma(t)}{2\pi} Q_d^2 \left[\tilde{P}_{ff}^V \otimes f_{\bar{d}_{L,i}} + N_c \tilde{P}_{f_{LV_s}}^f \otimes f_{\gamma_{-s}} \right] \\
&+ \frac{\alpha_2(t)}{2\pi c_W^2(t)} \left(\frac{1}{2} + Q_d s_W^2(t) \right)^2 \left[\tilde{P}_{ff}^V \otimes f_{\bar{d}_{L,i}} + N_c \tilde{P}_{f_{LV_s}}^f \otimes f_{Z_{-s}} \right] \\
&+ \frac{\alpha_2(t)}{2\pi} \frac{1}{2} \left[\tilde{P}_{ff}^V \otimes f_{\bar{u}_{L,i}} + N_c \tilde{P}_{f_{LV_s}}^f \otimes f_{W_{-s}^+} \right] \\
&- \frac{\alpha_{\gamma 2}(t)}{2\pi} Q_d N_c \left(\frac{1}{2} + Q_d s_W^2(t) \right) \tilde{P}_{f_{LV_s}}^f \otimes f_{Z_{\gamma_{-s}}} \\
&+ \frac{\alpha_3(t)}{2\pi} \left[C_F \tilde{P}_{ff}^V \otimes f_{\bar{d}_{L,i}} + T_F \tilde{P}_{f_{LV_s}}^f \otimes f_{g_{-s}} \right] \\
&+ \tilde{U}_{\bar{d}_{L,\bar{u}_L}^-} \otimes f_{\bar{u}_{L,i}} + \tilde{U}_{\bar{d}_{L,W_L}^+} \otimes f_{W_L^+} + \tilde{U}_{\bar{d}_{L,\bar{d}_L}^{Z_L}} \otimes f_{\bar{d}_{L,i}} + \tilde{U}_{\bar{d}_{L,Z_L}^{d_L}} \otimes f_{Z_L} ,
\end{aligned} \tag{D.14}$$

$$\begin{aligned}
\frac{df_{b_L}}{dt} &= P_{b_L}^v f_{b_L} + \frac{\alpha_\gamma(t)}{2\pi} Q_d^2 \left[\tilde{P}_{ff}^V \otimes f_{b_L} + N_c \tilde{P}_{f_{LV_s}}^f \otimes f_{\gamma_s} \right] \\
&+ \frac{\alpha_2(t)}{2\pi c_W^2(t)} \left(\frac{1}{2} + Q_d s_W^2(t) \right)^2 \left[\tilde{P}_{ff}^V \otimes f_{b_L} + N_c \tilde{P}_{f_{LV_s}}^f \otimes f_{Z_s} \right] \\
&+ \frac{\alpha_2(t)}{2\pi} \frac{1}{2} \left[\tilde{P}_{ff}^V \otimes f_{t_L} + N_c \tilde{P}_{f_{LV_s}}^f \otimes f_{W_s^-} \right] \\
&- \frac{\alpha_{\gamma 2}(t)}{2\pi} Q_d N_c \left(\frac{1}{2} + Q_d s_W^2(t) \right) \tilde{P}_{f_{LV_s}}^f \otimes f_{Z_{\gamma_s}} \\
&+ \frac{\alpha_3(t)}{2\pi} \left[C_F \tilde{P}_{ff}^V \otimes f_{b_L} + T_F \tilde{P}_{f_{LV_s}}^f \otimes f_{g_s} \right] \\
&+ \frac{\alpha_y(t)}{2\pi} \left[\tilde{P}_{ff}^h \otimes f_{t_R} + N_c \tilde{P}_{f_{hL}}^f \otimes f_{W_L^-} \right] \\
&+ \tilde{U}_{b_{L,t_R}^{W^+}} \otimes f_{t_R} + \tilde{U}_{b_{L,W_L}^-} \otimes f_{W_L^-} \\
&+ \tilde{U}_{b_{L,t_L}^{W^+}} \otimes f_{t_L} + \tilde{U}_{b_{L,W_L}^-} \otimes f_{W_L^-} + \tilde{U}_{b_{L,b_L}^{Z_L}} \otimes f_{b_L} + \tilde{U}_{b_{L,Z_L}^{\bar{b}_L}} \otimes f_{Z_L} ,
\end{aligned} \tag{D.15}$$

$$\begin{aligned}
\frac{df_{\bar{b}_L}}{dt} &= P_{\bar{b}_L}^v f_{\bar{b}_L} + \frac{\alpha_\gamma(t)}{2\pi} Q_d^2 \left[\tilde{P}_{ff}^V \otimes f_{\bar{b}_L} + N_c \tilde{P}_{fLV_s}^f \otimes f_{\gamma_{-s}} \right] \\
&+ \frac{\alpha_2(t)}{2\pi c_W^2(t)} \left(\frac{1}{2} + Q_d s_W^2(t) \right)^2 \left[\tilde{P}_{ff}^V \otimes f_{\bar{b}_L} + N_c \tilde{P}_{fLV_s}^f \otimes f_{Z_{-s}} \right] \\
&+ \frac{\alpha_2(t)}{2\pi} \frac{1}{2} \left[\tilde{P}_{ff}^V \otimes f_{\bar{t}_L} + N_c \tilde{P}_{fLV_s}^f \otimes f_{W_{-s}^+} \right] \\
&- \frac{\alpha_{\gamma 2}(t)}{2\pi} Q_d N_c \left(\frac{1}{2} + Q_d s_W^2(t) \right) \tilde{P}_{fLV_s}^f \otimes f_{Z_{\gamma_{-s}}} \\
&+ \frac{\alpha_3(t)}{2\pi} \left[C_F \tilde{P}_{ff}^V \otimes f_{\bar{b}_L} + T_F \tilde{P}_{fLV_s}^f \otimes f_{g_{-s}} \right] \\
&+ \frac{\alpha_y(t)}{2\pi} \left[\tilde{P}_{ff}^h \otimes f_{\bar{t}_R} + N_c \tilde{P}_{fh}^f \otimes f_{W_L^+} \right] \\
&+ \tilde{U}_{\bar{b}_L \bar{t}_R}^{W^-} \otimes f_{\bar{t}_R} + \tilde{U}_{\bar{b}_L W^+}^{tR} \otimes f_{W^+} \\
&+ \tilde{U}_{\bar{b}_L \bar{t}_L}^{W^-} \otimes f_{\bar{t}_L} + \tilde{U}_{\bar{b}_L W_L^+}^{tL} \otimes f_{W_L^+} + \tilde{U}_{\bar{b}_L \bar{b}_L}^{Z_L} \otimes f_{\bar{b}_L} + \tilde{U}_{\bar{b}_L Z_L}^{tL} \otimes f_{Z_L} ,
\end{aligned} \tag{D.16}$$

$$\begin{aligned}
\frac{df_{u_{R,i}}}{dt} &= P_{u_{R,i}}^v f_{u_{R,i}} + \frac{\alpha_\gamma(t)}{2\pi} Q_u^2 \left[\tilde{P}_{ff}^V \otimes f_{u_{R,i}} + N_c \tilde{P}_{fLV_s}^f \otimes f_{\gamma_{-s}} \right] \\
&+ \frac{\alpha_2(t)}{2\pi c_W^2(t)} Q_u^2 s_W^4(t) \left[\tilde{P}_{ff}^V \otimes f_{u_{R,i}} + N_c \tilde{P}_{fLV_s}^f \otimes f_{Z_{-s}} \right] \\
&- N_c \frac{\alpha_{\gamma 2}(t)}{2\pi c_W(t)} Q_u^2 s_W^2(t) \tilde{P}_{fLV_s}^f \otimes f_{Z_{\gamma_{-s}}} \\
&+ \frac{\alpha_3(t)}{2\pi} \left[C_F \tilde{P}_{ff}^V \otimes f_{u_{R,i}} + T_F \tilde{P}_{fLV_s}^f \otimes f_{g_{-s}} \right] \\
&+ \tilde{U}_{u_R u_R}^{Z_L} \otimes f_{u_{R,i}} + \tilde{U}_{u_R Z_L}^{\bar{u}R} \otimes f_{Z_L} ,
\end{aligned} \tag{D.17}$$

$$\begin{aligned}
\frac{df_{\bar{u}_{R,i}}}{dt} &= P_{\bar{u}_{R,i}}^v f_{\bar{u}_{R,i}} + \frac{\alpha_\gamma(t)}{2\pi} Q_u^2 \left[\tilde{P}_{ff}^V \otimes f_{\bar{u}_{R,i}} + N_c \tilde{P}_{fLV_s}^f \otimes f_{\gamma_s} \right] \\
&+ \frac{\alpha_2(t)}{2\pi c_W^2(t)} Q_u^2 s_W^4(t) \left[\tilde{P}_{ff}^V \otimes f_{\bar{u}_{R,i}} + N_c \tilde{P}_{fLV_s}^f \otimes f_{Z_s} \right] \\
&- N_c \frac{\alpha_{\gamma 2}(t)}{2\pi c_W(t)} Q_u^2 s_W^2(t) \tilde{P}_{fLV_s}^f \otimes f_{Z_{\gamma_s}} \\
&+ \frac{\alpha_3(t)}{2\pi} \left[C_F \tilde{P}_{ff}^V \otimes f_{\bar{u}_{R,i}} + T_F \tilde{P}_{fLV_s}^f \otimes f_{g_s} \right] \\
&+ \tilde{U}_{\bar{u}_R \bar{u}_R}^{Z_L} \otimes f_{\bar{u}_{R,i}} + \tilde{U}_{\bar{u}_R Z_L}^{uR} \otimes f_{Z_L} ,
\end{aligned} \tag{D.18}$$

$$\begin{aligned}
\frac{df_{t_R}}{dt} &= P_{t_R}^v f_{t_R} + \frac{\alpha_\gamma(t)}{2\pi} Q_u^2 \left[\tilde{P}_{ff}^V \otimes f_{t_R} + N_c \tilde{P}_{f_L V_s}^f \otimes f_{\gamma-s} \right] \\
&+ \frac{\alpha_2(t)}{2\pi c_W^2(t)} Q_u^2 s_W^4(t) \left[\tilde{P}_{ff}^V \otimes f_{t_R} + N_c \tilde{P}_{f_L V_s}^f \otimes f_{Z-s} \right] \\
&- N_c \frac{\alpha_{\gamma 2}(t)}{2\pi c_W(t)} Q_u^2 s_W^2(t) \tilde{P}_{f_L V_s}^f \otimes f_{Z\gamma-s} \\
&+ \frac{\alpha_3(t)}{2\pi} \left[C_F \tilde{P}_{ff}^V \otimes f_{t_R} + T_F \tilde{P}_{f_L V_s}^f \otimes f_{g-s} \right] \\
&+ \frac{\alpha_y(t)}{2\pi} \left[\tilde{P}_{ff}^h \otimes \left(\frac{f_{t_L}^{(h)} + f_{t_L}^{(Z_L)}}{2} + f_{b_L} \right) + N_c \tilde{P}_{fh}^f \otimes \left(\frac{f_h + f_{Z_L} - f_{hZ_L}}{2} + f_{W_L^+} \right) \right] \\
&+ \tilde{U}_{tt}^g \otimes f_{t_L} + \tilde{U}_{tg}^t \otimes f_{g_+} \\
&+ \tilde{U}_{tt}^\gamma \otimes f_{t_L} + \tilde{U}_{t\gamma}^t \otimes f_{\gamma_+} + \tilde{U}_{t_R t_L}^{Z-} \otimes f_{t_L} + \tilde{U}_{t_R Z_+}^{\bar{t}L} \otimes f_{Z_+} + \tilde{U}_{t_R Z/\gamma_+}^{\bar{t}L} \otimes f_{Z/\gamma_+} \\
&+ \tilde{U}_{t_R b_L}^{W-} \otimes f_{b_L} + \tilde{U}_{t_R W_+}^{\bar{b}L} \otimes f_{W_+} \\
&+ \tilde{U}_{t_R t_R}^{Z_L} \otimes f_{t_R} + \tilde{U}_{t_R Z_L}^{\bar{t}R} \otimes f_{Z_L} + \tilde{U}_{tt}^h \otimes f_{t_R} + \tilde{U}_{th}^t \otimes f_h + \tilde{U}_{t_R h Z_L}^{\bar{t}R} \otimes f_{hZ_L} ,
\end{aligned} \tag{D.19}$$

$$\begin{aligned}
\frac{df_{\bar{t}_R}}{dt} &= P_{\bar{t}_R}^v f_{\bar{t}_R} + \frac{\alpha_\gamma(t)}{2\pi} Q_u^2 \left[\tilde{P}_{ff}^V \otimes f_{\bar{t}_R} + N_c \tilde{P}_{f_L V_s}^f \otimes f_{\gamma_s} \right] \\
&+ \frac{\alpha_2(t)}{2\pi c_W^2(t)} Q_u^2 s_W^4(t) \left[\tilde{P}_{ff}^V \otimes f_{\bar{t}_R} + N_c \tilde{P}_{f_L V_s}^f \otimes f_{Z_s} \right] \\
&- N_c \frac{\alpha_{\gamma 2}(t)}{2\pi c_W(t)} Q_u^2 s_W^2(t) \tilde{P}_{f_L V_s}^f \otimes f_{Z\gamma_s} \\
&+ \frac{\alpha_3(t)}{2\pi} \left[C_F \tilde{P}_{ff}^V \otimes f_{\bar{t}_R} + T_F \tilde{P}_{f_L V_s}^f \otimes f_{g_s} \right] \\
&+ \frac{\alpha_y(t)}{2\pi} \left[\tilde{P}_{ff}^h \otimes \left(\frac{f_{\bar{t}_L}^{(h)} + f_{\bar{t}_L}^{(Z_L)}}{2} + f_{\bar{b}_L} \right) + N_c \tilde{P}_{fh}^f \otimes \left(\frac{f_h + f_{Z_L} + f_{hZ_L}}{2} + f_{W_L^-} \right) \right] \\
&+ \tilde{U}_{tt}^g \otimes f_{\bar{t}_L} + \tilde{U}_{tg}^t \otimes f_{g_-} \\
&+ \tilde{U}_{tt}^\gamma \otimes f_{\bar{t}_L} + \tilde{U}_{t\gamma}^t \otimes f_{\gamma_-} + \tilde{U}_{\bar{t}_R \bar{t}_L}^{Z+} \otimes f_{\bar{t}_L} + \tilde{U}_{\bar{t}_R Z_-}^{\bar{t}L} \otimes f_{Z_-} + \tilde{U}_{\bar{t}_R Z/\gamma_-}^{\bar{t}L} \otimes f_{Z/\gamma_-} \\
&+ \tilde{U}_{\bar{t}_R \bar{b}_L}^{W+} \otimes f_{\bar{b}_L} + \tilde{U}_{\bar{t}_R W_-}^{\bar{b}L} \otimes f_{W_-} \\
&+ \tilde{U}_{\bar{t}_R \bar{t}_R}^{Z_L} \otimes f_{\bar{t}_R} + \tilde{U}_{\bar{t}_R Z_L}^{\bar{t}R} \otimes f_{Z_L} + \tilde{U}_{tt}^h \otimes f_{\bar{t}_R} + \tilde{U}_{th}^t \otimes f_h + \tilde{U}_{\bar{t}_R h Z_L}^{\bar{t}R} \otimes f_{hZ_L} ,
\end{aligned} \tag{D.20}$$

$$\begin{aligned}
\frac{df_{d_{R,i}}}{dt} &= P_{d_{R,i}}^v f_{d_{R,i}} + \frac{\alpha_\gamma(t)}{2\pi} Q_d^2 \left[\tilde{P}_{ff}^V \otimes f_{d_{R,i}} + N_c \tilde{P}_{f_L V_s}^f \otimes f_{\gamma-s} \right] \\
&+ \frac{\alpha_2(t)}{2\pi c_W^2(t)} Q_d^2 s_W^4(t) \left[\tilde{P}_{ff}^V \otimes f_{d_{R,i}} + N_c \tilde{P}_{f_L V_s}^f \otimes f_{Z-s} \right] \\
&- N_c \frac{\alpha_\gamma 2(t)}{2\pi c_W(t)} Q_d^2 s_W^2(t) \tilde{P}_{f_L V_s}^f \otimes f_{Z\gamma-s} \\
&+ \frac{\alpha_3(t)}{2\pi} \left[C_F \tilde{P}_{ff}^V \otimes f_{d_{R,i}} + T_F \tilde{P}_{f_L V_s}^f \otimes f_{g-s} \right] \\
&+ \tilde{U}_{d_R d_R}^{Z_L} \otimes f_{d_{R,i}} + \tilde{U}_{d_R Z_L}^{\bar{d}_R} \otimes f_{Z_L},
\end{aligned} \tag{D.21}$$

$$\begin{aligned}
\frac{df_{\bar{d}_{R,i}}}{dt} &= P_{\bar{d}_{R,i}}^v f_{\bar{d}_{R,i}} + \frac{\alpha_\gamma(t)}{2\pi} Q_d^2 \left[\tilde{P}_{ff}^V \otimes f_{\bar{d}_{R,i}} + N_c \tilde{P}_{f_L V_s}^f \otimes f_{\gamma_s} \right] \\
&+ \frac{\alpha_2(t)}{2\pi c_W^2(t)} Q_d^2 s_W^4(t) \left[\tilde{P}_{ff}^V \otimes f_{\bar{d}_{R,i}} + N_c \tilde{P}_{f_L V_s}^f \otimes f_{Z_s} \right] \\
&- N_c \frac{\alpha_\gamma 2(t)}{2\pi c_W(t)} Q_d^2 s_W^2(t) \tilde{P}_{f_L V_s}^f \otimes f_{Z\gamma_s} \\
&+ \frac{\alpha_3(t)}{2\pi} \left[C_F \tilde{P}_{ff}^V \otimes f_{\bar{d}_{R,i}} + T_F \tilde{P}_{f_L V_s}^f \otimes f_{g_s} \right] \\
&+ \tilde{U}_{\bar{d}_R \bar{d}_R}^{Z_L} \otimes f_{\bar{d}_{R,i}} + \tilde{U}_{\bar{d}_R Z_L}^{\bar{d}_R} \otimes f_{Z_L}.
\end{aligned} \tag{D.22}$$

D.3 Transverse gauge bosons

$$\begin{aligned}
\frac{df_{g_+}}{dt} &= P_{g_+}^v f_{g_+} + \frac{\alpha_3(t)}{2\pi} \left[C_A^{(3)} P_{V_+ V_s}^V \otimes f_{g_s} + C_F^{(3)} \tilde{P}_{V_+ f_L}^f \otimes \sum_i (f_{u_{L,i}} + f_{d_{L,i}} + f_{\bar{u}_{R,i}} + f_{\bar{d}_{R,i}}) \right. \\
&\left. + C_F^{(3)} \tilde{P}_{V_- f_L}^f \otimes \sum_i (f_{u_{R,i}} + f_{d_{R,i}} + f_{\bar{u}_{L,i}} + f_{\bar{d}_{L,i}}) \right] + \tilde{U}_{gt}^t \otimes (f_{t_R} + f_{\bar{t}_L}),
\end{aligned} \tag{D.23}$$

$$\begin{aligned}
\frac{df_{g_-}}{dt} &= P_{g_-}^v f_{g_-} + \frac{\alpha_3(t)}{2\pi} \left[C_A^{(3)} P_{V_- V_s}^V \otimes f_{g_s} + C_F^{(3)} \tilde{P}_{V_- f_L}^f \otimes \sum_i (f_{u_{L,i}} + f_{d_{L,i}} + f_{\bar{u}_{R,i}} + f_{\bar{d}_{R,i}}) \right. \\
&\left. + C_F^{(3)} \tilde{P}_{V_+ f_L}^f \otimes \sum_i (f_{u_{R,i}} + f_{d_{R,i}} + f_{\bar{u}_{L,i}} + f_{\bar{d}_{L,i}}) \right] + \tilde{U}_{gt}^t \otimes (f_{t_L} + f_{\bar{t}_R}),
\end{aligned} \tag{D.24}$$

$$\begin{aligned}
\frac{df_{\gamma_+}}{dt} &= P_{\gamma_+}^v f_{\gamma_+} + \frac{\alpha_\gamma(t)}{2\pi} \tilde{P}_{V_+ V_s}^V \otimes (f_{W_s^+} + f_{W_s^-}) + \frac{\alpha_\gamma(t)}{2\pi} \tilde{P}_{V_+ h}^h \otimes (f_{W_L^+} + f_{W_L^-}) \\
&+ \frac{\alpha_\gamma(t)}{2\pi} \sum_f Q_f^2 \left[\tilde{P}_{V_+ f_L}^f \otimes (f_{f_L} + f_{\bar{f}_R}) + \tilde{P}_{V_- f_L}^f \otimes (f_{f_R} + f_{\bar{f}_L}) \right] \\
&+ \tilde{U}_{\gamma t}^t \otimes (f_{t_R} + f_{\bar{t}_L}) + \tilde{U}_{\gamma T W_T}^{W_L} \otimes (f_{W_+^+} + f_{W_+^-}) + \tilde{U}_{\gamma T W_L}^{W_T} \otimes (f_{W_L^+} + f_{W_L^-}),
\end{aligned} \tag{D.25}$$

$$\begin{aligned}
\frac{df_{\gamma_-}}{dt} &= P_{\gamma_-}^v f_{\gamma_-} + \frac{\alpha_\gamma(t)}{2\pi} \tilde{P}_{V_- V_s}^V \otimes (f_{W_s^+} + f_{W_s^-}) + \frac{\alpha_\gamma(t)}{2\pi} \tilde{P}_{V_- h}^h \otimes (f_{W_L^+} + f_{W_L^-}) \\
&+ \frac{\alpha_\gamma(t)}{2\pi} \sum_f Q_f^2 \left[\tilde{P}_{V_- f_L}^f \otimes (f_{f_L} + f_{\bar{f}_R}) + \tilde{P}_{V_+ f_L}^f \otimes (f_{f_R} + f_{\bar{f}_L}) \right] \\
&+ \tilde{U}_{\gamma t}^t \otimes (f_{t_L} + f_{\bar{t}_R}) + \tilde{U}_{\gamma T W_T}^{W_L} \otimes (f_{W_-^+} + f_{W_-^-}) + \tilde{U}_{\gamma T W_L}^{W_T} \otimes (f_{W_L^+} + f_{W_L^-}),
\end{aligned} \tag{D.26}$$

$$\begin{aligned}
\frac{df_{Z_+}}{dt} &= P_{Z_+}^v f_{Z_+} + \frac{\alpha_2(t)}{2\pi} c_W^2(t) \tilde{P}_{V_+V_s}^V \otimes (f_{W_s^+} + f_{W_s^-}) \\
&+ \frac{\alpha_2(t)}{2\pi} \frac{c_{2W}^2}{4c_W^2} \tilde{P}_{V_+h}^h \otimes (f_{W_L^+} + f_{W_L^-}) + \frac{\alpha_2(t)}{2\pi} \frac{1}{4c_W^2} \tilde{P}_{V_+h}^h \otimes (f_h + f_{Z_L}) \\
&+ \frac{\alpha_2(t)}{2\pi c_W^2} \sum_f \left[\tilde{P}_{V_+f_L}^f \otimes (Z_{f_L}^2 f_{f_L} + Z_{f_R}^2 f_{f_R}) + \tilde{P}_{V_-f_L}^f \otimes (Z_{f_R}^2 f_{f_R} + Z_{f_L}^2 f_{f_L}) \right] \quad (D.27) \\
&+ \tilde{U}_{Z_+t_R}^{tL} \otimes f_{t_R} + \tilde{U}_{Z_-t_L}^{tR} \otimes f_{t_L} \\
&+ \tilde{U}_{Z_T W_T}^{W_L} \otimes (f_{W_+^+} + f_{W_+^-}) + \tilde{U}_{Z_T W_L}^{W_T} \otimes (f_{W_L^+} + f_{W_L^-}) \\
&+ \tilde{U}_{Z_T Z_T}^h \otimes f_{Z_+} + \tilde{U}_{Z_T h}^{Z_T} \otimes f_h,
\end{aligned}$$

$$\begin{aligned}
\frac{df_{Z_-}}{dt} &= P_{Z_-}^v f_{Z_-} + \frac{\alpha_2(t)}{2\pi} c_W^2(t) \tilde{P}_{V_-V_s}^V \otimes (f_{W_s^+} + f_{W_s^-}) \\
&+ \frac{\alpha_2(t)}{2\pi} \frac{c_{2W}^2}{4c_W^2} \tilde{P}_{V_-h}^h \otimes (f_{W_L^+} + f_{W_L^-}) + \frac{\alpha_2(t)}{2\pi} \frac{1}{4c_W^2} \tilde{P}_{V_-h}^h \otimes (f_h + f_{Z_L}) \\
&+ \frac{\alpha_2(t)}{2\pi c_W^2} \sum_f \left[\tilde{P}_{V_-f_L}^f \otimes (Z_{f_L}^2 f_{f_L} + Z_{f_R}^2 f_{f_R}) + \tilde{P}_{V_+f_L}^f \otimes (Z_{f_R}^2 f_{f_R} + Z_{f_L}^2 f_{f_L}) \right] \quad (D.28) \\
&+ \tilde{U}_{Z_-t_L}^{tR} \otimes f_{t_L} + \tilde{U}_{Z_+t_R}^{tL} \otimes f_{t_R} \\
&+ \tilde{U}_{Z_T W_T}^{W_L} \otimes (f_{W_+^+} + f_{W_+^-}) + \tilde{U}_{Z_T W_L}^{W_T} \otimes (f_{W_L^+} + f_{W_L^-}) \\
&+ \tilde{U}_{Z_T Z_T}^h \otimes f_{Z_-} + \tilde{U}_{Z_T h}^{Z_T} \otimes f_h,
\end{aligned}$$

$$\begin{aligned}
\frac{df_{Z\gamma_+}}{dt} &= \frac{\alpha_{\gamma 2}(t)}{2\pi} 2c_W(t) \tilde{P}_{V_+V_s}^V \otimes (f_{W_s^+} + f_{W_s^-}) + \frac{\alpha_{\gamma 2}(t)}{2\pi} \frac{c_{2W}(t)}{c_W(t)} \tilde{P}_{V_+h}^h \otimes (f_{W_L^+} + f_{W_L^-}) \\
&+ \frac{\alpha_{\gamma 2}(t)}{2\pi} \frac{2}{c_W(t)} \sum_f Q_f \left[\tilde{P}_{V_+f_L}^f \otimes (Z_{f_L} f_{f_L} + Z_{f_R} f_{f_R}) + \tilde{P}_{V_-f_L}^f \otimes (Z_{f_R} f_{f_R} + Z_{f_L} f_{f_L}) \right] \\
&+ \tilde{U}_{Z/\gamma_+t_R}^{tL} \otimes f_{t_R} + \tilde{U}_{Z/\gamma_-t_L}^{tR} \otimes f_{t_L} \\
&+ \tilde{U}_{Z/\gamma_T W_T}^{W_L} \otimes (f_{W_+^+} + f_{W_+^-}) + \tilde{U}_{Z/\gamma_T W_L}^{W_T} \otimes (f_{W_L^+} + f_{W_L^-}), \quad (D.29)
\end{aligned}$$

$$\begin{aligned}
\frac{df_{Z\gamma_-}}{dt} &= \frac{\alpha_{\gamma 2}(t)}{2\pi} 2c_W(t) \tilde{P}_{V_-V_s}^V \otimes (f_{W_s^+} + f_{W_s^-}) + \frac{\alpha_{\gamma 2}(t)}{2\pi} \frac{c_{2W}(t)}{c_W(t)} \tilde{P}_{V_-h}^h \otimes (f_{W_L^+} + f_{W_L^-}) \\
&+ \frac{\alpha_{\gamma 2}(t)}{2\pi} \frac{2}{c_W(t)} \sum_f Q_f \left[\tilde{P}_{V_-f_L}^f \otimes (Z_{f_L} f_{f_L} + Z_{f_R} f_{f_R}) + \tilde{P}_{V_+f_L}^f \otimes (Z_{f_R} f_{f_R} + Z_{f_L} f_{f_L}) \right] \\
&+ \tilde{U}_{Z/\gamma_-t_L}^{tR} \otimes f_{t_L} + \tilde{U}_{Z/\gamma_+t_R}^{tL} \otimes f_{t_R} \\
&+ \tilde{U}_{Z/\gamma_T W_T}^{W_L} \otimes (f_{W_+^+} + f_{W_+^-}) + \tilde{U}_{Z/\gamma_T W_L}^{W_T} \otimes (f_{W_L^+} + f_{W_L^-}), \quad (D.30)
\end{aligned}$$

$$\begin{aligned}
\frac{df_{W_+^+}}{dt} &= P_{W_+^+}^v f_{W_+^+} + \frac{\alpha_2(t)}{2\pi} c_W^2(t) \tilde{P}_{V_+V_s}^V \otimes (f_{W_s^+} + f_{Z_s}) + \frac{\alpha_\gamma(t)}{2\pi} \tilde{P}_{V_+V_s}^V \otimes (f_{W_s^+} + f_{\gamma_s}) \\
&+ \frac{\alpha_{\gamma 2}(t)}{2\pi} c_W(t) \tilde{P}_{V_+V_s}^V \otimes f_{Z\gamma_s} + \frac{\alpha_2(t)}{2\pi} \frac{1}{4} \tilde{P}_{V_+h}^h \otimes (f_h + f_{Z_L} + f_{hZ_L} + f_{W_L^+}^{(h)} + f_{W_L^+}^{(Z_L)}) \\
&+ \frac{\alpha_2(t)}{2\pi} \frac{1}{2} \sum_i \left[\tilde{P}_{V_+f_L}^f \otimes (f_{u_{L,i}} + f_{\nu_i}) + \tilde{P}_{V_-f_L}^f \otimes (f_{\bar{d}_{L,i}} + f_{\bar{\ell}_{L,i}}) \right] \\
&+ \tilde{U}_{W_+^+t_R}^{bL} \otimes f_{t_R} + \tilde{U}_{W_-^+b_L}^{tR} \otimes f_{b_L} \\
&+ \left(\tilde{U}_{W_T W_L}^{\gamma T} + \tilde{U}_{W_T W_L}^{Z T} \right) \otimes f_{W_L^+} + \left(\tilde{U}_{W_T W_T}^h + \tilde{U}_{W_T W_T}^{Z L} \right) \otimes f_{W_+^+} \\
&+ \tilde{U}_{W_T \gamma T}^{W_L} \otimes f_{\gamma_+} + \tilde{U}_{W_T Z T}^{W_L} \otimes f_{Z_+} + \tilde{U}_{W_T Z \gamma T}^{W_L} \otimes f_{Z\gamma_+} \\
&+ \tilde{U}_{W_T h}^{W_T} \otimes f_h + \tilde{U}_{W_T Z_L}^{W_T} \otimes f_{Z_L} + \tilde{U}_{W_T h Z_L}^{W_T} \otimes f_{hZ_L} ,
\end{aligned} \tag{D.31}$$

$$\begin{aligned}
\frac{df_{W_-^+}}{dt} &= P_{W_-^+}^v f_{W_-^+} + \frac{\alpha_2(t)}{2\pi} c_W^2(t) \tilde{P}_{V_-V_s}^V \otimes (f_{W_s^+} + f_{Z_s}) + \frac{\alpha_\gamma(t)}{2\pi} \tilde{P}_{V_-V_s}^V \otimes (f_{W_s^+} + f_{\gamma_s}) \\
&+ \frac{\alpha_{\gamma 2}(t)}{2\pi} c_W(t) \tilde{P}_{V_-V_s}^V \otimes f_{Z\gamma_s} + \frac{\alpha_2(t)}{2\pi} \frac{1}{4} \tilde{P}_{V_-h}^h \otimes (f_h + f_{Z_L} + f_{hZ_L} + f_{W_L^+}^{(h)} + f_{W_L^+}^{(Z_L)}) \\
&+ \frac{\alpha_2(t)}{2\pi} \frac{1}{2} \sum_i \left[\tilde{P}_{V_-f_L}^f \otimes (f_{u_{L,i}} + f_{\nu_i}) + \tilde{P}_{V_+f_L}^f \otimes (f_{\bar{d}_{L,i}} + f_{\bar{\ell}_{L,i}}) \right] \\
&+ \left(\tilde{U}_{W_T W_L}^{\gamma T} + \tilde{U}_{W_T W_L}^{Z T} \right) \otimes f_{W_L^+} + \left(\tilde{U}_{W_T W_T}^h + \tilde{U}_{W_T W_T}^{Z L} \right) \otimes f_{W_-^+} \\
&+ \tilde{U}_{W_T \gamma T}^{W_L} \otimes f_{\gamma_-} + \tilde{U}_{W_T Z T}^{W_L} \otimes f_{Z_-} + \tilde{U}_{W_T Z \gamma T}^{W_L} \otimes f_{Z\gamma_-} \\
&+ \tilde{U}_{W_T h}^{W_T} \otimes f_h + \tilde{U}_{W_T Z_L}^{W_T} \otimes f_{Z_L} + \tilde{U}_{W_T h Z_L}^{W_T} \otimes f_{hZ_L} ,
\end{aligned} \tag{D.32}$$

$$\begin{aligned}
\frac{df_{W_+^-}}{dt} &= P_{W_+^-}^v f_{W_+^-} + \frac{\alpha_2(t)}{2\pi} c_W^2(t) \tilde{P}_{V_+V_s}^V \otimes (f_{W_s^-} + f_{Z_s}) + \frac{\alpha_\gamma(t)}{2\pi} \tilde{P}_{V_+V_s}^V \otimes (f_{W_s^-} + f_{\gamma_s}) \\
&+ \frac{\alpha_{\gamma 2}(t)}{2\pi} c_W(t) \tilde{P}_{V_+V_s}^V \otimes f_{Z\gamma_s} + \frac{\alpha_2(t)}{2\pi} \frac{1}{4} \tilde{P}_{V_+h}^h \otimes (f_h + f_{Z_L} - f_{hZ_L} + f_{W_L^-}^{(h)} + f_{W_L^-}^{(Z_L)}) \\
&+ \frac{\alpha_2(t)}{2\pi} \frac{1}{2} \sum_i \left[\tilde{P}_{V_+f_L}^f \otimes (f_{d_{L,i}} + f_{\ell_{L,i}}) + \tilde{P}_{V_-f_L}^f \otimes (f_{\bar{u}_{L,i}} + f_{\bar{\nu}_i}) \right] \\
&+ \left(\tilde{U}_{W_T W_L}^{\gamma T} + \tilde{U}_{W_T W_L}^{Z T} \right) \otimes f_{W_L^-} + \left(\tilde{U}_{W_T W_T}^h + \tilde{U}_{W_T W_T}^{Z L} \right) \otimes f_{W_+^-} \\
&+ \tilde{U}_{W_T \gamma T}^{W_L} \otimes f_{\gamma_+} + \tilde{U}_{W_T Z T}^{W_L} \otimes f_{Z_+} + \tilde{U}_{W_T Z \gamma T}^{W_L} \otimes f_{Z\gamma_+} \\
&+ \tilde{U}_{W_T h}^{W_T} \otimes f_h + \tilde{U}_{W_T Z_L}^{W_T} \otimes f_{Z_L} - \tilde{U}_{W_T h Z_L}^{W_T} \otimes f_{hZ_L} ,
\end{aligned} \tag{D.33}$$

$$\begin{aligned}
\frac{df_{W_-^-}}{dt} &= P_{W_-^-}^v f_{W_-^-} + \frac{\alpha_2(t)}{2\pi} c_W^2(t) \tilde{P}_{V_{-}V_s}^V \otimes (f_{W_s^-} + f_{Z_s}) + \frac{\alpha_\gamma(t)}{2\pi} \tilde{P}_{V_{-}V_s}^V \otimes (f_{W_s^-} + f_{\gamma_s}) \\
&+ \frac{\alpha_{\gamma 2}(t)}{2\pi} c_W(t) \tilde{P}_{V_{-}V_s}^V \otimes f_{Z_{\gamma_s}} + \frac{\alpha_2(t)}{2\pi} \frac{1}{4} \tilde{P}_{V_{-}h}^h \otimes (f_h + f_{Z_L} - f_{hZ_L} + f_{W_L^{(h)}} + f_{W_L^{(Z_L)}}) \\
&+ \frac{\alpha_2(t)}{2\pi} \frac{1}{2} \sum_i \left[\tilde{P}_{V_{-}f_L}^f \otimes (f_{d_{L,i}} + f_{\ell_{L,i}}) + \tilde{P}_{V_{+}f_L}^f \otimes (f_{\bar{u}_{L,i}} + f_{\bar{\nu}_i}) \right] \\
&+ \tilde{P}_{W_-^-b_L}^{t_R} \otimes f_{b_L} + \tilde{P}_{W_+^+t_R}^{b_L} \otimes f_{t_R} \\
&+ \left(\tilde{U}_{W_T W_L}^{\gamma T} + \tilde{U}_{W_T W_L}^{Z T} \right) \otimes f_{W_L^-} + \left(\tilde{U}_{W_T W_T}^h + \tilde{U}_{W_T W_T}^{Z L} \right) \otimes f_{W_-} \\
&+ \tilde{U}_{W_T \gamma T}^{W_L} \otimes f_{\gamma_-} + \tilde{U}_{W_T Z T}^{W_L} \otimes f_{Z_-} + \tilde{U}_{W_T Z \gamma T}^{W_L} \otimes f_{Z \gamma_-} \\
&+ \tilde{U}_{W_T h}^{W_T} \otimes f_h + \tilde{U}_{W_T Z_L}^{W_T} \otimes f_{Z_L} - \tilde{U}_{W_T h Z_L}^{W_T} \otimes f_{h Z_L} .
\end{aligned} \tag{D.34}$$

D.4 Higgs and longitudinal gauge bosons

$$\begin{aligned}
\frac{df_h}{dt} &= P_h^v f_h + \frac{\alpha_2(t)}{2\pi} \frac{1}{4} \left[\tilde{P}_{hh}^V \otimes (f_{W_+^+} + f_{W_-^-}) + \tilde{P}_{hV}^h \otimes (f_{W_+^+} + f_{W_-^-} + f_{W_+^-} + f_{W_-^+}) \right] \\
&+ \frac{\alpha_2(t)}{2\pi} \frac{1}{4c_W^2} \left[\tilde{P}_{hh}^V \otimes f_{Z_L} + \tilde{P}_{hV}^h \otimes (f_{Z_+} + f_{Z_-}) \right] \\
&+ \frac{\alpha_y(t)}{2\pi} \frac{1}{2} \tilde{P}_{hf}^f \otimes (f_{t_L} + f_{t_R} + f_{\bar{t}_L} + f_{\bar{t}_R}) \\
&+ \tilde{U}_{ht}^t \otimes (f_{t_L} + f_{t_R} + f_{\bar{t}_L} + f_{\bar{t}_R}) \\
&+ \tilde{U}_{hW_T}^{W_T} \otimes (f_{W_+^+} + f_{W_-^-} + f_{W_+^-} + f_{W_-^+}) + \tilde{U}_{hZ_T}^{Z T} \otimes (f_{Z_+} + f_{Z_-}) \\
&+ \tilde{U}_{hW_L}^{W_L} \otimes (f_{W_+^+} + f_{W_-^-}) + \tilde{U}_{hZ_L}^{Z L} \otimes f_{Z_L} + \tilde{U}_{hh}^h \otimes f_h ,
\end{aligned} \tag{D.35}$$

$$\begin{aligned}
\frac{df_{Z_L}}{dt} &= P_{Z_L}^v f_{Z_L} + \frac{\alpha_2(t)}{2\pi} \frac{1}{4} \left[\tilde{P}_{hh}^V \otimes (f_{W_+^+} + f_{W_-^-}) + \tilde{P}_{hV}^h \otimes (f_{W_+^+} + f_{W_-^-} + f_{W_+^-} + f_{W_-^+}) \right] \\
&+ \frac{\alpha_2(t)}{2\pi} \frac{1}{4c_W^2} \left[\tilde{P}_{hh}^V \otimes f_h + \tilde{P}_{hV}^h \otimes (f_{Z_+} + f_{Z_-}) \right] \\
&+ \frac{\alpha_y(t)}{2\pi} \frac{1}{2} \tilde{P}_{hf}^f \otimes (f_{t_L} + f_{t_R} + f_{\bar{t}_L} + f_{\bar{t}_R}) \\
&+ \sum_{f_L} \tilde{U}_{Z_L f_L}^{f_L} \otimes f_{f_L} + \sum_{f_R} \tilde{U}_{Z_L f_R}^{f_R} \otimes f_{f_R} \\
&+ \sum_{\bar{f}_L} \tilde{U}_{Z_L \bar{f}_L}^{\bar{f}_L} \otimes f_{\bar{f}_L} + \sum_{\bar{f}_R} \tilde{U}_{Z_L \bar{f}_R}^{\bar{f}_R} \otimes f_{\bar{f}_R} \\
&+ \tilde{U}_{Z_L W_T}^{W_T} \otimes (f_{W_+^+} + f_{W_-^-} + f_{W_+^-} + f_{W_-^+}) \\
&+ \tilde{U}_{Z_L Z_L}^h \otimes f_{Z_L} + \tilde{U}_{Z_L h}^{Z L} \otimes f_h + \tilde{U}_{Z_L W_L}^{W_L} \otimes (f_{W_+^+} + f_{W_-^-}) ,
\end{aligned} \tag{D.36}$$

$$\begin{aligned}
\frac{df_{W_L^+}}{dt} &= P_{W_L^+}^v f_{W_L^+} + \frac{\alpha_2(t)}{2\pi} \frac{1}{4} \left[\tilde{P}_{hh}^V \otimes (f_h + f_{Z_L} - f_{hZ_L}) + \tilde{P}_{hV}^h \otimes \left(f_{W_+^+}^{(h)} + f_{W_+^+}^{(Z_L)} + f_{W_-^+}^{(h)} + f_{W_-^+}^{(Z_L)} \right) \right] \\
&+ \frac{\alpha_2(t)}{2\pi} \frac{c_{2W}^2}{4c_W^2} \left[\tilde{P}_{hh}^V \otimes f_{W_L^+} + \tilde{P}_{hV}^h \otimes (f_{Z_+} + f_{Z_-}) \right] \\
&+ \frac{\alpha_\gamma(t)}{2\pi} \left[\tilde{P}_{hh}^V \otimes f_{W_L^+} + \tilde{P}_{hV}^h \otimes (f_{\gamma_+} + f_{\gamma_-}) \right] + \frac{\alpha_{\gamma 2}(t)}{2\pi} \frac{c_{2W}}{2c_W} \tilde{P}_{hV}^h \otimes (f_{Z\gamma_+} + f_{Z\gamma_-}) \\
&+ \frac{\alpha_y(t)}{2\pi} \tilde{P}_{hf}^f \otimes (f_{t_R} + f_{b_L}) \\
&+ \sum_{f_L^{(1)} f_L^{(2)}} \tilde{U}_{W_L^+ f_L^{(1)}}^{f_L^{(2)}} \otimes f_{f_L^{(1)}} + \sum_{\bar{f}_L^{(1)} \bar{f}_L^{(2)}} \tilde{U}_{W_L^+ \bar{f}_L^{(1)}}^{\bar{f}_L^{(2)}} \otimes f_{\bar{f}_L^{(1)}} \\
&+ \tilde{U}_{W_L W_T}^{\gamma_T} \otimes (f_{W_+^+} + f_{W_-^+}) + \tilde{U}_{W_L W_T}^{Z_T} \otimes (f_{W_+^+} + f_{W_-^+}) \\
&+ \tilde{U}_{W_L \gamma_T}^{W_T} \otimes (f_{\gamma_+} + f_{\gamma_-}) + \tilde{U}_{W_L Z_T}^{W_T} \otimes (f_{Z_+} + f_{Z_-}) \\
&+ \tilde{U}_{W_L Z\gamma_T}^{W_T} \otimes (f_{Z\gamma_+} + f_{Z\gamma_-}) \\
&+ \tilde{U}_{W_L h}^{W_L} \otimes f_h + \tilde{U}_{W_L Z_L}^{W_L} \otimes f_{Z_L} + \tilde{U}_{W_L h Z_L}^{W_L} \otimes f_{hZ_L} \\
&+ \tilde{U}_{W_L W_L}^h \otimes f_{W_L^+} + \tilde{U}_{W_L W_L}^{Z_L} \otimes f_{W_L^+} ,
\end{aligned} \tag{D.37}$$

$$\begin{aligned}
\frac{df_{W_L^-}}{dt} &= P_{W_L^-}^v f_{W_L^-} + \frac{\alpha_2(t)}{2\pi} \frac{1}{4} \left[\tilde{P}_{hh}^V \otimes (f_h + f_{Z_L} + f_{hZ_L}) + \tilde{P}_{hV}^h \otimes \left(f_{W_+^-}^{(h)} + f_{W_+^-}^{(Z_L)} + f_{W_-^-}^{(h)} + f_{W_-^-}^{(Z_L)} \right) \right] \\
&+ \frac{\alpha_2(t)}{2\pi} \frac{c_{2W}^2}{4c_W^2} \left[\tilde{P}_{hh}^V \otimes f_{W_L^-} + \tilde{P}_{hV}^h \otimes (f_{Z_+} + f_{Z_-}) \right] \\
&+ \frac{\alpha_\gamma(t)}{2\pi} \left[\tilde{P}_{hh}^V \otimes f_{W_L^-} + \tilde{P}_{hV}^h \otimes (f_{\gamma_+} + f_{\gamma_-}) \right] + \frac{\alpha_{\gamma 2}(t)}{2\pi} \frac{c_{2W}}{2c_W} \tilde{P}_{hV}^h \otimes (f_{Z\gamma_+} + f_{Z\gamma_-}) \\
&+ \frac{\alpha_y(t)}{2\pi} \tilde{P}_{hf}^f \otimes (f_{b_L} + f_{t_R}) \\
&+ \sum_{f_L^{(1)} f_L^{(2)}} \tilde{U}_{W_L^- f_L^{(1)}}^{f_L^{(2)}} \otimes f_{f_L^{(1)}} + \sum_{\bar{f}_L^{(1)} \bar{f}_L^{(2)}} \tilde{U}_{W_L^- \bar{f}_L^{(1)}}^{\bar{f}_L^{(2)}} \otimes f_{\bar{f}_L^{(1)}} \\
&+ \tilde{U}_{W_L W_T}^{\gamma_T} \otimes (f_{W_+^-} + f_{W_-^-}) + \tilde{U}_{W_L W_T}^{Z_T} \otimes (f_{W_+^-} + f_{W_-^-}) \\
&+ \tilde{U}_{W_L \gamma_T}^{W_T} \otimes (f_{\gamma_+} + f_{\gamma_-}) + \tilde{U}_{W_L Z_T}^{W_T} \otimes (f_{Z_+} + f_{Z_-}) \\
&+ \tilde{U}_{W_L Z\gamma_T}^{W_T} \otimes (f_{Z\gamma_+} + f_{Z\gamma_-}) \\
&+ \tilde{U}_{W_L h}^{W_L} \otimes f_h + \tilde{U}_{W_L Z_L}^{W_L} \otimes f_{Z_L} - \tilde{U}_{W_L h Z_L}^{W_L} \otimes f_{hZ_L} \\
&+ \tilde{U}_{W_L W_L}^h \otimes f_{W_L^-} + \tilde{U}_{W_L W_L}^{Z_L} \otimes f_{W_L^-} ,
\end{aligned} \tag{D.38}$$

$$\begin{aligned}
\frac{df_{hZ_L}}{dt} &= \frac{\alpha_y(t)}{2\pi} \tilde{P}_{hf}^f \otimes (f_{t_{L+}} + f_{\bar{t}_R} - f_{t_R} - f_{\bar{t}_L}) \\
&+ \frac{\alpha_2(t)}{2\pi} \frac{1}{4} \left[\tilde{P}_{hh}^V \otimes (f_{W_L^-} - f_{W_L^+}) + \tilde{P}_{hV}^h \otimes (f_{W_+^+} + f_{W_-^+} - f_{W_+^-} - f_{W_-^-}) \right] \\
&+ \tilde{U}_{hZ_L t_L}^{t_L} \otimes (f_{t_L} - f_{\bar{t}_L}) + \tilde{U}_{hZ_L t_R}^{t_R} \otimes (f_{t_R} - f_{\bar{t}_R}) \\
&+ \tilde{U}_{hZ_L W_L}^{W_L} \otimes (f_{W_L^+} - f_{W_L^-}) + \tilde{U}_{hZ_L W_T}^{W_T} \otimes (f_{W_+^+} + f_{W_-^+} - f_{W_+^-} - f_{W_-^-}) .
\end{aligned} \tag{D.39}$$

E Numerical implementation

Here we show the details of our numerical implementation of the DGLAP equations. We discretize the x -space from a minimum value x_0 up to 1 in N_x bins, $x_\alpha = \{x_0, x_1, \dots, x_{N_x} \equiv 1\}$, with spacing $\delta x_\alpha = x_\alpha - x_{\alpha-1}$. We choose a spacing that is denser near $x = 1$ and sparser at small values, in practice we set $x_\alpha = 10^{-6((N_x-\alpha)/N_x)^{2.5}}$ for $\alpha = 0, 1, \dots, N_x$ to get values from $x_0 = 10^{-6}$ to $x_{N_x} = 1$. This allows us to obtain a set of ODEs, where the integrals are computed using the rectangles method.⁸

For the non-divergent terms or when $z_{\max}^{ABC} \neq 1$ we obtain

$$\frac{df_B(x_\beta, t)}{dt} \supset \int_{x_\beta}^{z_{\max}^{ABC}} \frac{dz}{z} \tilde{P}_{BA}^C \left(\frac{x_\beta}{z} \right) f_A(z, t) = \sum_{\alpha=\beta+1}^{N_{\max}^{ABC}} \frac{\delta x_\alpha}{x_\alpha} \tilde{P}_{BA}^C \left(\frac{x_\beta}{x_\alpha} \right) f_A(x_\alpha, t), \tag{E.1}$$

where N_{\max}^{ABC} is the index of the greatest point of the grid which is smaller than z_{\max}^{ABC} . The remaining case is that of the splitting functions with the $+$ distribution, which we can write as

$$\tilde{P}_{BA}^C(z) = \frac{\tilde{D}_{BA}^C(z)}{(1-z)_+}. \tag{E.2}$$

Using the definition in Eq. (B.1) the corresponding terms in the DGLAP equations are:

$$\begin{aligned}
\frac{df_B(x_\beta, t)}{dt} &\supset \int_{x_\beta}^1 \frac{dy}{y(1-y)_+} \tilde{D}_{BA}^C(y) f_A \left(\frac{x_\beta}{y}, t \right) = \tilde{D}_{BA}^C(1) \log(1-x_\beta) f_A(x_\beta, t) \\
&+ \int_{x_\beta}^{z_{\max}^{ABC}} \frac{dy}{(1-y)} \left(\frac{\tilde{D}_{BA}^C(y) f_A \left(\frac{x_\beta}{y}, t \right)}{y} - \tilde{D}_{BA}^C(1) f_A(x_\beta, t) \right).
\end{aligned} \tag{E.3}$$

⁸Due to the use of the rectangles method, we note that special care should be taken when interpolating the LePDFs near the region of $x = 1$, where the muon PDF changes very steeply. In this case we recommend using zeroth order interpolation for consistency.

With our discretization, the last integral becomes

$$\begin{aligned}
& \int_{x_\beta}^1 \frac{dy}{(1-y)} \left(\frac{\tilde{D}_{BA}^C(y) f_A\left(\frac{x_\beta}{y}, t\right)}{y} - \tilde{D}_{BA}^C(1) f_A(x_\beta, t) \right) \\
&= \int_{x_\beta}^1 dz \frac{x_\beta}{z^2} \frac{1}{1-\frac{x_\beta}{z}} \left[\frac{z}{x_\beta} \tilde{D}_{BA}^C\left(\frac{x_\beta}{z}\right) f_A(z, t) - \tilde{D}_{BA}^C(1) f_A(x_\beta, t) \right] \\
&= \int_{x_\beta}^1 dz \left[\frac{1}{z \left(1-\frac{x_\beta}{z}\right)} \tilde{D}_{BA}^C\left(\frac{x_\beta}{z}\right) f_A(z, t) - \frac{x_\beta}{z^2} \frac{1}{1-\frac{x_\beta}{z}} \tilde{D}_{BA}^C(1) f_A(x_\beta, t) \right] \\
&= \sum_{\alpha=\beta+1}^{N_x} \frac{\delta x_\alpha}{x_\alpha} \tilde{P}_{BA}^C\left(\frac{x_\beta}{x_\alpha}\right) f_A(x_\alpha, t) - \tilde{D}_{BA}^C(1) f_A(x_\beta, t) x_\beta \sum_{\alpha=\beta+1}^{N_x} \frac{\delta x_\alpha}{x_\alpha^2} \frac{1}{1-\frac{x_\beta}{x_\alpha}} \\
&\equiv \sum_{\alpha=\beta+1}^{N_x} \frac{\delta x_\alpha}{x_\alpha} \tilde{P}_{BA}^C\left(\frac{x_\beta}{x_\alpha}\right) f_A(x_\alpha, t) - \tilde{D}_{BA}^C(1) X_\beta f_A(x_\beta, t) ,
\end{aligned} \tag{E.4}$$

where X_β is given by

$$X_\beta \equiv x_\beta \sum_{\alpha=\beta+1}^{N_x} \frac{\delta x_\alpha}{x_\alpha^2} \frac{1}{1-\frac{x_\beta}{x_\alpha}} . \tag{E.5}$$

With this discretization, starting with N_f PDFs we get a set of $(N_x + 1)N_f$ equations for the variables $f_{B\beta}(t) \equiv f_B(x_\beta, t)$, with $\beta = \{0, \dots, N_x\}$ and $B = \{1, \dots, N_f\}$

$$\begin{aligned}
\frac{df_{B\beta}(t)}{dt} &= P_B^v(t) f_{B\beta}(t) + \sum_{A,C} \frac{\alpha_{ABC}(t)}{2\pi} (\log(1-x_\beta) - X_\beta) \tilde{D}_{BA}^C(1) f_{A\beta} \\
&+ \sum_{A,C} \frac{\alpha_{ABC}(t)}{2\pi} \sum_{\alpha=\beta+1}^{N_{\max}^{ABC}} \frac{\delta x_\alpha}{x_\alpha} \tilde{P}_{BA}^C\left(\frac{x_\beta}{x_\alpha}\right) f_{A\alpha}(t) .
\end{aligned} \tag{E.6}$$

Once we have the equations with the proper initial conditions, we solve them numerically using a fourth order Runge-Kutta with integration step dt . For a set of equations of the form $y'_i(t) = F_i(t, y)$, starting with the solution $y_{i,n}$ at $t = t_n$ the step of the algorithm is

$$\begin{aligned}
k_{1,i} &= dt F_i(t_n, y_{i,n}) \\
k_{2,i} &= dt F_i\left(t_n + \frac{dt}{2}, y_{i,n} + \frac{k_{1,i}}{2}\right) \\
k_{3,i} &= dt F_i\left(t_n + \frac{dt}{2}, y_{i,n} + \frac{k_{2,i}}{2}\right) \\
k_{4,i} &= dt F_i(t_n + dt, y_{i,n} + k_{3,i}) \\
y_{i,n+1} &= y_{i,n} + \frac{k_{1,i}}{6} + \frac{k_{2,i}}{3} + \frac{k_{3,i}}{3} + \frac{k_{4,i}}{6} + \mathcal{O}(dt^5) .
\end{aligned} \tag{E.7}$$

We then reduce the number of variables imposing momentum conservation after every step of the evolution, since performing a numerical integration it will be more and more violated, as done in [34]. With our discretization Eq. (C.2) becomes

$$\sum_{i=1}^{N_f} \sum_{\alpha=1}^{N_x} \delta x_\alpha x_\alpha f_{i\alpha}(t) = 1 . \tag{E.8}$$

Since the initial conditions on PDFs are given by

$$f_\mu(0, x_\alpha) = \delta(1 - x_\alpha) = \frac{1}{\delta x_{N_x}} \delta_{\alpha N_x} , \quad f_{i \neq \mu}(0, x) = 0 , \quad (\text{E.9})$$

only $f_{\mu\alpha}$ will be nonzero for $\alpha = N_x$ throughout the evolution. Then we fix

$$f_{i N_x}(t) = \begin{cases} \frac{L(t)}{\delta x_{N_x}} & i = \mu \\ 0 & i \neq \mu \end{cases} , \quad (\text{E.10})$$

reducing by N_f the number of variables and solving the remaining equations. The factor $L(t)$ is computed using momentum conservation

$$1 = \sum_{i=1}^{N_f} \sum_{\alpha=1}^{N_x-1} \delta x_\alpha x_\alpha f_{i\alpha}(t) + L(t) , \quad (\text{E.11})$$

that is

$$L(t) = 1 - \sum_{i=1}^{N_f} \sum_{\alpha=1}^{N_x-1} \delta x_\alpha x_\alpha f_{i\alpha}(t) . \quad (\text{E.12})$$

The uncertainties due to the discretizations in x and t spaces are discussed in Section 4.6.

F LHAPDF format

We publish our numerical results in a format inspired by the LHAPDF6 [75] one used for proton PDFs. Some changes are required due to the polarisation of PDFs. The structure of the output is then as follows:

- the first three lines just specify the format;
- in the fourth and fifth line are reported respectively the grids in x and in Q (the grid in Q is a subset of the grid used in the numerical solution of the DGLAP equations);
- the next three lines report the particles' list as in Table 4: name, PDG ID (for the Z/γ and h/Z_L interference we join the PDG ID of the two states) and the additional label specifying the helicity (it is understood that for fermions or vectors it will be $\pm 1/2$ or ± 1 , respectively);
- in all the remaining lines we report the quantities $xf(x, Q)$: each column corresponds to a particle, following the order of the previous lines. We start at $x = x_0$ increasing Q at each row and repeating for each x , so that the data have the form reported in Table 5.

e_L	eL	11	-	d_L	dL	1	-	g_+	gp	21	+
e_R	eR	11	+	d_R	dR	1	+	g_-	gm	21	-
ν_e	nue	12	-	u_L	uL	2	-	γ_+	gap	22	+
μ_L	muL	13	-	u_R	uR	2	+	γ_-	gam	22	-
μ_R	muR	13	+	s_L	sL	3	-	Z_+	Zp	23	+
ν_μ	numu	14	-	s_R	sR	3	+	Z_-	Zm	23	-
τ_L	taL	15	-	c_L	cL	4	-	Z_L	ZL	23	0
τ_R	taR	15	+	c_R	cR	4	+	Z/γ_+	Zgap	2223	+
ν_τ	nuta	16	-	b_L	bL	5	-	Z/γ_-	Zgam	2223	-
\bar{e}_L	eLb	-11	+	b_R	bR	5	+	W_+^+	Wpp	24	+
\bar{e}_R	eRb	-11	-	t_L	tL	6	-	W_+^-	Wpm	24	-
$\bar{\nu}_e$	nueb	-12	+	t_R	tR	6	+	W_L^+	WpL	24	0
$\bar{\mu}_L$	muLb	-13	+	\bar{d}_L	dLb	-1	+	W_+^-	Wmp	-24	+
$\bar{\mu}_R$	muRb	-13	-	\bar{d}_R	dRb	-1	-	W_-^+	Wmp	-24	+
$\bar{\nu}_\mu$	numub	-14	+	\bar{u}_L	uLb	-2	+	W_-^-	Wmm	-24	-
$\bar{\tau}_L$	taLb	-15	+	\bar{u}_R	uRb	-2	-	W_L^-	WmL	-24	0
$\bar{\tau}_R$	taRb	-15	-	\bar{s}_L	sLb	-3	+	h	h	25	0
$\bar{\nu}_\tau$	nutab	-16	+	\bar{s}_R	sRb	-3	-	h/Z_L	hZL	2523	0
				\bar{c}_L	cLb	-4	+				
				\bar{c}_R	cRb	-4	-				
				\bar{b}_L	bLb	-5	+				
				\bar{b}_R	bRb	-5	-				
				\bar{t}_L	tLb	-6	+				
				\bar{t}_R	tRb	-6	-				

Table 4. Names, PDG ID and polarisations of the particles. In particular, the second, third and fourth columns of the tables correspond to the sixth, seventh and eighth lines of the output file.

References

- [1] FCC collaboration, A. Abada et al., *FCC-ee: The Lepton Collider: Future Circular Collider Conceptual Design Report Volume 2*, *Eur. Phys. J. ST* **228** (2019) 261–623.
- [2] CEPC STUDY GROUP collaboration, M. Dong et al., *CEPC Conceptual Design Report: Volume 2 - Physics & Detector*, [1811.10545](#).
- [3] *The International Linear Collider Technical Design Report - Volume 1: Executive Summary*, [1306.6327](#).
- [4] CLIC collaboration, J. de Blas et al., *The CLIC Potential for New Physics*, [1812.02093](#).
- [5] M. Bai et al., *C³: A "Cool" Route to the Higgs Boson and Beyond*, in *Snowmass 2021*, 10, 2021, [2110.15800](#).
- [6] MUON COLLIDER collaboration, D. Stratakis et al., *A Muon Collider Facility for Physics Discovery*, [2203.08033](#).
- [7] MUON COLLIDER collaboration, S. Jindariani et al., *Promising Technologies and R&D Directions for the Future Muon Collider Detectors*, [2203.07224](#).

$xf_{e_L}(x_0, Q_0)$	$xf_{h/Z_L}(x_0, Q_0)$
$xf_{e_L}(x_0, Q_1)$	$xf_{h/Z_L}(x_0, Q_1)$
\vdots	\vdots	\vdots	\vdots
$xf_{e_L}(x_0, Q_{N_Q})$	$xf_{h/Z_L}(x_0, Q_{N_Q})$
$xf_{e_L}(x_1, Q_0)$	$xf_{h/Z_L}(x_1, Q_0)$
$xf_{e_L}(x_1, Q_1)$	$xf_{h/Z_L}(x_1, Q_1)$
\vdots	\vdots	\vdots	\vdots
$xf_{e_L}(x_1, Q_{N_Q})$	$xf_{h/Z_L}(x_1, Q_{N_Q})$
\vdots	\vdots	\vdots	\vdots
\vdots	\vdots	\vdots	\vdots
$xf_{e_L}(x_{N_x}, Q_0)$	$xf_{h/Z_L}(x_1, Q_0)$
$xf_{e_L}(x_{N_x}, Q_1)$	$xf_{h/Z_L}(x_1, Q_1)$
\vdots	\vdots	\vdots	\vdots
$xf_{e_L}(x_{N_x}, Q_{N_Q})$	$xf_{h/Z_L}(x_{N_x}, Q_{N_Q})$

Table 5. Structure of our PDF data in the LHAPDF6 format.

- [8] C. Aime et al., *Muon Collider Physics Summary*, [2203.07256](#).
- [9] MUON COLLIDER collaboration, J. de Blas et al., *The physics case of a 3 TeV muon collider stage*, [2203.07261](#).
- [10] C. Accettura et al., *Towards a Muon Collider*, [2303.08533](#).
- [11] E. Fermi, *On the Theory of the impact between atoms and electrically charged particles*, *Z. Phys.* **29** (1924) 315–327.
- [12] C. F. von Weizsacker, *Radiation emitted in collisions of very fast electrons*, *Z. Phys.* **88** (1934) 612–625.
- [13] E. J. Williams, *Nature of the high-energy particles of penetrating radiation and status of ionization and radiation formulae*, *Phys. Rev.* **45** (1934) 729–730.
- [14] L. D. Landau and E. M. Lifschitz, *ON THE PRODUCTION OF ELECTRONS AND POSITRONS BY A COLLISION OF TWO PARTICLES*, *Phys. Z. Sowjetunion* **6** (1934) 244.
- [15] V. N. Gribov and L. N. Lipatov, *Deep inelastic $e p$ scattering in perturbation theory*, *Sov. J. Nucl. Phys.* **15** (1972) 438–450.
- [16] Y. L. Dokshitzer, *Calculation of the Structure Functions for Deep Inelastic Scattering and $e+e-$ Annihilation by Perturbation Theory in Quantum Chromodynamics.*, *Sov. Phys. JETP* **46** (1977) 641–653.
- [17] G. Altarelli and G. Parisi, *Asymptotic Freedom in Parton Language*, *Nucl. Phys. B* **126** (1977) 298–318.
- [18] S. Frixione, *Initial conditions for electron and photon structure and fragmentation functions*, *JHEP* **11** (2019) 158, [[1909.03886](#)].
- [19] V. Bertone, M. Cacciari, S. Frixione and G. Stagnitto, *The partonic structure of the electron at the next-to-leading logarithmic accuracy in QED*, *JHEP* **03** (2020) 135, [[1911.12040](#)].
[Erratum: *JHEP* 08, 108 (2022)].

- [20] V. Bertone, M. Cacciari, S. Frixione, G. Stagnitto, M. Zaro and X. Zhao, *Improving methods and predictions at high-energy e^+e^- colliders within collinear factorisation*, *JHEP* **10** (2022) 089, [[2207.03265](#)].
- [21] P. Ciafaloni and D. Comelli, *Electroweak evolution equations*, *JHEP* **11** (2005) 022, [[hep-ph/0505047](#)].
- [22] V. Bertone, S. Carrazza, D. Pagani and M. Zaro, *On the Impact of Lepton PDFs*, *JHEP* **11** (2015) 194, [[1508.07002](#)].
- [23] A. Manohar, P. Nason, G. P. Salam and G. Zanderighi, *How bright is the proton? A precise determination of the photon parton distribution function*, *Phys. Rev. Lett.* **117** (2016) 242002, [[1607.04266](#)].
- [24] A. V. Manohar, P. Nason, G. P. Salam and G. Zanderighi, *The Photon Content of the Proton*, *JHEP* **12** (2017) 046, [[1708.01256](#)].
- [25] B. Fornal, A. V. Manohar and W. J. Waalewijn, *Electroweak Gauge Boson Parton Distribution Functions*, *JHEP* **05** (2018) 106, [[1803.06347](#)].
- [26] L. Buonocore, P. Nason, F. Tramontano and G. Zanderighi, *Leptons in the proton*, *JHEP* **08** (2020) 019, [[2005.06477](#)].
- [27] P. Ciafaloni and D. Comelli, *Sudakov enhancement of electroweak corrections*, *Phys. Lett. B* **446** (1999) 278–284, [[hep-ph/9809321](#)].
- [28] M. Ciafaloni, P. Ciafaloni and D. Comelli, *Bloch-Nordsieck violating electroweak corrections to inclusive TeV scale hard processes*, *Phys. Rev. Lett.* **84** (2000) 4810–4813, [[hep-ph/0001142](#)].
- [29] M. Ciafaloni, P. Ciafaloni and D. Comelli, *Bloch-Nordsieck violation in spontaneously broken Abelian theories*, *Phys. Rev. Lett.* **87** (2001) 211802, [[hep-ph/0103315](#)].
- [30] J. Chen, T. Han and B. Tweedie, *Electroweak Splitting Functions and High Energy Showering*, *JHEP* **11** (2017) 093, [[1611.00788](#)].
- [31] C. W. Bauer and B. R. Webber, *Polarization Effects in Standard Model Parton Distributions at Very High Energies*, *JHEP* **03** (2019) 013, [[1808.08831](#)].
- [32] A. Azatov, F. Garosi, A. Greljo, D. Marzocca, J. Salko and S. Trifinopoulos, *New physics in $b \rightarrow s\mu\mu$: FCC-hh or a muon collider?*, *JHEP* **10** (2022) 149, [[2205.13552](#)].
- [33] T. Han, Y. Ma and K. Xie, *High energy leptonic collisions and electroweak parton distribution functions*, *Phys. Rev. D* **103** (2021) L031301, [[2007.14300](#)].
- [34] T. Han, Y. Ma and K. Xie, *Quark and gluon contents of a lepton at high energies*, *JHEP* **02** (2022) 154, [[2103.09844](#)].
- [35] A. Costantini, F. De Lillo, F. Maltoni, L. Mantani, O. Mattelaer, R. Ruiz et al., *Vector boson fusion at multi-TeV muon colliders*, *JHEP* **09** (2020) 080, [[2005.10289](#)].
- [36] H. Al Ali et al., *The muon Smasher’s guide*, *Rept. Prog. Phys.* **85** (2022) 084201, [[2103.14043](#)].
- [37] R. Ruiz, A. Costantini, F. Maltoni and O. Mattelaer, *The Effective Vector Boson Approximation in high-energy muon collisions*, *JHEP* **06** (2022) 114, [[2111.02442](#)].
- [38] S. Coleman and R. E. Norton, *Singularities in the physical region*, *Nuovo Cim.* **38** (1965) 438–442.
- [39] I. F. Ginzburg, *Initial particle instability in muon collisions*, *Nucl. Phys. B Proc. Suppl.* **51** (1996) 85–89, [[hep-ph/9601272](#)].

- [40] K. Melnikov and V. G. Serbo, *New type of beam size effect and the W boson production at $mu^+ mu^-$ colliders*, *Phys. Rev. Lett.* **76** (1996) 3263–3266, [[hep-ph/9601221](#)].
- [41] F. Borzumati and G. A. Schuler, *Real and virtual photon contributions to inelastic $e p$ scattering*, *Z. Phys. C* **58** (1993) 139–152, [[hep-ph/9211271](#)].
- [42] P. Aurenche, J. P. Guillet, M. Fontannaz, Y. Shimizu, J. Fujimoto and K. Kato, *Jets in photon-photon collisions: from TRISTAN to J/N-LC*, *Prog. Theor. Phys.* **92** (1994) 175–188, [[hep-ph/9401269](#)].
- [43] M. Drees and R. M. Godbole, *Virtual photon structure functions and the parton content of the electron*, *Phys. Rev. D* **50** (1994) 3124–3133, [[hep-ph/9403229](#)].
- [44] G. A. Schuler and T. Sjostrand, *Low and high mass components of the photon distribution functions*, *Z. Phys. C* **68** (1995) 607–624, [[hep-ph/9503384](#)].
- [45] G. A. Schuler and T. Sjostrand, *Parton distributions of the virtual photon*, *Phys. Lett. B* **376** (1996) 193–200, [[hep-ph/9601282](#)].
- [46] M. Ciafaloni, P. Ciafaloni and D. Comelli, *Towards collinear evolution equations in electroweak theory*, *Phys. Rev. Lett.* **88** (2002) 102001, [[hep-ph/0111109](#)].
- [47] C. W. Bauer, N. Ferland and B. R. Webber, *Standard Model Parton Distributions at Very High Energies*, *JHEP* **08** (2017) 036, [[1703.08562](#)].
- [48] C. W. Bauer, N. Ferland and B. R. Webber, *Combining initial-state resummation with fixed-order calculations of electroweak corrections*, *JHEP* **04** (2018) 125, [[1712.07147](#)].
- [49] M. Ciafaloni, P. Ciafaloni and D. Comelli, *Electroweak double logarithms in inclusive observables for a generic initial state*, *Phys. Lett. B* **501** (2001) 216–222, [[hep-ph/0007096](#)].
- [50] G. Cuomo, L. Vecchi and A. Wulzer, *Goldstone Equivalence and High Energy Electroweak Physics*, *SciPost Phys.* **8** (2020) 078, [[1911.12366](#)].
- [51] F. Bloch and A. Nordsieck, *Note on the Radiation Field of the electron*, *Phys. Rev.* **52** (1937) 54–59.
- [52] M. Ciafaloni, P. Ciafaloni and D. Comelli, *Electroweak Bloch-Nordsieck violation at the TeV scale: ‘Strong’ weak interactions?*, *Nucl. Phys. B* **589** (2000) 359–380, [[hep-ph/0004071](#)].
- [53] D. Amati, A. Bassetto, M. Ciafaloni, G. Marchesini and G. Veneziano, *A Treatment of Hard Processes Sensitive to the Infrared Structure of QCD*, *Nucl. Phys. B* **173** (1980) 429–455.
- [54] A. V. Manohar and W. J. Waalewijn, *Electroweak Logarithms in Inclusive Cross Sections*, *JHEP* **08** (2018) 137, [[1802.08687](#)].
- [55] A. Denner and S. Pozzorini, *One loop leading logarithms in electroweak radiative corrections. 1. Results*, *Eur. Phys. J. C* **18** (2001) 461–480, [[hep-ph/0010201](#)].
- [56] A. Denner, *Electroweak radiative corrections at high-energies*, *PoS HEP2001* (2001) 129, [[hep-ph/0110155](#)].
- [57] D. Pagani and M. Zaro, *One-loop electroweak Sudakov logarithms: a revisit and automation*, *JHEP* **02** (2022) 161, [[2110.03714](#)].
- [58] S. Chen, A. Glioti, R. Rattazzi, L. Ricci and A. Wulzer, *Learning from radiation at a very high energy lepton collider*, *JHEP* **05** (2022) 180, [[2202.10509](#)].
- [59] J. Chay and T. Kwon, *N -jettiness for muon jet pairs in electroweak high-energy processes*, *JHEP* **12** (2022) 091, [[2207.05425](#)].

- [60] C. W. Bauer, D. Provasoli and B. R. Webber, *Standard Model Fragmentation Functions at Very High Energies*, *JHEP* **11** (2018) 030, [[1806.10157](#)].
- [61] R. M. Barnett, H. E. Haber and D. E. Soper, *Ultraheavy Particle Production from Heavy Partons at Hadron Colliders*, *Nucl. Phys. B* **306** (1988) 697–745.
- [62] F. I. Olness and W.-K. Tung, *When Is a Heavy Quark Not a Parton? Charged Higgs Production and Heavy Quark Mass Effects in the QCD Based Parton Model*, *Nucl. Phys. B* **308** (1988) 813.
- [63] S. Dawson, A. Ismail and I. Low, *Redux on “When is the top quark a parton?”*, *Phys. Rev. D* **90** (2014) 014005, [[1405.6211](#)].
- [64] T. Han, J. Sayre and S. Westhoff, *Top-Quark Initiated Processes at High-Energy Hadron Colliders*, *JHEP* **04** (2015) 145, [[1411.2588](#)].
- [65] R. N. Cahn and S. Dawson, *Production of Very Massive Higgs Bosons*, *Phys. Lett. B* **136** (1984) 196. [Erratum: *Phys.Lett.B* 138, 464 (1984)].
- [66] S. Dawson, *The Effective W Approximation*, *Nucl. Phys. B* **249** (1985) 42–60.
- [67] M. S. Chanowitz and M. K. Gaillard, *Multiple Production of W and Z as a Signal of New Strong Interactions*, *Phys. Lett. B* **142** (1984) 85–90.
- [68] G. L. Kane, W. W. Repko and W. B. Rolnick, *The Effective W⁺⁻, Z⁰ Approximation for High-Energy Collisions*, *Phys. Lett. B* **148** (1984) 367–372.
- [69] Z. Kunszt and D. E. Soper, *On the Validity of the Effective W Approximation*, *Nucl. Phys. B* **296** (1988) 253–289.
- [70] P. Borel, R. Franceschini, R. Rattazzi and A. Wulzer, *Probing the Scattering of Equivalent Electroweak Bosons*, *JHEP* **06** (2012) 122, [[1202.1904](#)].
- [71] D. Buttazzo, D. Redigolo, F. Sala and A. Tesi, *Fusing Vectors into Scalars at High Energy Lepton Colliders*, *JHEP* **11** (2018) 144, [[1807.04743](#)].
- [72] Z. Alam and S. P. Martin, *Standard model at 200 GeV*, *Phys. Rev. D* **107** (2023) 013010, [[2211.08576](#)].
- [73] PARTICLE DATA GROUP collaboration, R. L. Workman et al., *Review of Particle Physics*, *PTEP* **2022** (2022) 083C01.
- [74] M. Cacciari, A. Deandrea, G. Montagna and O. Nicosini, *QED structure functions: A Systematic approach*, *EPL* **17** (1992) 123–128.
- [75] A. Buckley, J. Ferrando, S. Lloyd, K. Nordström, B. Page, M. Rüfenacht et al., *LHAPDF6: parton density access in the LHC precision era*, *Eur. Phys. J. C* **75** (2015) 132, [[1412.7420](#)].